NGT-21-002-080

N6T-80001

AERONAUTICS

CALIFORNIA STATE POLYTECHNIC UNIVERSITY, POMONA

NASA / USRA ADVANCED DESIGN PROGRAM

JUNE 11, 1988

NASA / USRA ADVANCED DESIGN PROJECT

Final Report 1987-1988

Volume II

WAVERIDER

Design Team Members:

Pat Nightingale   Project Leader

Toan Duong

Chris Gillotte

Ron Mangio

Pablo Martinez

ABSTRACT

Because of the anticipated growth in airline travel within the next decade, the construction of a High-Speed Civilian Transport has been a topic of interest in the aerospace industry. It has been proposed that the new transport has a M = 3 - 6 cruise speed and carry 250 passengers on a 6,500 nm journey (the distance from Los Angeles to Sydney)> Working in conjunction with NASA/USRA, Cal Poly Pomona has been evaluating the viability of four configurations for this mission requirement.

One of the configurations under evaluation is the Waverider configuration (an evolution of the Caret configuration). The Waverider creates lift in a unique fashion. The craft is designed to produce lift at high speeds through the use of shock waves. This 'shock lift' when combined with conventionally created lift produce higher L/D values at high speeds than conventional configurations.

The Waverider cruises at M = 5.5, has a range of 6,500 nm, and seats 250 passengers and baggage in first class comfort for the trip. The aircraft is operable from existing airfields and does not require any special traffic control considerations when operating in controlled airspace.

TABLE OF CONTENTS

List of Symbols

A_c — intake capture area

A_e — nozzle exit area

C — local thermal conductivity constant

C_D — drag coefficient

C_{Dq} — drag change with pitch rate

C_{Du} — drag change with speed

C_{D0} — zero lift drag coefficient

C_{D0} — zero lift drag coefficient

$C_{D\alpha}$ — drag change with angle of attack

$C_{D\dot\alpha}$ — drag change with angle of attack rate

C_L — lift coefficient

C_{Lmax} — maximum lift coefficient

C_{LB} — break lift coefficient

C_{Lq} — lift change with pitch rate

C_{Lu} — lift change with speed

$C_{L\alpha}$ — lift change with angle of attack

$C_{L\dot\alpha}$ — lift change with angle of attack rate

C_{Txu} — thrust coefficient change with speed

C_a — nozzle losses due to flow angularity

C_{fg} — nozzle thrust coefficient

C_{macWB} — mean aerodynamic center:wingbody

C_{mq} — pitching moment change with pitch rate

C_{mu} — pitching moment change with speed

$C_{m\alpha}$ — pitching moment change with

$C_{m\dot\alpha}$ — pitching moment change with pitch rate

C_{lp} — rolling moment change with roll rate

C_{lr} — rolling moment change with yaw rate

$C_{l\beta}$ — rolling moment change with sideslip

C_{np} — yawing moment change with roll rate

C_{nr} — yawing moment change with yaw rate

$C_{n\beta}$ — yawing moment change with sideslip

C_{p0} — specific heat of freestream

C_{p4} — specific heat of gas generator

C_v — nozzle friction losses

C_{yp} — side force change with roll rate

C_{yr} — side force change with yaw rate

$C_{y\beta}$ — side force change with sideslip

C_1 — vortex lift constant, conductivity const

C_2 — thermal conductivity constant

D — drag

D_{reqd} — required engine diameter

D_1 — engine diameter at analysis

E — energy rate emission

F — engine thrust force

F_{ram} - ram drag force

I - specific impulse

K_B - break constant

K' - constant based on Oswald efficiency

L - convection flow length

L_H - length from cg to horizontal ac

L_{WB} - length of wing body

M - Mach number

M_0 - freestream Mach number

M_4 - gas generator exit Mach number

Nu^* - Nusselt number

P_i - nozzle inlet pressure

Pr - Prandtl Number

P_0 - freestream static pressure

P_7 - freestream static pressure

R - gas constant of air, nose radius

Re^* - reference Reynolds Number

S - exposed wing area

S_A - airborne distance

S_B - breaking distance

S_{CL} - take off climb distance

S_{FR} - free roll distance

S_G - take off ground distance

S_R - take off rotation distance

S_{TR} - take off transition distance

T - thrust, freestream temperature

T_L - local temperature

T_{SL} - stagnation local temperature

T_{WS} - wall temperature

T_{aw} - adiabatic wall temperature

T_r - rolling mode, recovery temperature

T_{reqd} - thrust required

T_s - spiral mode, surface temperature

T_w - static wall temperature

T_{wf} - element final temperature

T_0 - static air temperature

T_1 - thrust at engine size analyzed

T_4 - rocket static exit temperature

T^* - reference temperature

U - forward speed

V_C - design cruise speed

V_{CL} - climb velocity

V_D - design diving speed

V_{TO} - takeoff velocity

V_a - design maneuvering speed

V_e - velocity of mass at nozzle exit

V_i - velocity of mass at nozzle inlet

V_{s1} - stall velocity

V_{50} - velocity required to clear 50 ft obstacle $\quad$ **W** - weight

X_{acH} - horizontal aerodynamic center $\quad$ X_{acWB} - wing-body aerodynamic center

X_{cg} - center of gravity location $\quad$ X_{mg} - distance from point to center of mass

Z_D - distance from point to drag axis $\quad$ Z_T - distance from point to thrust axis

Z_{mg} - distance from point to center of mass $\quad$ a_0 - freestream speed of sound

a_4 - gas generator speed of sound $\quad$ **c** - mean chord

h - fuel heating rate, heat transfer coefficent $\quad$ **g** - gravity

g_c - Newton's constant $\quad$ **k** - thermal conductivity

k_{32} - thermal conductivity constant $\quad$ k^* - reference thermal conductivity

l - wing length $\quad$ **m** - mass

$\dot{m}_e$ - nozzle exit mass flow rate $\quad$ $\dot{m}_f$ - fuel mass flow rate

$\dot{m}_0$ - freestream mass flow rate $\quad$ $\dot{m}_4$ - gas generator mass flow rate

p - freestream pressure $\quad$ p_L - local pressure

p_{02} - total pressure behind shock wave $\quad$ $q_{T.O.R.}$ - dynamic pressure at rotation

q_{bl} - convective heating rate $\quad$ q_{rad} - stagnation point radiation

q_s - stagnation point heating rate $\quad$ **r** - recovery factor

s - wing span $\quad$ t_c - skin thickness

ΔC_{fg} - nozzle losses for leakage and cooling air $\quad$ Δt - time increment

Θ - angle between velocity and surface $\quad$ α - bypass ratio

η_{spec} - MIL specification total pressure recovery $\quad$ δ - wedge angle

ε - emissivity $\quad$ γ - ratio of specific heat of air

θ_{CL} - angle of climb $\quad$ θ_{ab} - bypass total/freestream static pressure

θ_{ar} - rocket total/freestream static pressure $\quad$ θ_0 - freestream total/freestream static pres

θ_4 - turbine total/rocket static pressure $\quad$ μ_L - local viscosity

σ - Stephan-Boltzman constant $\qquad$ τ - volume/area ratio

τ_c - bypass total/inlet total temperature $\qquad$ τ_f - burner total/inlet total temperature

ω_D - high frequency Dutch Roll $\qquad$ ω_{nph} - high frequency phugoid

ω_{nsp} - high frequency short period $\qquad$ ζ_D - low frequency Dutch Roll

ζ_{ph} - low frequency phugoid $\qquad$ ζ_{sp} - low frequency short period

1 INTRODUCTION

California State Polytechnic University, Pomona (CSPUP) was invited to participate in the NASA / USRA Universities advanced Design Program. The purpose of this invitation was to investigate the planform effects of four different planform configurations on a viable High - Speed Civilian Transport. This investigation was started in the Fall and continued through the Winter and Spring quarters of the 1987 - 1988 academic year. The four planforms investigated were:

1. Blended Wing - Body
2. Caret
3. Joined Wing
4. Oblique Wing

During the first quarter of the investigation, Fall quarter (ARO 499), literature review pertaining to second generation supersonic transports was performed. In addition, each participating student was assigned to one of three disciplines, and reviewed the literature according to this assigned discipline. At the begining of the Winter quarter (ARO 446) the list of disciplines was expanded to include a fourth. The four disciplines were:

1. Aerodynamics
2. Propulsions
3. Structures / Heat Transfer
4. Noise and Pollution

Each group included seven students with the exception of the fourth discipline, Noise and Pollution. The Noise and Pollution analysis was completed by only one

student.

At the beginning of the Winter quarter, four project leaders were elected to assume responsibility for each of the four above mentioned configurations. The remaining students maitained their membership to their respective groups while also becoming responsible for a particular portion of a configuration. This caused the class organization to be similar to a " Matrix Management " style of organization. This organization continued through to the end of the Spring quarter (ARO 463).

This report contains the results of the analysis on the Waverider Project (an evolution of the Caret project). The Waverider design team consisted of five students; two from the Aerodynamics group, one from the Propulsions, and two from the Structures / Heat Transfer group (this includes the project engineer). Additionally, the Noise and Pollution analysis was completed by one individual who was responsible for the Noise and Pollution analysis of all four configurations.

2 MISSION REQUIRMENTS

Because of the increasing trans - Pacfic trade and the length of time required for the ocean crossing, the viability of a High - Speed Civil Transport has been the subject of study for some time by several companies.

2.1 REQUEST FOR PROPOSAL

After reviewing many economic and technological trade studies by several independent companies on the High - Speed Civil Transport and discussions with the Cal Poly, Pomona NASA advisor, a request for proposal (RFP) was formulated. The RFP called for the following:

Type of Aircraft	Commercial Transport
Speed	M = 3 - 6
Range	6,500 Nm
Payload	250 + Passengers
Operational Airfield	11,500 ft
Technology Level	Today's

This RFP is intentionally general enough to allow the individual configurations to optimize their attributes. In addition to the above mentioned requirements, the aircraft must be operable in today's Terminal Control Airspace.

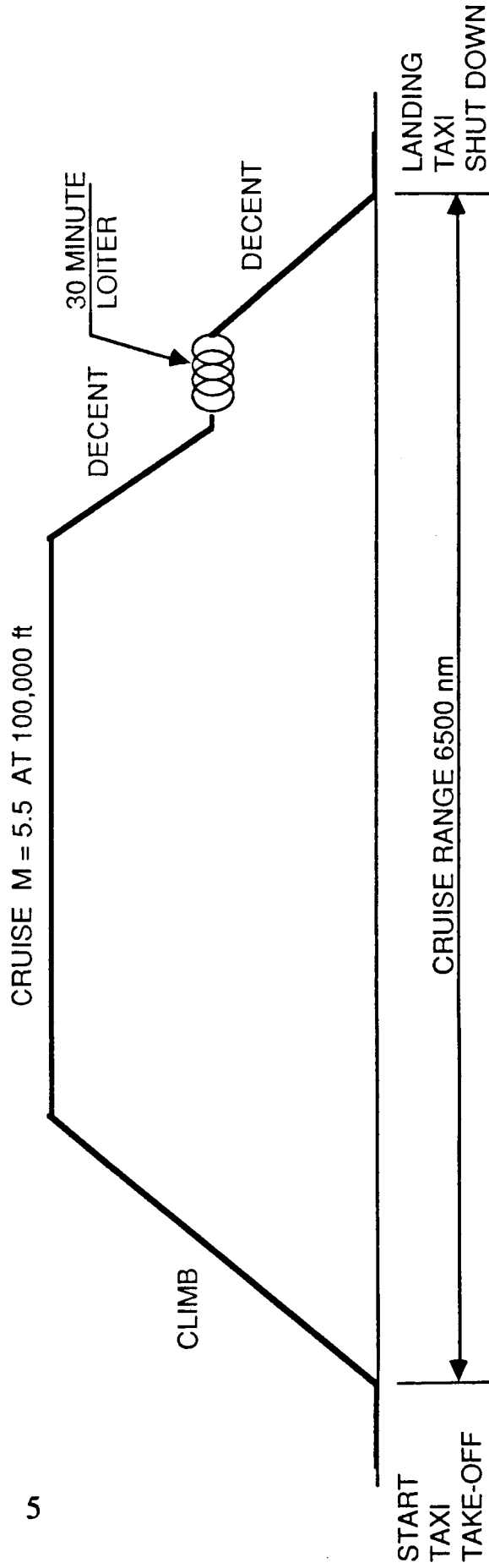The requirements fill many of the needs for the aircraft to be comercially viable. The 6,500 Nm range is the same distance as a non - stop flight from Los Angeles to Sydney. Also, all studies reviewed determined the optimum number of passengers to be in the range of 200 - 300 people. From these studies the passenger payload requirement was agreed to be 250 people. Based on the same studies, the

3

optimum aircraft speed was determined to be in the range of M = 3 - 6. Additionally, the aircraft was agreed to have the contraint of operating from existing airfields which lead to the 11,500 ft operational field length requirement. Finnally, the assumed technology level must be today's, as the aircraft must be operational by the late 1990's to fully take advantage of the expanding trans - Pacific travel.

2.2 MISSION PROFILE

Based on the performance requirements, Federal Aviation Regulations (FAR's) and inherent flight characteristics of the Waverider (the utilization of shock lift) a mission profile was derived (see Figure 2.1). The M = 5.5 cruise speed was determined because of several factors. Because of high temperatures and heating rates, above M = 5.5 the ability to cool the aircraft becomes impractical. The second factor is that the Waverider utilizes shock lift to increase the aerodynamic efficiency at cruise speeds. The production of this lift increases with Mach number. The compromise of these two criteria produced the M = 5.5 cruise speed. The 100,000 ft cruise altitude was deemed necessary because of pollution considerations, namely the ozone concentrations in the 80,000 - 95,000 ft range of the atmosphere. Additionally, because of an assumed dynamic pressure limitation of aerospace structures (1000 psf) the aircraft could not cruise below 80,000 ft at M= 5.5. The loiter and reserve portions of the mission profile were required by FAR 25 . The climb and decent distances were determined using the maximum decent and climb angle specified in FAR 25.119. Using these contraints in conjunction with the cruise altitude of 100,000 ft provides for a level cruise portion of the mission to be 490,000 Nm. The standard flight time (assuming no loiter) for the 6,500 Nm journey is 3.0 hrs.

MISSION PROFILE

CLIMB

CRUISE M = 5.5 AT 100,000 ft

DECENT

30 MINUTE LOITER

DECENT

START
TAXI
TAKE-OFF

LANDING
TAXI
SHUT DOWN

CRUISE RANGE 6500 nm

RESERVES = 5% OF TOTAL FUEL

FIGURE 2.1. MISSION PROFILE.

3 WAVERIDER CONFIGURATION

The Waverider is very similar to a tailess blended-wing-body planform. Figure 3.1 presents a three-view of the configuration.

3.1 GENERAL CONFIGURATION

The most notable feature of the Waverider is the anhedral and the flat bottom surface of the wings. The wings are anhedraled to take full advantage of the shock lift at hypersonic speeds. The 13,080 ft^2 wing area coupled with the 870,500 lb gross take-off weight produce a wing loading of 66.55 lbs/ ft^2 at take-off. Propulsive power is provided by four air turbo ramjet engines of 52,621 lbs static thrust each at sea level.

3.2 INTERNAL ARRANGEMENT

The inboard profile Figure 3.2, shows the internal arrangement of the fuselage. Additionally, Figure 3.3 shows a plan view of the internal arrangement.

The passenger cabin was designed for both comfort and safety. Fist class seating for 250 passengers and cargo space for baggage is provided for the 3.0 hour journey. The passengers are seated eight abreast in four individual cabins (see Figure 3.4). For normal operations the passengers deplane the aircraft through the two front cabin entrances. As required by FAR 25.807 ten emergency exits(two Type II, four Type III, and four Type A) are incorporated in the cabin. Additionally seating is provided for fourteen crew members (four flight crew and ten passenger cabin attendants).

The fuel system consists of four fuel tanks that together hold 455,000 lbs of

liquid natural gas (LNG) fuel. The forward fuel tank holds 215,000 lbs, the rear tank holds 76,000 lbs, and the two wing tanks hold 82,000 lbs of fuel each. The intent of the forward fuel tank is to allow managment of the c. g. location to reduce trim drag penalties. Additionally, it is anticipated that fuel will be circulated throughout the aircaft for the purpose of sinking heat from the structure and to increase the heat of combustion of the fuel before injection into the engines.

The propulsion system consists of four engines divided into three main parts; the inlet, the engine, and the nozzle. The inlets employ variable geometry ramps to help optomize the incoming flow properties over a wide range of speeds. The engine is an Air Turbo Ramjet (manufactured by General Electric Turbine Co.) that makes use of a liquid hydrogen rocket powered core surrounded by the LNG powered turbo-ramjet engine. The nozzle is actively cooled and employs variable geometry to optomize the integrated propulsive units effectiveness.

WAVERIDER

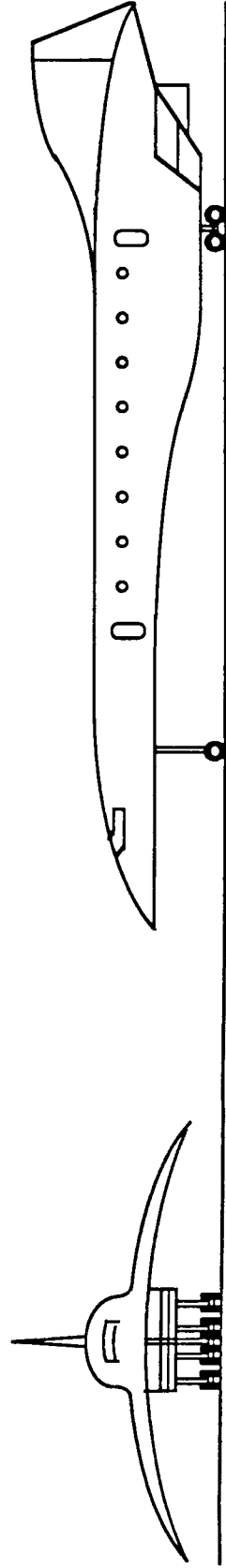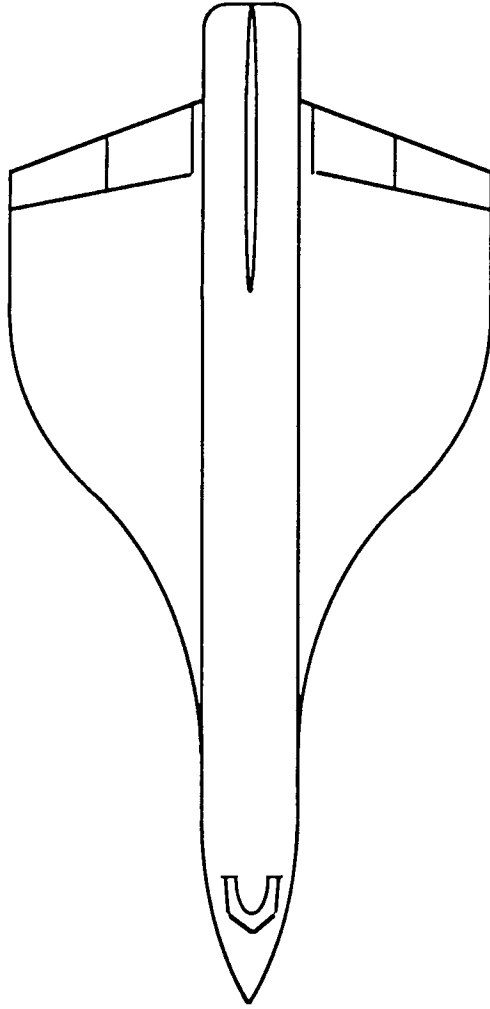|	
WING SPAN	120 FT
LENGTH	245 FT
HEIGHT	50 FT
WING AREA	13080 FT
GROSS TAKE-OFF WEIGHT	870,500 LB
PAYLOAD	250 PASSENGERS
CRUISE SPEED	M = 5.5
RANGE	6500 NM

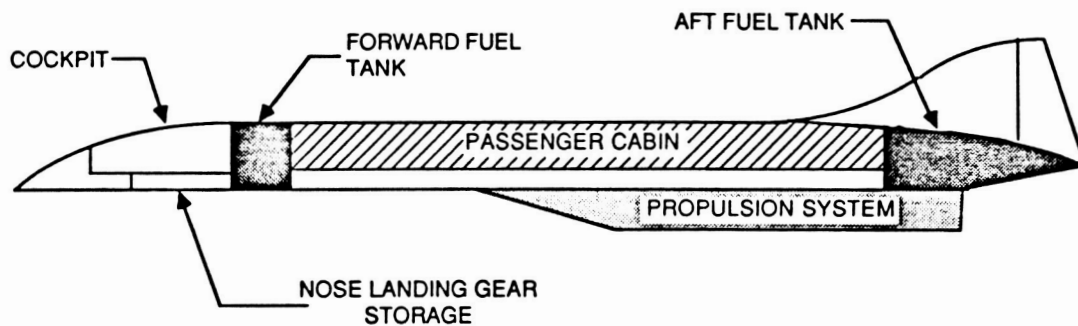FIGURE 3.1. WAVERIDER THREE-VIEW.
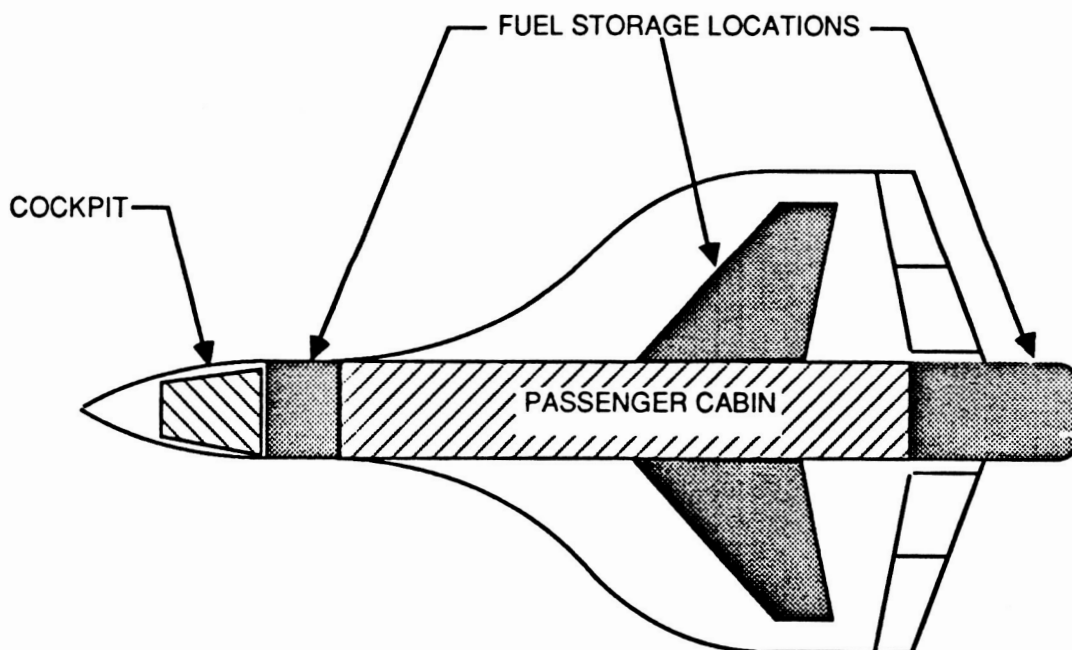
8

FIGURE 3.2. INBOARD PROFILE.

FIGURE 3.3. PLANVIEW PROFILE.

9

4 AERODYNAMICS

The Hypersonic Civil Transport was required to operate for a large range of Mach numbers and altitudes. Since the efficient production of lift at the higher Mach numbers (Mach numbers 4 - 6) possessed the greatest design challenge, the cruise Mach number was chosen as the aerodynamic design point. The configuration was constrained by the requirement that the planform be a single fixed geometry in order to minimize the weight and avoid heat problems associated with variable geometry structural designs. This led to a tradeoff between the hypersonic and the subsonic performance resulting in subsonic aerodynamic characteristics poorer than those found in current subsonic transports. However, due to the incorporation of compression lift, the hypersonic aerodynamic characteristics indicated that the high performance goals initiated to meet the cruise requirements for speed and range could be reached.

4.1 AERODYNAMIC CHARACTERISTICS

Since the aircraft cannot instantaneously accelerate to the cruise Mach number, all of the speed regimes must be analysed and the aerodynamic characteristics be determined for the Waverider configuration.

Throughout the entire flight mission, lift will be produced by conventional means. That is to say, lift will be produced by accelerating the flowstream over the upper surface which results in a pressure decrease over this surface creating lift by suction. This is the method of lift common to all aircraft today. In addition, delta wing planforms, have additional lift that is generated by vortex's over the leading edges. These vortex's are created by the flow of higher pressure air from the lower surface over the leading edges to the upper surface resulting in leading edge suction which in turn generates lift (Reference 1).

10

Compression lift is lift that is created when the flowstream is compressed on the lower surface of a lifting body which results in the production of shockwaves. These shockwaves are then employed to contain this high pressure flow on the lower surface. The goal of the aerodynamicist in this context is to design the configuration so that the shockwaves isolate the upper and lower surfaces. This produces compressed high pressure flow on the lower surface and expanded low pressure flow on the upper surface (Reference 2).

4.1.1 SUBSONIC AERODYNAMICS

A number of basic ideas and assumptions went into the analysis of the Waverider aircraft. These assumptions relate to the analysis techniques presented in Reference 3. These assumptions relate both to the aircraft and to its analysis. The Waverider was a blended wing-body aircraft. However, for purposes of analysis, the aircraft was considered to be flat plate and a cylindircal body section. The flat plate was considered to be without camber which led to the resulting assumption that the zero lift angle of attack was zero. The configuration was analysed under the clean aerodynamic conditions.

The zero lift drag coefficient was determined with the assumption that the entire wetted surface of the aircraft was subjected to turbulent flow. In addition, a constant altitude of 100,000 ft was used to calculate the Reynold's Number of the zero lift drag.

The drag due to lift was assumed to possess a parabolic behavior until the break lift coefficient was reached. This value was taken to be 0.8. In addition, the non-parabolic lift drag constant was assumed to be 0.1.

The drag due to empennage was taken to be 0.001 for the clean configuration.

The actual range of subsonic flow was selected to extend from a Mach

number of zero to a Mach number of 0.85.

The resulting aerodynamic performance showed that the Waverider's subsonic performance was below that of current transports. This was primarily due to the need to keep the aspect ratio of the wing down to a value of 1.2. This led to a small average lift curve slope of approximately 1.65. The vortex lift in this case was only able to produce a few percent to the lift. The drag coefficient values were low (Figure 4.1) but the corresponding lift drag values were still below those listed for various other transports.The maximum Lift / Drag ranged from 12.4 to 10.6 and increased as the Mach number increased (Figure 4.2).This decrease was due primarily to the increase in the friction drag as the Mach number increased (Figure 4.3). The lift coefficient and the lift drag altered only within a few percent as the Mach number changed. Figure 4.4 showed that the lift drag becomes more significant as the angle of attack is increased. This was to be expected and therefore it was assumed that the values obtained for the subsonic aerodynamics were precise in nature.

The equation for the lift coefficient assumes that the lift is produced by conventional methods and by vortex's. The drag coefficient assumes that the drag is produced by skin friction, interference, and by the production of lift. The equations for the lift coefficient and the drag coefficient are listed below:

$$C_D = C_{Do} + K'C_L^2 + K_B (C_L - C_{LB})^2$$

$$C_L = C_{L\alpha} \alpha + C_1 \alpha^2$$

C_{Do}	=	zero lift drag coefficent
K'	=	constant based on Oswald's efficiency
K_B	=	break constant = 0.1

12

$$C_{LB} \quad = \quad \text{Break lift coefficient} = 0.8$$

$$C_{L\alpha} \quad = \quad \text{lift curve slope}$$

$$C_1 \quad = \quad \text{vortex lift constant} = 0.95$$

4.1.2 TRANSONIC AERODYNAMICS

The general assumptions for the transonic performance are similar to those adopted for the subsonic performance. Lift is produced by the same means, but the lift curve slope must be estimated by using graphs and fairing in the transonic regions values. The same procedure was used to estimate the drag due to lift. The skin friction drag is assumed to the same values that were determined for the subsonic Mach number of 0.6. The values for the base pressure drag and the afterbody drag are zero due to the effect of exhaust gases.

As indicated in the previous paragraph, all of the transonic results were determined by fairing in the graphs of drag coefficient, friction drag coefficient, and lift curve slope versus Mach number. The divergent Mach number was determined empirically to be approximately 0.85 for the body and approximately 1.02 for the wing body combination. This Mach number indicated where the peak values of the various drag coefficients occured.

In spite of the elimination of the body and base pressure drag, the transonic drag was much larger than those values for the other flight Mach numbers. This drag was principally wave drag. Refering to the area ruling diagram (Figure 4.5), it was obvious that the wave drag would be significant due to the distribution of the majority of the area towards the aft of the aircraft.

The resulting L/Dmax values for this region did not compare favorably with those of the subsonic and supersonic regimes (Figure 4.2).This occured despite the fact that there was an increase in the lift coefficient values.

4.1.3 CONVENTIONAL SUPERSONIC AERODYNAMICS

For the conventional supersonic analysis, the same assumptions made in the transonic analysis were applied to this case.The nose and the boattail of the Waverider were analysed for a conical shape. The nose of the aircraft was assigned a fineness ratio (length / base diameter) of 3.5. The leading and trailing edges of the wing were both assumed to be relatively sharp, and the analysis of the wing drag reflected this concept.

The results of the data can be seen in Figures 4.6 - 4.8. Note that the lift, the drag, and the lift/drag values all decrease as the Mach numbers were increased. All of the drag components decreased with an increase in Mach number. The body drag comprised a significant portion of the total drag in all instances. This drag, in turn , was due mainly to drag induced on the nose of the aircraft. The short boattail in conjunction with the exhaust gases resulted in negligible wave drag from the afterbody.This resulted in a need to have a large nose fineness ratio of which the value selected was considered the smallest allowable to achieve the desired drag polar results.The decrease in the L/D max values indicates that the lift was decreasing at a greater rate than the drag.

4.1.4 COMPRESSION LIFT CHARACTERISTICS

The compression lift characteristics of the Waverider transport were analysed using a constrained set of aerodynamic equations for a caret body presented in Reference 4 and are shown in equations 2.3.1 - 2.3.3. The lift and drag characteristcs depended upon the three-dimensional shape of the body and certain flight aspects. The goal was to achieve a body that compressed the flow on the lower surface of the aircraft and expanded the flow on the upper surface. Oblique shocks

14

were to be attached to the leading edges in order to isolate the upper and lower surfaces to contain the higher pressure airflow. This in turn required that the leading edges be as sharp as the structural and heating requirements allowed.

$$C_P = \frac{4}{\S + 1}(\sin^2\partial - \frac{1}{M_\infty^2})$$

Eq. 2.3.1

$$C_L = \frac{C_P}{(1 + 9T^2 s/l)^{0.5}}$$

Eq. 2.3.2

$$C_D = C_{Do} + 3T\sqrt{s/l}\, C_L$$

Eq. 2.3.3

The volume - area ratio, the body slenderness, and the wedge angle formed by the leading edge determined the shock structure and, therefore, the aircraft performance. This diverges completely from the subsonic and conventional supersonic analysis where the aircraft was treated as a seperate wing + body. Since Equations 2.3.1 through 2.3.3 were for a mathematical model of a simplified shape (a caret) certain limits were imposed upon the range of figures to be employed in the analysis. The slenderness ratio was constrained to fall between 0.25 and 0.35. The leading edge wedge angle was allowed to fall between 5 and 10 degrees. The volume-area ratio was ranged from 0.045 to 0.075. These constraints were made by the suggestion of the author of Reference 4 and by personal recommendation. The final choice for the given figures is listed below:

volume - area ratio, $\tau = 0.07$

wedge angle, δ = 10 degrees

slenderness ratio, s/l = 0.30

The final values for the above variables were due to constraints ranging

15

aircraft from stability and control to structural and heating requirements. The volume-area ratio and the slenderness ratio were based on the required wingspan for stability, aircraft length for needed volume and conventional supersonic performance, and the minimum volume required for all systems. The wedge was constrained by a need to keep an oblique shock attached to the leading edge, less wave drag, and the heat induced by a sharp leading edge and the need to cool these edges.

Certain flight characteristcs also affected the performance of the transport at supersonic and hypersonic speeds. The altitude and the velocity determined the Mach number and the specific heat ratio combined with the Mach number and the aircraft shape determined the shock angles, and the peformance of the aircraft (Reference 5). The aircraft angle of attack affected the shock angles and the performance. Since the caret model depended upon this feature, the angle of attack was limited to a range of zero to ten degrees. This constraint was not considered severe since only the cruise phase was being examined, and it was felt that a high angle of attack would not be needed.

4.1.5 COMBINED COMPRESSION AND CONVENTIONAL

The area of greatest difficulty was in the area of integrating the conventional lift effects and the compression lift effects. What was finally employed was an extrapolation of the given information and are listed as follows:

1. The conventional delta lift and drag was significantly due to the vortexes that formed on the leading edges of the wings.

2. During supersonic flight, the resultant shocks were employed to isolate the upper and lower surfaces in order to contain the compressed high

16

pressure airflow on the lower surface.

3. According to Eq 3.2.1, the compression lift had a minimum speed which was assumed to be a Mach number of 2 for this analysis.

4. In Reference 6, the XB-70 accounted for 30 percent of its total lift from compression at a Mach number of 3.

From this information and a constraint to keep the analysis as workable as possible, the effects of compression were phased in as the Mach number was increased. At a Mach number of 2, only 10 percent of the lift and drag was due to compression (Figure 4.6). At Mach six, compression lift and drag accounted for 90 percent of the total effect (Figure 4.8). The contribution of compression lift was assumed to increase linearly as the Mach number was increased.

The final result of using compression lift was to give a greater lift-drag ratio at the required cruise Mach number than would have been possible otherwise. In fact, the Waverider's performance, based on L/D, impoved as the Mach number was increased(Figure 4.2).

5.2 CONCLUSIONS

The Waverider Hypersonic Civil Transport showed that high aerodynamic performance would be possible at low hypersonic speeds. The aircraft was severely hindered by the requirement that it have a single fixed geometry. However, this constraint was considered necessary in order to avoid additional weight and heating problems that are created by the use of hinges and spools found in variable geometry components. Consequently, the subsonic Lift to Drag ratios were well below those found in subsonic transports. However, due to primarily to

17

compression lift, the Waverider has high values of Lift-Drag ratio for the supersonic and hypersonics flight regimes.

CDmin VS MACH NUMBER
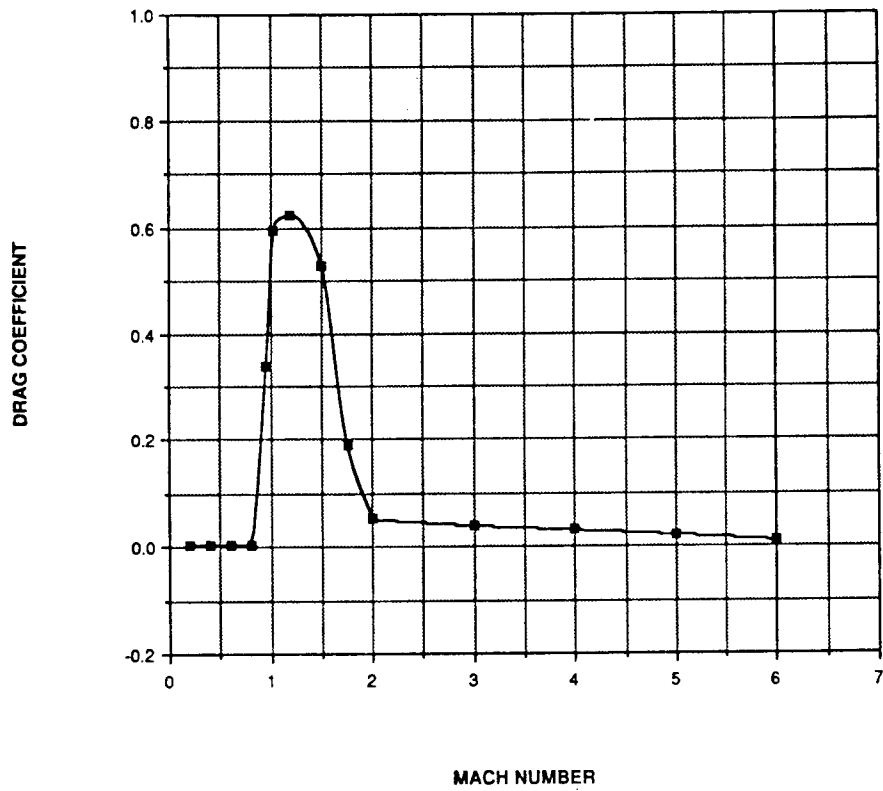

FIGURE 4.1. MINIMUM LIFT COEFFICIENT.

Lift/Drag Versus Mach Number

FIGURE 4.2. MAXIMUM L/D.   MACH NUMBER
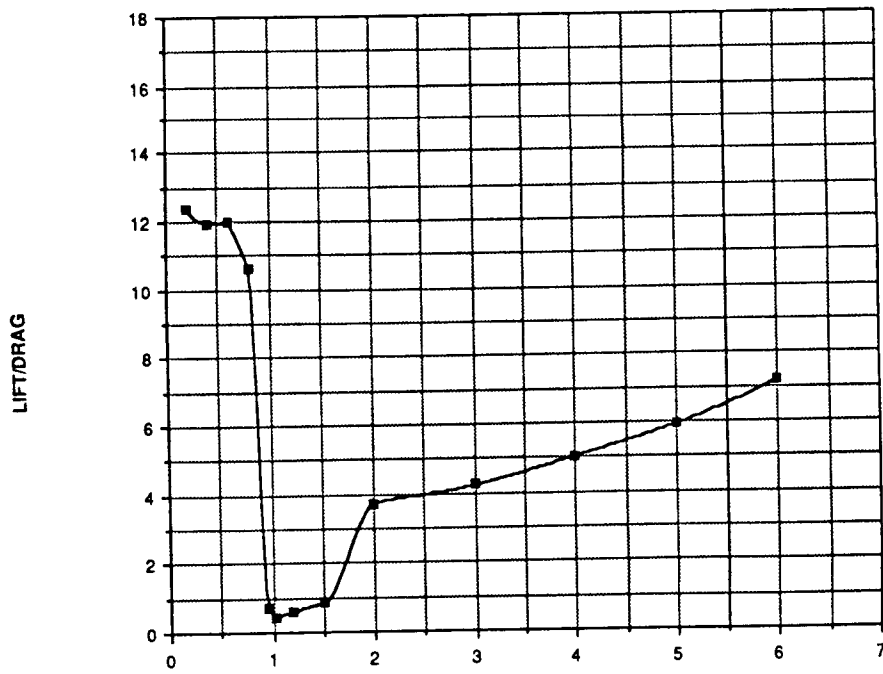
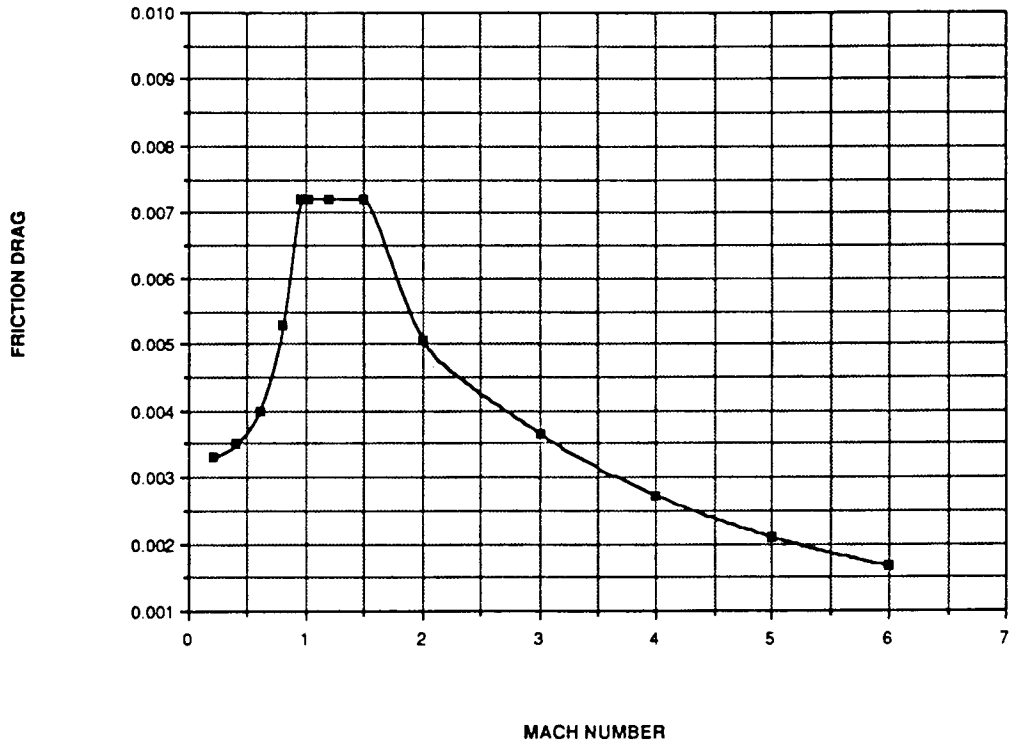19

CDo VERSUS MACH NUMBER

FIGURE 4.3. FRICTION DRAG.

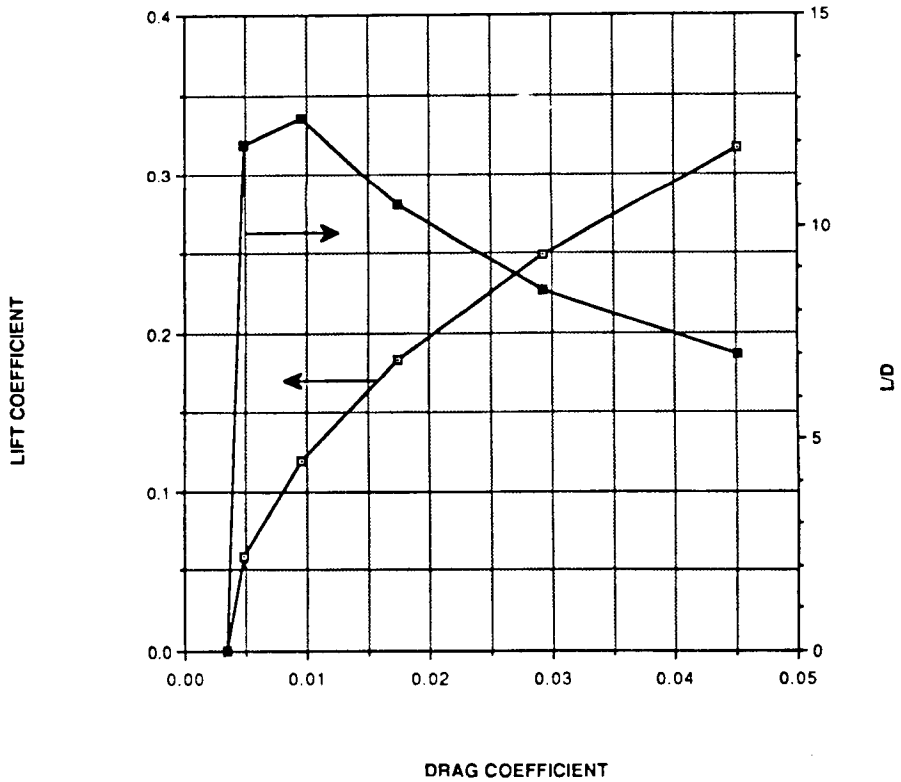DRAG POLAR AT MACH NUMBER 0.4

FIGURE 4.4. MACH 0.4 DRAG POLAR.
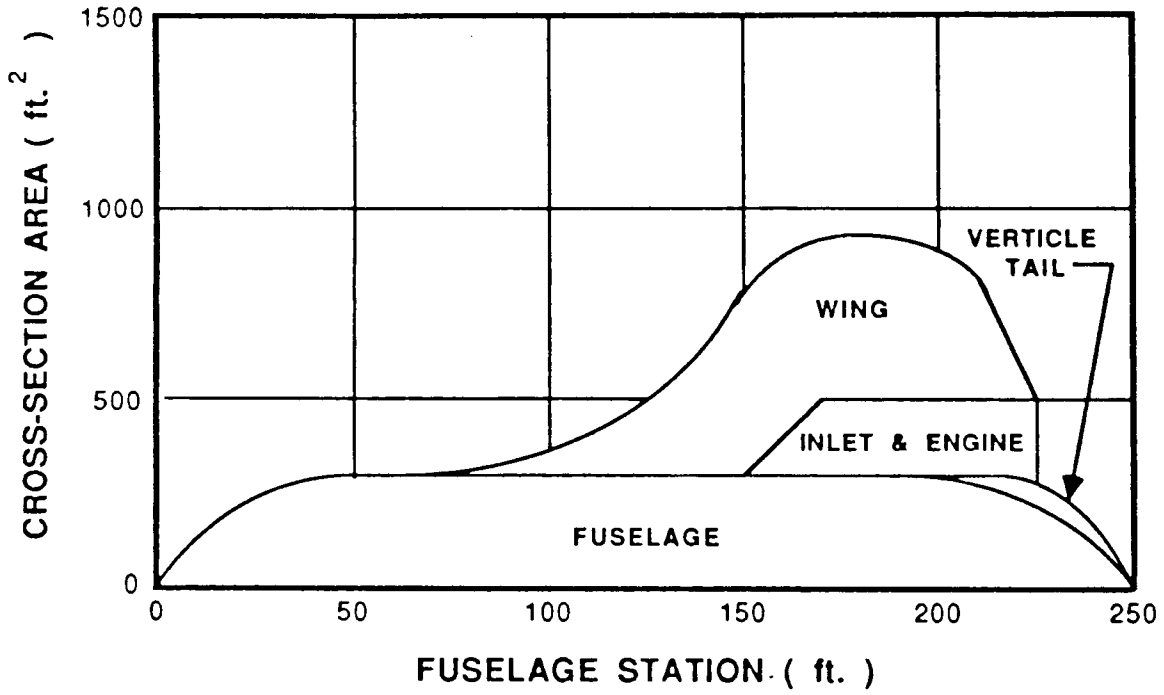
AREA DISTRIBUTION

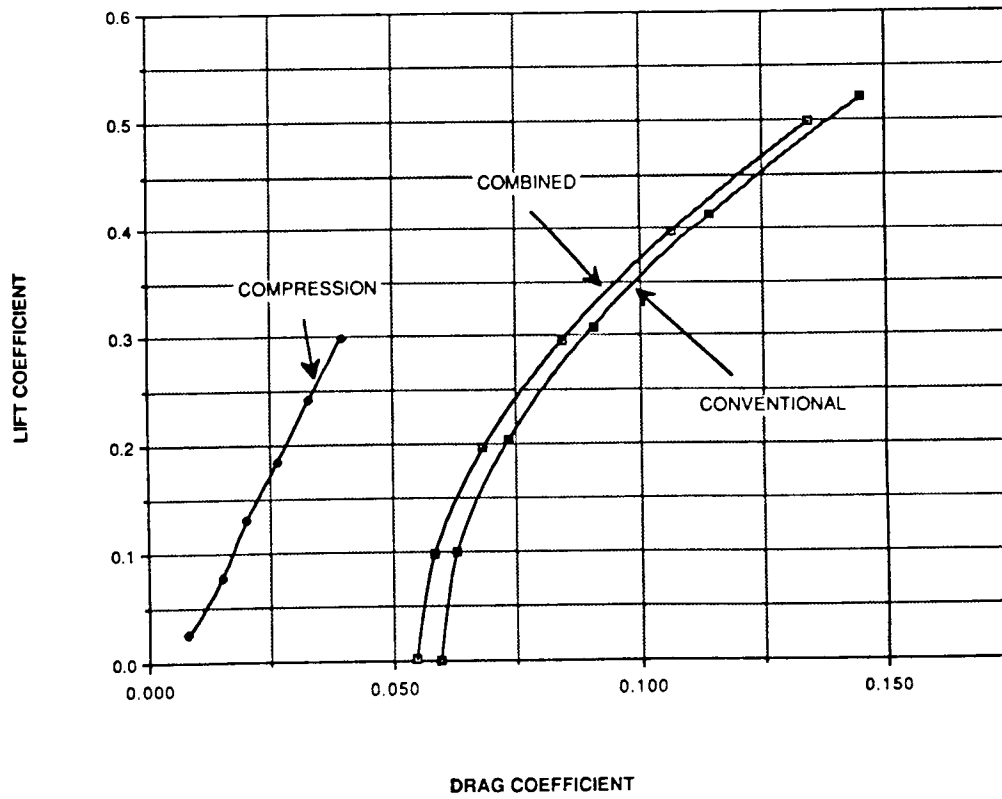FIGURE 4.5. AREA DISTRIBUTION.

DRAG POLARS AT MACH 2

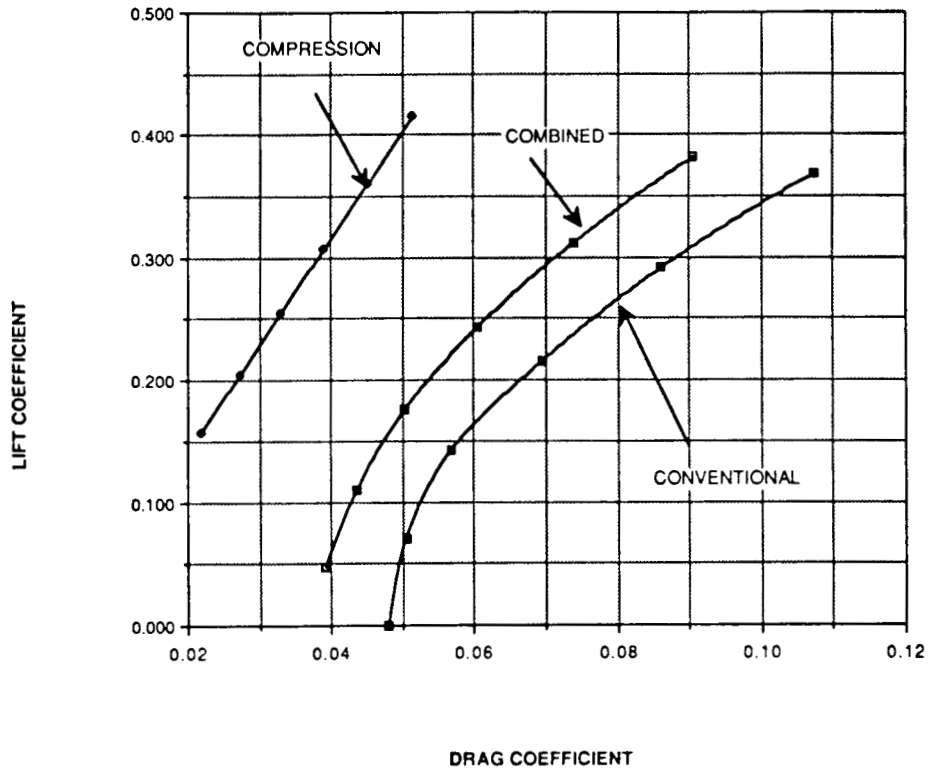FIGURE 4.6. MACH 2.0 DRAG POLAR.

DRAG POLARS AT MACH 3

FIGURE 4.7. MACH 3.0 DRAG POLAR.
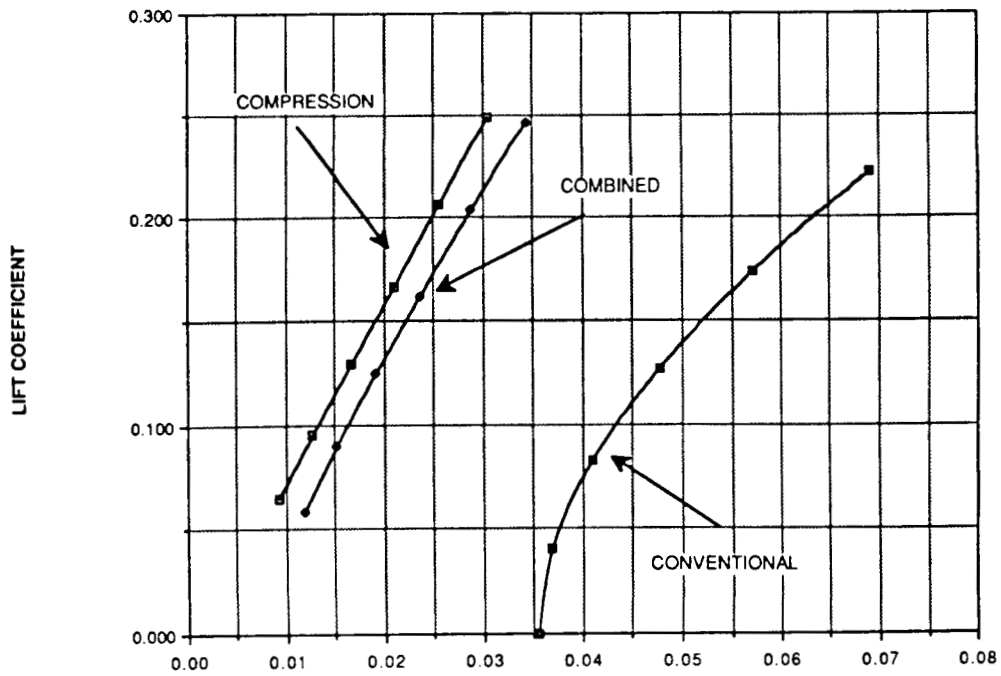
DRAG POLARS AT MACH 6

FIGURE 4.8. MACH 6.0 DRAG POLAR.

22

5 STABILITY AND CONTROL

One of the most important aspects in aircraft design is the stability and control of the aircraft. This will decided whether the aircraft is or is not qualified for certification under the guideline of the MIL-SPEC 8785C. The purpose of this section is to verify whether the aircraft is static and dynamic stable under the guideline of MIL-SPEC 8785C.

The longitudinal and lateral stability analysis for the High Speed Civilian Transport aircraft used methods presented by Roskam in Reference 11. All the notation used in this section are similar to notation used by Roskam.

5.1 SUBSONIC STABILITY

It is generally required that the aircraft has to be statically and dynamically stable. Static stability as is defined as the tendency of the aircraft to develop forces or moments to counteract an instantaneous pertubation from the steady-state flight condition (Reference 11). Reference 11 suggests that if the aircraft follows the stability criteria, it is almost safe to consider it as statically stable. The vehicle must also be dynamically stable. With the aid of "Flight Dynamics" program, the dynamic analysis was completed and results compared to MIL-SPEC 8785C level 1 criteria. Another topic of this subsection is the Waverider's ability to meet take-off rotation criteria..

5.1.1 STATIC STABILITY

Static stability criteria is defined as a rule by which steady-state flight conditions are separated into the categories of stable, unstable or neutrally stable. In order to achieve stable conditions, the following criteria must be sastified

23

(Reference 11).

As a variation of forward speed , the aircraft has to exert a force to oppose the variation. That is,

$$C_{T_{x_u}} - C_{D_u} < 0$$

Based on Table 5.1 , this expression is sastified. Therefore , this aircraft is statically stable in forward speed disturbance.

As side speed varied, the aircraft has to exert a force to return the aircraft to steady state (static). That is,

$$C_{y_\beta} < 0 \quad .$$

Based on Table 5.2, this expression is sastified. Therefore, the aircraft is statically stable in side speed disturbance.

Once the aircraft experienced a vertical speed disturbance, it will generate a force which tends to return itself back to the steady state. Based on table 5.1, the following expression is sastified

$$C_{l_a} > 0 \quad .$$

Therefore, it is safe to say that this aircraft is statically stable in vertical speed. This characteristic is generally true except in case of stalling.

As a result of an angle of sideslip disturbance, the aircraft weathercocks into the new relative wind. To have this characteristics, the following expression has to be sastified,

$$C_{n_\beta} > 0 \quad .$$

A look at the Table 5.2 will show that this expression is indeed sastified.

As the aircraft experience a disturbance in angle-of-attack, it will weathercocks into the relative new wind. This is desirable that the aircraft returns to its trim angle-of-attack once disturbed away from it. To sastify this criterion, the following expression applies

$$C_{m_a} < 0.$$

From Table 5.1 , this criterion is sastified.

The aircraft generates moments to counteract the increase in roll. Which implies that the following expression must be sastified,

$$C_{l_p} < 0.$$

With the value in Table 5.2, this expression is sastified implying that the aircraft is statically stable in roll rate.

As the aircraft pitches, there is an internal moment which tends to oppose the increase in pitching velocity. This internal moment is generated if the aircraft has the following characteristic

$$C_{m_q} < 0.$$

A look at the Table 5.1 will show that the aircraft indeed has this characteristic.

An internal moment is generated when the aircraft increase its yawing velocity which opposes any further increase in yawing velocity. To have this internal moment generated, the aircraft has to have the following criterion

$$C_{n_r} < 0.$$

From Table 5.2 , this criterion is sastified. A moment is generated every there is an increase in yawing velocity.

One characteristic that ensures the steady speed is: as the aircraft increases in forward speed, the aircraft pitches up and tends to have additional drags which will decrease its speed. The following criterion is required to have this characteristic,

$$C_{m_u} > 0.$$

From Table 5.2 this aircraft indeed has the above characteristic.

The following expression is need to have lateral stability. That is,

25

$$C_{l_\beta} < 0 .$$

With the value in Table 5.2, this aircraft do have lateral stability.

5.1.2 DYNAMIC STABILITY

The dynamic stability was analyzed about both the longitudinal and lateral axes. The results of the longitudinal analysis are presented in Table 5.3. Even though the short period frequency is within the stable region, it seems that this short period frequency is too small. Therefore , stability augmentation system is suggested to be installed. The results of the lateral analysis are presented in Table 5.4. All requirements of the MIL-SPEC 8785C level 1 are sastified except the product of Dutch roll frequency and damping ratio. Therefore, stability augmentation system is definitely required for this aircraft to sastify the MIL-SPEC.

5.1.3 TAKE-OFF ROTATION

It is generally required that the aircraft could rotate and take off at low take-off speed and maximum gross weight. Summing the moment at the main landing gear contact point at the instant of take-off rotation, the following equation is derived (Reference 11),

$$C_{m_{ac_{WB}}} \bar{q}_{T.O.R} \, S \, \bar{c} \; - T(Z_{mg} - Z_T) \; - W(X_{mg} - X_{cg}) + L_{WB}(X_{mg} - X_{ac_{WB}})$$

$$+ D(Z_{mg} - Z_D) + \frac{W}{g} \overset{\circ}{U} Z_{mg} - L_H (X_{ac_H} - X_{mg}) \geq 0$$

Replacing all characteristics of the aircraft, it could indeed rotate and lift off at take-off speed.

5.2 SUPERSONIC STABILITY

The supersonic stability and control derivatives are analyzed throughout the Mach range of the Waverider. It is expected that as the Mach number increases, moments acting on the vehicle will decrease and some potentially will be small enough to neglect.

The analysis for the Waverider involve slender body methods with an aft delta-wing configuration. There is no horizontal tail in this configuration so the methods are wing-body. This analysis is performed using two references, the Air Force DATCOM (Reference 13), and the text of University of Kansas Professor, Jan Roskam (Reference 11). It should be mentioned that some methods are not available for supersonic/hypersonic conditions.

Throughout the calculations, many variables and charts require constants which are functions of vehicle geometry such as Aspect Ratio, wing span, wing station sweep angles, and others. Once these constants are determined, equations for stability derivatives supplied by DATCOM are reduced to the basic variable parameters such as Mach Number, lift curve slope, lift coefficient, and others. Several derivatives also depend upon various charts and graphs which may or may not be constant. This involves continuous dashing through the DATCOM text. However, efforts are directed to simplifying each equation as a function of the previously variable parameters.

However, the primary concern is to coment on the static and dynamic stability of the Waverider.

5.2.1 STATIC STABILITY

Tables 5.1 and 5.2 display the longitudinal stability derivatives and the

lateral stability derivatives, respectively. Static stability is defined as the 'tendency to oppose disturbances' from a steady-state flight condition. It is based on the stability derivatives applied for perturbations on steady-state components.

For speed perturbations, the Waverider exibits decreasing tendency to resist the forward increase in speed. Although C_{du} is positive or very small, the Waverider undesireably reduces the resistance to increases in velocity. The side speed disturbance is very favorable as Mach number increases. This will allow comfortable turning capability. However, at low Mach numbers the Waverider does may experience some sideslipping as is seen in a positive $C_{y\beta}$. This is due to the anhedral of 18 degrees. For $C_{L\alpha}$, the Waverider experiences an upward force with decrease in speed. This is a desirable characteristic along with a positive lift curve slope throughout the Mach range.

In weathercock stability, the criteria is that $C_{n\beta}$ is greater than zero. This criteria is satisfied throughout the Mach range so that the Waverider weathercocks into a new wind when a sideslip disturbance occurs sending the aircraft to a straight flight path. This derivative does not vary with Mach number. Because of the closeness of location of the center of gravity and aerodynamic center, the moment lift curve slope, $C_{m\alpha}$ is small, but negative. This is desirable because, again, of the ability of the Waverider to weathercock to a straight direction at an angle of attack disturbance.

For rotational stability, C_{lp}, is the tendency of the aircraft to oppose rolling moments. This handling quality parameter is the roll damping derivative and since is is negative throughout the supersonic regime, the criteria for stability is met. The pitch damping derivative, C_{mq}, is a moment opposing the pitching velocity. Its value

is also negative throughout supersonic/hypersonic Mach numbers. C_{nr} is the yaw damping derivative. This handling quality parameter controls Dutch Roll Damping. At Mach numbers greater than one, this derivative is expected to approach or become zero. However, there are no methods that exist to approximate this parameter at supersonic/hypersonic Mach numbers.

Many of the static derivatives are well within acceptable ranges except for a couple which is discussed in the following. Although the rolling handling quality mentioned earlier is favorable, the other roll-rate derivatives are not favorable. C_{yp} and C_{np} show adverse affects in pitch roll-rate and yaw roll-rate, respectively. The large leading edge sweep angle combined with high Mach numbers and the large anhedral produce rolling moments. Stability augmentation for roll is suggested.

5.2.2 DYNAMIC STABILITY

Dynamic stability is difficult to pridict due to aerolastic effects. However, this text will neglect these effects and can predict the high and low frequency short period and phugoid modes.

From Reference 11, these mode shapes are a function of pitching moment of inertia. On Figure 2.4 of this reference, this parameter is estimated for the Waverider as 10^8 slug ft^2. These shapes are also functions of other stability derivatives.

At the cruise Mach number, the high frequency short period, ω_{nsp}, is .565 rad/sec. The low frequency short period, ζ_{sp}, is .0447 rad/sec. These values are small for pitch damping and suggest stability augmentation is necessary for cruise Mach numbers.

For the high frequency phugoid mode, ω_{nph}, the value calculated is .0184 rad/sec. The low frequency phugoid mode, ζ_{ph}, is 2.137 rad/sec. The high frequency is low and unstable. However, the low frequncy phugoid is high which indicates some damping capability. From the examination of the static and dynamic stability, it is recommended that a stability augmentation system be implemented on the Waverider.

LONGITUDINAL DERIVATIVES			
Cm_u	.17	C_{L_u}	.964
Cm_α	−.19	C_{D_α}	.481
$Cm_{\dot\alpha}$	−.1	C_{D_u}	.17
Cm_q	−.485	$C_{T_{X_U}}$	0
Cm_{T_u}	0	$C_{L_{\delta_f}}$	.25
Cm_{T_α}	0	$C_{D_{\delta_f}}$	0
C_{L_u}	.052	$C_{m_{\delta_f}}$	−.75
C_{L_α}	1.704		
$C_{L_{\dot\alpha}}$	1.1		

TABLE 5.1. LONGITUDINAL SUBSONIC DERIVATIVES.

LATERAL DIRECTIONAL DERIVATIVES			
C_{l_β}	−.25	$C_{n_{\delta_R}}$	−.109
C_{l_p}	−.39	C_{y_β}	−1.07
C_{l_r}	.15	C_{y_p}	−.00861
$C_{l_{\delta_A}}$	.05	C_{y_r}	.008
$C_{l_{\delta_R}}$	.01	$C_{y_{\delta_A}}$	0
C_{n_β}	.15	$C_{y_{\delta_R}}$	.19
C_{n_p}	−.2025		
C_{n_r}	−.35		
$C_{n_{\delta_A}}$	−.005		

TABLE 5.2. LATERAL SUBSONIC DERIVATIVES.

Longitudinal

HSCT			REQUIRED				
$\omega_{n_{sp}}$	ζ_{sp}	ζ_p	$\omega_{n_{sp}}$		ζ_{sp}		ζ_p
			MIN	MAX	MIN	MAX	MIN
.8189	.509	.041	.78	3.2	.35	1.3	.04

TABLE 5.3. LONGITUDINAL DYNAMIC CHATRACTERISTICS.

Lateral

HSCT					REQUIRED				
T_s	T_r	ω_D	$\omega_D \zeta_D$	ζ_D	MIN T_s	MAX T_r	MIN ω_D	MIN $\omega_D \zeta_D$	MIN ζ_D
15.99	.936	.833	.0732	.0878	12	1.4	.4	.1	.08

TABLE 5.4. LATERAL DYNAMIC CHARACTERISTICS.

	Mach Number				
	1.5	2.0	3.0	4.0	5.5
C_{L_α}	6.031	2.309	1.414	1.033	0.817
C_{D_α}	0.256	0.071	0.030	0.018	0.002
C_{m_α}	-0.018	-0.007	-0.004	-0.003	-0.002
C_{L_u}	0.209	0.077	0.027	0.015	0.011
C_{D_u}	0.004	~0	~0	~0	~0
C_{m_u}	0.003	~0	~0	~0	~0
C_{L_q}	11.276	3.846	2.287	1.649	1.291
C_{D_q}	•	•	•	•	•
C_{m_q}	-2.472	-0.928	-0.548	-0.392	-0.279
$C_{L_{\dot\alpha}}$	-6.028	-0.768	-0.206	-0.072	0.137
$C_{D_{\dot\alpha}}$	•	•	•	•	•
$C_{m_{\dot\alpha}}$	-8.004	-0.989	-0.281	-0.115	~0

NOTE : • represents no method available

TABLE 5.5. LONGITUDINAL SUPERSONIC DERIVATIVES.

	Mach Number				
	1.5	2.0	3.0	4.0	5.5
C_{y_β}	0.016	-0.084	-0.196	-0.287	-0.356
C_{l_β}	-0.006	-0.001	~0	~0	~0
C_{n_β}	-0.014	-0.014	-0.014	-0.014	-0.014
C_{y_p}	-2.000	-1.400	-0.800	-0.500	-0.300
C_{l_p}	-0.370	-0.286	-0.203	-0.137	-0.081
C_{n_p}	0.768	0.505	0.422	0.356	0.300
C_{y_r}	•	•	•	•	•
C_{l_r}	•	•	•	•	•
C_{n_r}	•	•	•	•	•

NOTE : • represents no method available

TABLE 5.6. LATERAL SUBSONIC DERIVATIVES.

33

I ongitudinal

HSCT			REQUIRED				
$\omega_{n_{sp}}$	ζ_{sp}	ζ_p	$\omega_{n_{sp}}$		ζ_{sp}		ζ_p
			MIN	MAX	MIN	MAX	MIN
.565	.0447	2.137	.78	3.2	.35	1.3	.04

TABLE 5.7. LONGITUDINAL DYNAMIC CHARACTERISTICS.

6 PROPULSION SYSTEM

The propulsion system for the Waverider is, again, one of the more major tasks. The primary obstacle is to analyze and choose a system that operates efficiently within the Mach 3-6 range from altitudes at sea level to 100,000 feet. The system familiar within this range, the ramjet, is, as most realize, not efficient at subsonic and high Mach numbers. Therefore, the challenge is to determine a system that provides adequate thrust, efficient operation (minimize fuel), and is not a complicated system (minimize weight).

To operate within the mission profile, the engine is the primary concern. Surprisingly, however, the concept for hypersonic propulsion is not a recent development. One of the engines that is discussed was designed and a small model produced by Aerojet in 1955. This is the Air-Turbo Ramjet which is discussed later. Recently, a hybrid turbojet-ramjet similar to the SR-71's General Electric J-58 motors has been proposed as a capable hypersonic transport propulsion system. This is the Wraparound-Turbo Ramjet which is also considered in this project and is discussed in detail later.

For the propulsion system, five tasks are to be completed. First, is the type of fuel to be used. Because of the size of the vehicle, an inherent amount of fuel is necessary and many factors determine its choice. Next, an inlet must be developed that meets sizing criteria and adequately recovers total pressure. Third, and as mentioned previously, most important, the engine analysis is performed. Fourth, an efficient nozzle is designed to minimize losses for mass exiting the system. And finally an integration of each component of the system is achieved and a program is written to produce data for analysis.

6.1 FUEL CONSIDERATIONS

One of the more important parameters of the hypersonic commercial transport is weight. And much of this contribution concerns the volume of fuel required for the trip. Therefore, a major requirement is to determine a fuel that provides sufficient energy extraction and a high density so that the volume of fuel is kept at a minimum. Also, since active cooling is necessary due to the high operating temperatures of the engine, a sufficient heat sink capability is required. Through these constraints, three fuels have been chosen for analysis: 1). JP-7 , 2). Methane, and 3). Hydrogen. For the discussion of these fuels it is necessary to refer to the data for fuel heat of combustion, fuel heat sink capacity, and fuel density in Figure 6.1 (Reference 14).

6.1.1 JP-7

The aerospace industry is familiar with the JP fuels in use today. JP-4 is the most common fuel for the turbojet/turbofans in operation. However, do the JP fuels provide the necessary heating rates to provide adequate thrust? A recent derivative of JP-4 is JP-7. This is a high temperature fuel base on JP-4. The attractive aspect of this fuel is that there is little need to drastically change or reconstruct the fueling systems existing today. Another attractive parameter is its density. Its density exceeds many other fuels, therefore requiring less weight. It has an adequate heating rate to provide sufficient thrust, but the engine size to provide this may be too large. Also, the heat sinking capacity is still far from promising for the Waverider. This fuel may not provide requirements for the mission profile.

6.1.2 METHANE

Methane, or Liquid Natural Gas, is similar in some ways to JP-7. It has a heat of combustion similar to the JP fuels and, although less dense than JP-7, it volume requirement is several times less than hydrogen. It has many advantages in that the heat sink capacity is over five times that over JP fuels. Also, the heating rate is somewhat greater than that of JP fuels providing greater impulse. An attractive aspect of Methane is that production is plentiful and conversion of existing production plants is certainly feasible and financially sound. Its disadvantages are that the fuel is a cryogenic and storage may present a problem due to the low temperatures required for storage. But, if material limits permit, methane may be burned up to 7000 degrees Rankine.

6.1.3 HYDROGEN

For thrust requirements of the Waverider and heat sink capability, hydrogen is certainly a most attractive fuel. However, hydrogen has several major disadvantages. Like methane, hydrogen is a cryogenic and requires extensive systems design and insulation for this low temperature fuel. The heating rate is quite low for hydrogen therefore providing a low specific impulse which would require more fuel constraints. Adding to the fuel constraint is the very low density of hydrogen. Therefore, because of the previous two constraints, a much larger volume of hydrogen is necessary. Also, production of hydrogen is scarce and a special production line is required.

6.1.4 COMPARISON

A review of the parameters involved illustrates that Methane is the

37

appropriate choice of fuel for the Waverider. This choice is based on two parameters. One, is the physical characteristics provided in the previous three sections. The second is the cost parameter. Again, a review of the physical attributes are in order.

Hydrogen presents the most attractive qualities in the areas of heat sink and heat of combustion. The inherent active cooling capabilities are desirable for the Waverider. However, the small density and small heating rate do not meet the fuel volume criteria. The weight of the Waverider would exceed practical operation. Plus, manufacture of hydrogen as a fuel is scarce and the production system would be an added burden. Therefore, hydrogen is eliminated as the primary fuel source. However, hydrogen is used as a secondary fuel source for the Air-Turbo Ramjet. This application and its motivations are detailed later. Between Methane and JP-7, Methane again is most attractive in all physical aspects except density. A small weight penalty is seen since it is less dense than JP-7, but certainly a significant advantage over hydrogen. However, heat sink capacity is non-existent in JP fuels at hight Mach numbers. It would be necessary to involve additional active cooling systems for a JP based engine.

In the area of financial parameters, a cost trade analysis is performed. A cost trade on fuels for a fixed return on investment for a hypersonic transport is estimated. The surcharges show hydrogen fuels incur six times the amount than JP-7 and Methane. Also, since Methane production methods and facilities exist today, construction and production costs are minimal.

Because of the physical and financial data, Methane is certainly the logical choice of the primary fuel source for the Waverider.

6.2 INLET DESIGN

Of major concern in inlet design is to adequately provide pressure recovery entering the compressor face. Military specification MIL-E-5008B requires the following ram recovery for supersonic flight (Reference 15):

$$\eta_{spec} = 1 - 0.075(M_o - 1)^{1.35}$$

At the cruise Mach number, the pressure recovery specification is 42.9%. At the high Mach numbers required in the mission profile, total pressure recovery in the range of 50%-60% is certainly a great accomplishment. Any higher recovery would entail an inlet in excess of one hundred feet! Of course, this is not practical so a shock system must be developed to provide sufficient recovery in a short amount of length. This shock arrangement, or number of internal/external shocks, will determine the presure recovery and length of the inlet. Another constraint is that the inlet must provide adequate mass flow to supply the engine with the proper thrust requirements. Therefore, height and width of the inlet is another consideration. The first task though is to consider what Mach number is seen just outside the capture area. In other words, does the nose of the Waverider provide an initial shock.

6.2.1 NOSE SHOCK

Because the inlets are located on the lowere fuselage, the freestream flow first encounters compression and expansion at the nose. First, the flow is compressed at the nose. Although the nose is an ojive, a wedge analysis is used to calculate the Mach number along the surface since the ojive is sliced to an edge on the lower surface. The half-angle of the cone is ten degrees. At this parameter the shock angle at the cruise Mach number of 5.5 is 18.5 degrees. The Mach number along the

surface behind the compression shock is 4.257. Next, a Mach number is calculated behind the expansion shock using Prandtl-Meyer expansion theory (Reference 16). After expansion, the Mach number seen at the inlet is 5.224.

6.2.2 SHOCK SYSTEM

Initially, the inlet is designed at cruise without considering the shock produced by the nose. Although incorrect, this enabled a more efficient system to be developed: one that reduces length of the inlet with efficient pressure recovery. Originally, a two internal shock system was developed and employed, but the length of the inlet for this configuration was approximately sixty feet. The Waverider could not sustain this added weight. Now, a mixed compression inlet is developed that installs two external compression and one internal compression shock. The external compression is located at the upper lip and lower cowl of the inlet. The internal compression is located along the upper ramp. A normal shock is also included. This system reduces the length of the inlet to 43.0 feet. Figure 6.2 illustrates this inlet which have several geometric quantities to elaborate on.

Because of the amount of machinery required for variable geometry, the upper ramp surface is fixed. The inlet's upper ramp is a fixed ramp for 10.0 feet at a ramp angle of 8.0 degrees. This ramp is designed at angle for cruise conditions, which, for the Waverider, the Mach number is 5.5. As is seen, the lower half of the upper ramp is variable as well as the lower cowl. The shock and ramp arrangement is dependent on geometry in which the shocks are designed to be "swallowed" at Mach numbers of 0.1 above design to offset any disturbances during flight. Designing shocks to be captured at the design Mach number may allow inlet stalling to occur in the event of repeated disturbances (Reference 17).

6.2.3 MASS FLOW

The final requirement in inlet design is to allow enough area to adequately capture the appropriate streamtube for the massflow requirements to the engine. First, a general massflow value is obtained for thrust requirements. Considering atmospheric conditions, an estimation of the capture area is obtained. Appropriately rounding for greater thrust requirements, a 56 sqare foot area is required, or, again, as Figure 6.2 illustrates, an 8.0 foot high, 7.0 foot wide inlet is required. Any excess mass detected during actual operation is appropriately bypassed.

6.2.4 RAM DRAG

At supersonic Mach numbers there is a pressure force that must be considered. This force is the ram drag which is the force required to compress the flow from a large streamtube to a smaller area. This force can be estimated in many forms, but the one in use for this project is:

$$F_{ram} = P_o A_c \gamma M^2$$

(Reference 17)

6.2.5 RESULTS

Figure 6.3 illustrates the inlet pressure recovery. In this figure, the military specification is plotted versus Mach number. With a program written in FORTRAN, the actual pressure recovery is also plotted. As is seen, the actual pressure recovery is less than the MIL specification. For the cruise Mach number

41

of 5.5, only 34.0% of the total pressure is recovered. Further research indicates that the variable geometry ramps are less dependent on geometric capture. Rather, equalizing the normal Mach number value in the oblique shock relations tends to maximize pressure recovery (Reference 17). For future studies, this information will be transmitted and the computer algorithm adjusted to meet this requirement.

6.3 ENGINE ANALYSIS

As previously mentioned in the introductory section, two engine configurations are analyzed: the Air-Turbo Ramjet and the Wraparound-Turbo Ramjet. The Air-Turbo Ramjet has had prior research and development. In 1955, Aerojet developed a 26" engine and was tested for high Mach number simulations (Reference 18). The Lewis Research Center has conducted parametric studies on this engine. The Wraparound-Turbo Ramjet is more of a recent idea, although its concept is based on the J-58 engine which is on the SR-71. The engine analyses attempt to accompany today's technology limits. More detail is now presented for each engine.

6.3.1 AIR-TURBO RAMJET

The Air-Turbo Ramjet (ATR), illustrated in Figure 6.4, uses a gas generator that burns a liquid fuel and oxidizer. This "rocket" exhausts through the turbine which drives the compressor. Because of this independent cycle, a smaller compressor is necessary and much of the turbomachinery is smaller, thereby producing a higher thrust to weight ratio (Reference 19). However, because of the useage of hydrogen, a specific impulse penalty is seen and the contribution to thrust by the core is essentially non-existent. Because of the use of hydrogen, the

possibility of a weight penalty comes to attention. However, the core fuel of hydrogen may be advantageous because of the extra heat sink capability for active cooling.

6.3.2 WRAPAROUND-TURBO RAMJET

The Wraparound-Turbo Ramjet (WTR) is an attempt to make more efficient use of the ramjet operation in an ordinary afterburning, low-bypass, turbojet. At low Mach numbers the turbojet allows proper acceleration to higher Mach operation. The core flow is then closed off. With todays present afterburning engines, the aft burners are too small to allow efficient operation. Therefore, by placing burners in the bypass flow, the efficiency improvement of ramjet operation is very attractive. This engine is illustrated in Figure 6.5. However, the disadvantages are the bypass ducts are subjected to high pressures and temperatures (Reference 19). The active cooling system may require extensive routing throughout this engine for an added weight penalty. Plus, with the number of Methane fuel burning locations, an additional fuel penalty counters the fuel burning efficiency.

6.3.3 CYCLE ANALYSIS

A cycle analysis is done on each engine. The control volume for each is the outside surface of each motor. A vector analysis of the pressure forces determines that the upper and lower surface quantities cancel and the only components remaining are the pressure forces entering and exiting the engines. This method is used on both engines. Since these engines are not in production, cycle equations are developed for both engines for specific thrust and specific impulse. Also, pressures

43

and temperature are calculated at each station so that a cycle is presented in the form of a temperature versus entropy diagram. These diagrams are presented in Figure 6.6. The ATR, as expected, recieves most of the contribution from the bypass and little from the core. Since the engine could not make the thrust requirements, material limits were increased to potential future levels. The total temperature at the afterburner (station 6) is 6000 degrees Rankine and the total turbine temperature (station 4) is 4000 degrees Rankine. Since the cycle for the core and the bypass are independent, two specific thrust equations are derived. The equation for specific thrust for the rocket and bypass, respectively are as follows:

$$\frac{F}{m_4 a_4} = M_4 \left[\sqrt{ \frac{\theta_{ar}}{\theta_4 - 1} \left[1 - \frac{(P_o / P_7)^{\frac{\gamma - 1}{\gamma}}}{\theta_4 - \frac{m_o C_{po}}{C_{p4}} \left[\frac{T_o \theta_o}{T_4} (\tau_c - 1) \right]} \right] } - 1 \right]$$

$$\frac{F}{m_o a_o} = M_o \left[\sqrt{ \theta_{ab} \left(\frac{\theta_o \tau_c - 1}{\theta_o - 1} \right) } - 1 \right]$$

Also, the equation for specific impulse is:

$$I = \frac{F}{g \, m_f} = \frac{F \, h}{g \, m_o C_{po} T_o (\theta_{ab} - \theta_o)}$$

The WTR, as expected recieves most of the contribution from the augmented ramjet operation. Station 3a illustrates the added contribution, and there is more contribution from the core stations than from the ATR. As in the ATR,

future material technical increases were used. Again, this motor has little publication, and cycle equations had to be derived. The equation for specific thrust is:

$$\frac{F}{m_o\,a_o} = M_o\,(1 + \alpha)\,[\ \sqrt{\frac{\theta_a}{\theta_o\,\tau_f}\,(\frac{\theta_o\,\tau_f^2 - 1}{\theta_o - 1})}\ -\ 1\ ]$$

And for specific impulse:

$$I = \frac{F}{g\,m_f} = \frac{F\,h}{g\,m_o\,(1 + \alpha)\,C_{po}\,T_o\,(\theta_a - \theta_o)}$$

For results of the cycle, a program is written in FORTRAN to generate appropriate data.

6.3.4 ENGINE CHOICE

The choice of engine is a very difficult one. There are many compromising factors to consider. Both systems require cooling and insulation systems for the reduced temperature requirements. For efficient operation, the WTR wins outright. Again, though, it is necessary to be reminded that through efficient operation, the added burner locations add a fuel burden. With this added burden, the systems operations added a tremendous weight penalty. The ATR provided the thrust necessary for the requirements of the Waverider. The reduced weight due to the smaller compressor and reduced systems made this engine system more attractive. Plus, the hydrogen provides the necessary cooling at burner and nozzle locations for engine operation. Therefore, the choice for the Waverider engine is the ATR.

6.4 NOZZLE ANALYSIS

In the area of nozzle configurations, three nozzle types are investigated (Reference 15). They are described below:

Simple Converging Nozzle: Good performance at subsonic cruise and quick accelerations to high speeds. However, inefficient at supersonic cruise.

Fixed Geometry Convergent/   Unstable in under-expanded conditions, and poor
Divergent Nozzle: off-design performance.

Variable Geometry Convergent/ Excellent off-design performance, but complex
Divergent Nozzle: machinery is added weight penalty.

Since a large range of supersonic/hypersonic Mach numbers are required, a large range of throat/exit area ratios is expected. Off-design performance efficiency is a premium. Therefore, the variable geometry, two-dimensional convergent/divergent nozzle (2D-CD) is selected. The weight penalty is overcome by minimization of interference penalties and the bonus of integration with aft fuselage for better expansion. This nozzle is not in use with today's aircraft, but significant research has been performed and a full working model developed with favorable results. An illustration of subsonic, sonic, and supersonic configurations of the 2D-CD nozzle are shown in Figure 6.7.

6.4.1 NOZZLE GEOMETRY

The nozzle geometry was determined from a parametric analyses of

46

performance and weight. Of course, a large area ratio is desired, but weight penalties exist for values above 4.0 (Reference 15). From seperate analysis of primary nozzle half-angle and secondary nozzle half-angle on thrust coefficient and nozzle length reveal a final nozzle configuration in Figure 6.8.

6.4.2 NOZZLE PERFORMANCE

Performance of the nozzle is a function of friction losses, expansion, leakage, flow angularity, cooling air throttling, and off-design performance. The losses for leakage and cooling air can be estimated assuming no losses through the seals of moving parts (Reference 20). It is given as:

$$\Delta C_{fg} = 0.01$$

Under expansion occurs throughout the cruise profile. Aft fuselage expansion (afterbody expansion) is neccessary. The upper portion of the nozzle sees small losses due to afterbody assistance. However, the lower portion of the nozzle incur larger portion of losses because of the non-augmented length. This off-design performance is given as (Reference 15) :

$$C_{fg} = \frac{C_v \, C_a \, m_e \, V_1 / g_c + (P_1 - P_o) A_e}{m_e \, V_e / g_c} - \Delta C_{fg}$$

The thrust coefficient for the cruise Mach number of 5.5 is 0.942. This value is included in the FORTRAN program to account for the loss in thrust from the nozzle.

47

6.4.3 THRUST VECTORING

Since the Waverider touchdown speed is approximately 153 feet per second, the need for thrust vectoring is essential to ensure safe landing on commercial runways. Along with this convenience, thrust reversers also supplement the braking system. Figure 6.9 illustrates two types of thrust reversers, the cascade reverser and the clam shell reverser. For reduction of machinery and, therefore, weight, the clam shell reversers are employed for the Waverider (Reference 15).

6.4.4 NOZZLE COOLING

Since the afterburner is operation at a total temperature of 6000 degrees Rankine, the mass exiting the burner cannot run along the fuselage afterbody. Some bypass control of atmospheric air along cold fuel locations must be injected along the nozzle flow. Cooling is attained by approximately injecting 8% of the exit flow. The afterbody is actively cooled for the locations subjected to the nozzle exhaust.

6.5 DESIGN INTEGRATION

With the design of the components complete, the final step is to integrate each component to the FORTRAN program. Since each step has been completed seperately, the process of coding the entire system should be straight-forward. To view the entire propulsion system integration, refer to Figure 6.10.

6.5.1 PROPULSION ALGORITHIM

48

The program simulates actual flight conditions, varying Mach number and altitudes. The algorithm is as follows:

1). Read Input Conditions
2). Calculate Atmospheric Conditions
3). Calculate Inlet Conditions Supplying Compressor
4). Calculate Core Specific Thrust and Specific Impulse
5). Calculate Bypass Specific Thrust and Specific Impulse
6). Calculate Gross Thrust
7). Include Nozzle Losses
8). Determine Ram Drag
9). Determine Total Net Thrust
10). Output Information

For a sample program output, refer to Figure 6.11. The output reveals flight conditions, inlet conditions (shock data, compressor conditions), engine gross thrust, ram drag, net thrust, specific impulse, and specific fuel consumption. The execution of the program involved flight conditions of Mach number from zero to six at increments of 0.5 and altitudes from sea level to 100,000 feet at increments of 5,000 feet.

6.5.2 RESULTS

The program results for a six foot diameter compressor and engine are distributed. Figure 6.12 illustrates thrust versus Mach number at altitude increments of 20,000 feet. As is seen, there is sufficient thrust to meet the takeoff requirements and cruise requirements of the Waverider. However, it is noted that at high Mach numbers and lower altitudes, the ram drag overcomes any thrust

49

contributions. At higher altitudes, the static pressure is very small and the ram drag contribution is appropriately less. Figure 6.13 illustrates the specific fuel consumption versus Mach number at 20,000 foot increments of altitude. As mentioned earlier in Section 6.3.1, this engine does have an impulse penalty. However, the present rate of future technology may reduce this penalty by an estimated 25%. As is seen by the figure, with increase in altitude, the fuel consumption expectedly decreases.

The six foot diameter, again is sufficient for the Waverider thrust requirements at all conditions. However, if future sizing is necessary, a relationship exists for this. Since massflow is proportional to thrust and massflow is proportional to the square of the diameter, the following relationship is used for sizing of the engine (Reference 21):

$$D_{reqd} = \sqrt{\frac{D_1^2 T_{reqd}}{T_1}}$$

Therefore, the propulsion system is capable of meeting Waverider RFP requirements.

HEAT OF COMBUSTION

BTU / LB

JP-7 ▨ 18500.0

METHANE ▨ 21460.0

HYDROGEN ▨ 51600.0

0 10 20 30 40 50 60 (X 1000)
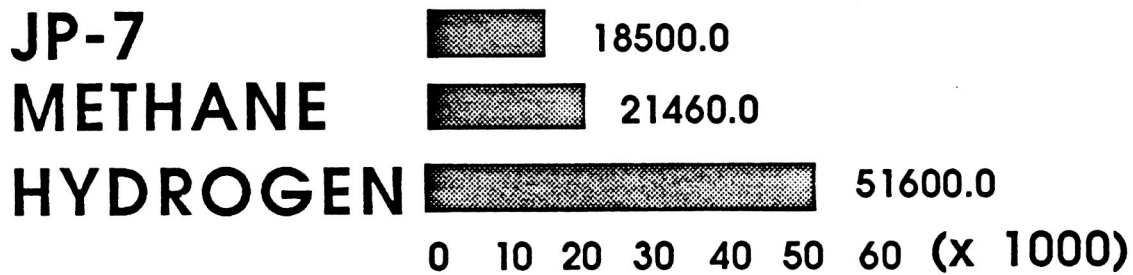
HEAT SINK CAPACITY

BTU / LBM

JP-7 ▨ 269.0

METHANE ▨ 1350.0

HYDROGEN ▨ 6700.0

0 1000 2000 3000 4000 5000 6000 7000

DENSITY

LB / CU. FT.

JP-7 ▨ 48.0

METHANE ▨ 28.0

HYDROGEN ▨ 4.7

0 10 20 30 40 50
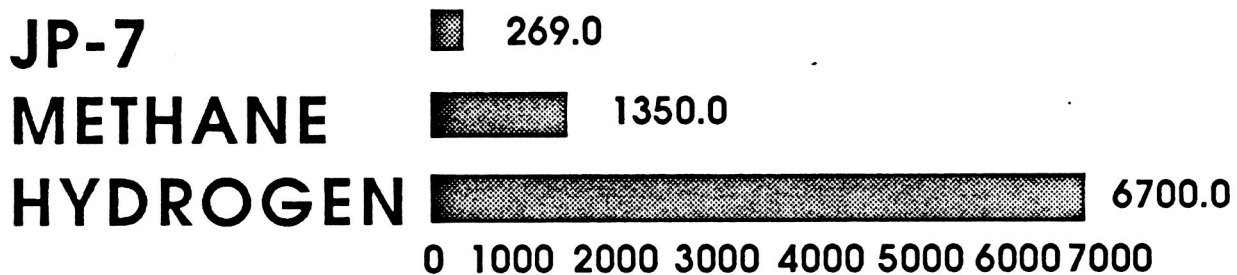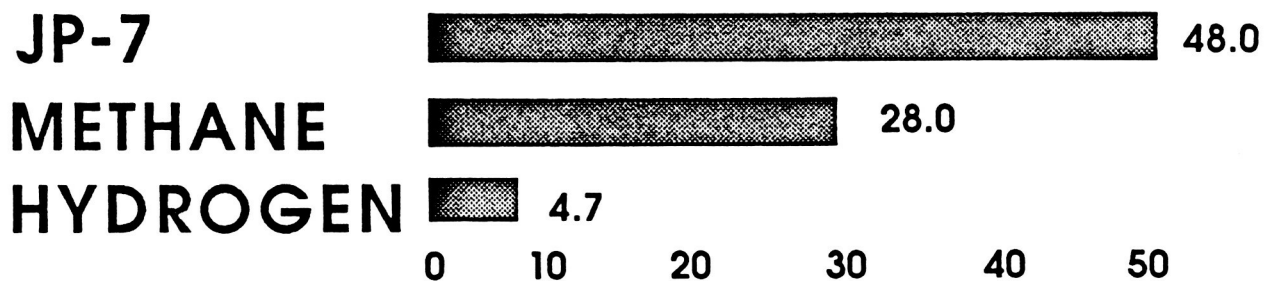
Figure 6.1 -- Fuel Characteristics

51
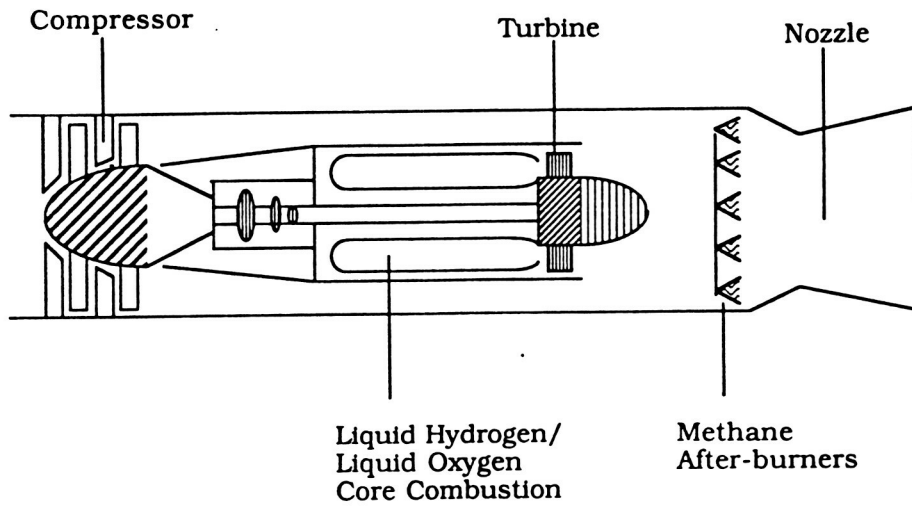
Figure 6.4 -- Schematic of the Air-Turbo Ramjet
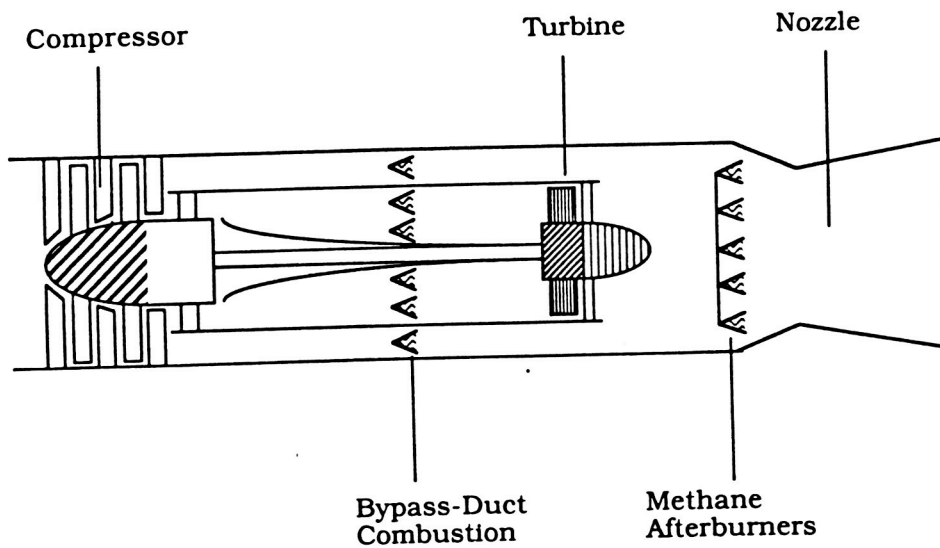
Figure 6.5 -- Schematic of the Wraparound-Turbo Ramjet
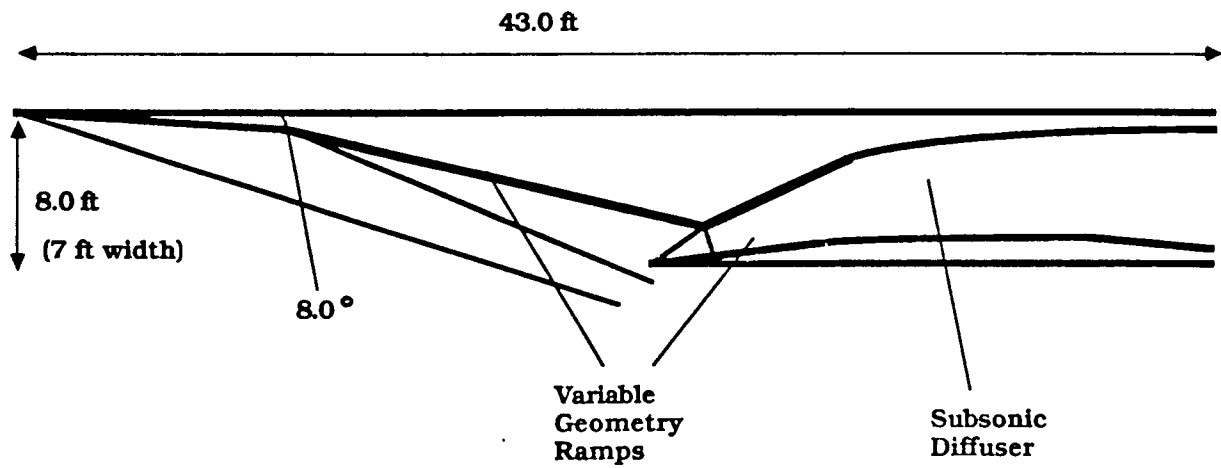
Figure 6.2 -- Mixed Compression Inlet for the Waverider

Figure 6.3 -- Mixed Compression Inlet Pressure Recovery

Mach Number

52
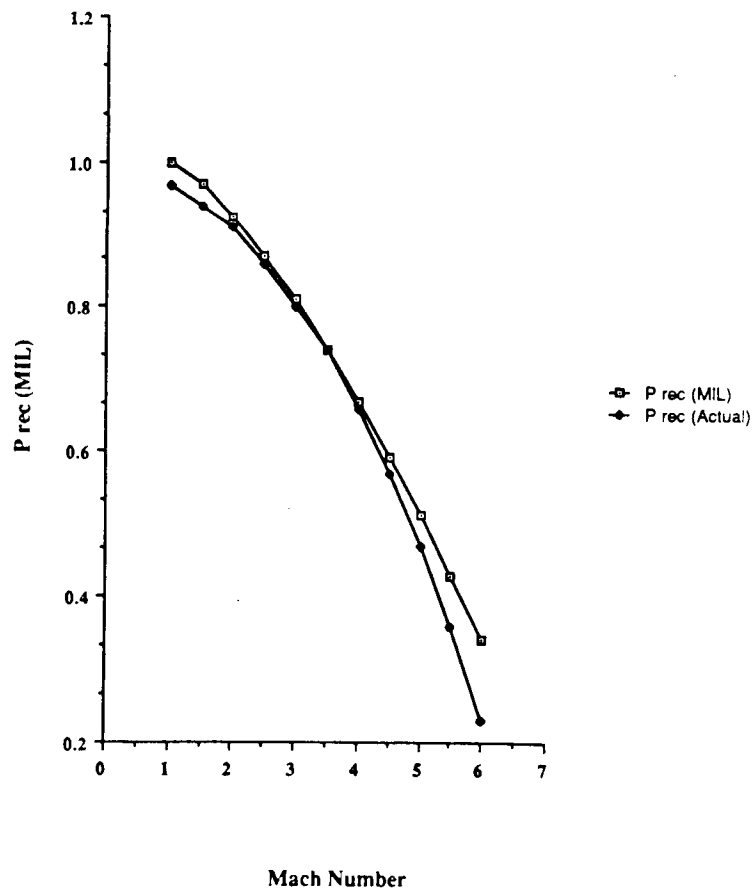
AIR TURBO-RAMJET CYCLE
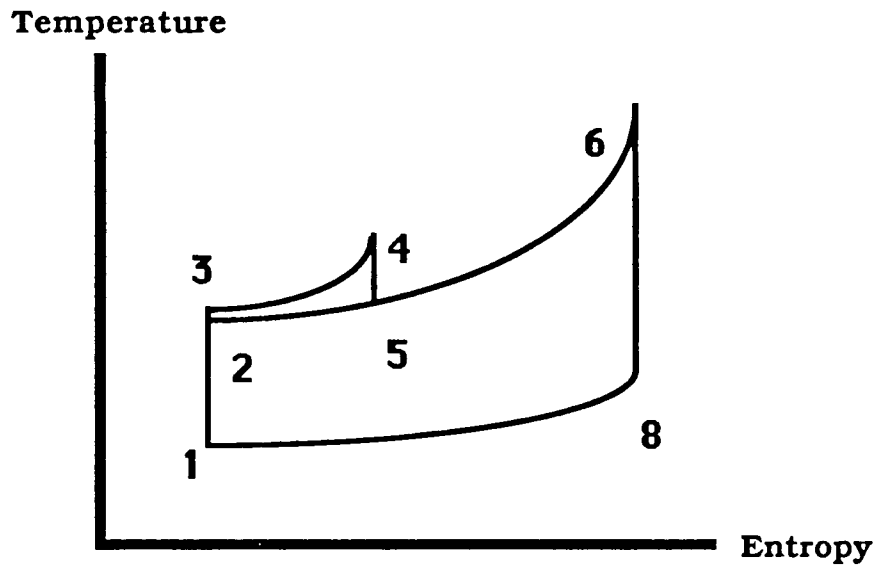
WRAPAROUND CYCLE
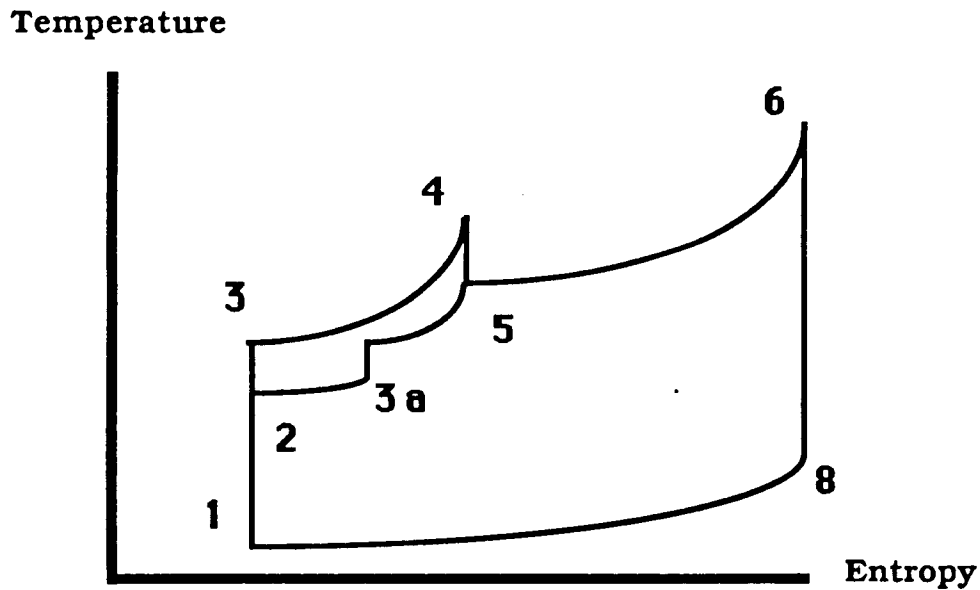
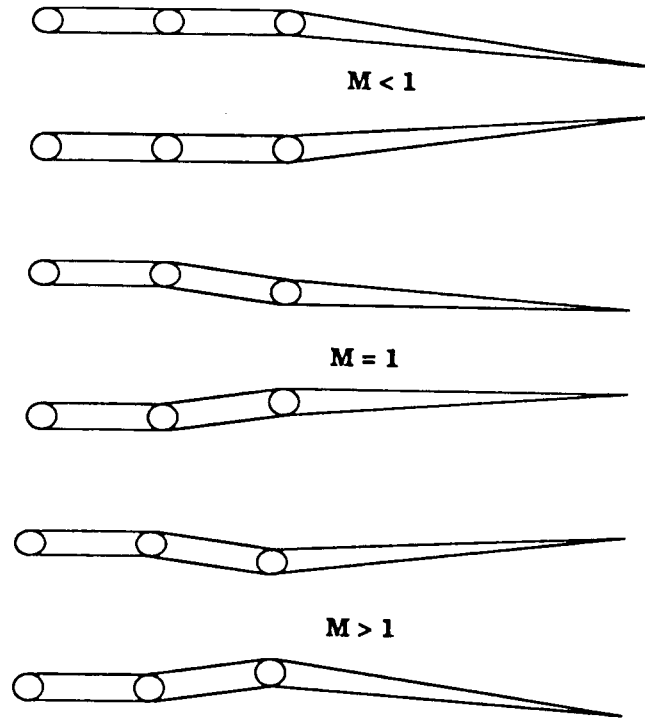Figure 6.6 -- Cycle Diagrams for Engine Analysis

54

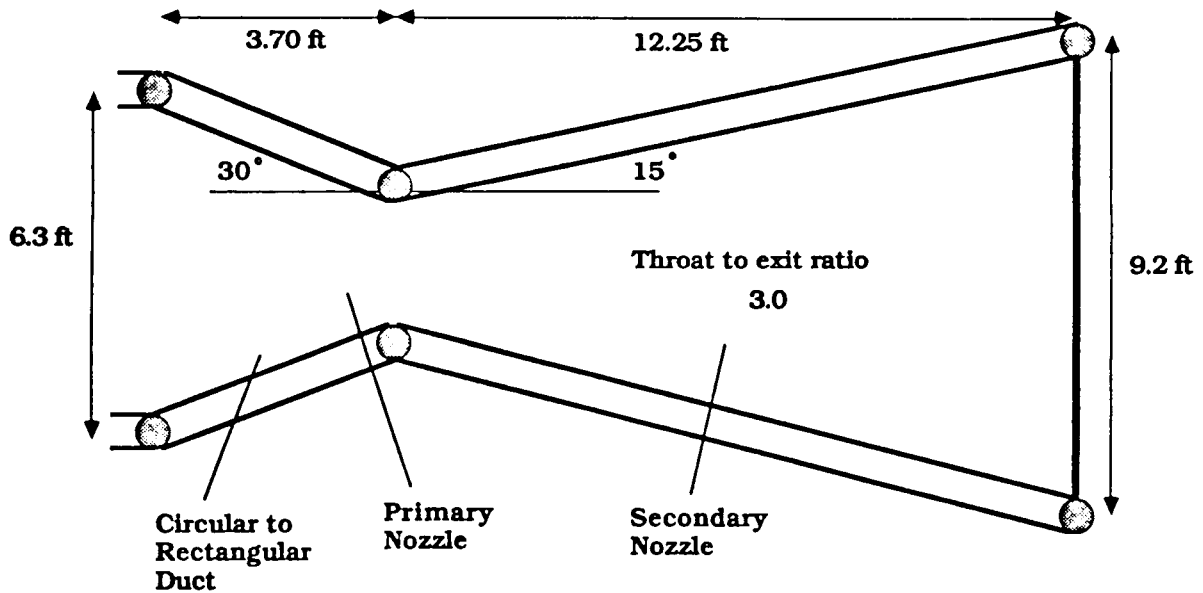**Figure 6.7 -- Variable Geometry Nozzle Configurations**
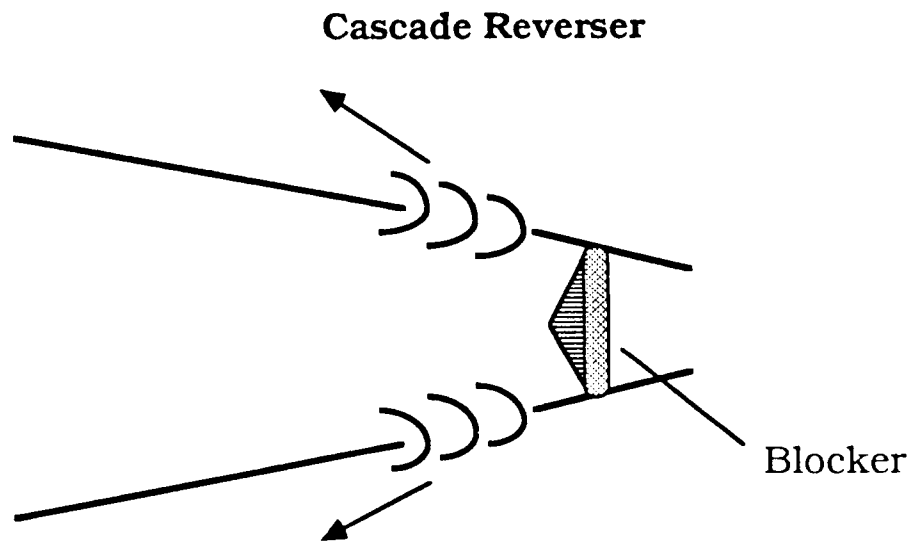

Figure 6.8 -- Cruise Mach Number Nozzle Geometry

55

Clam Shell Reverser

Deployed
Clam Shell

Cascade Reverser

Blocker
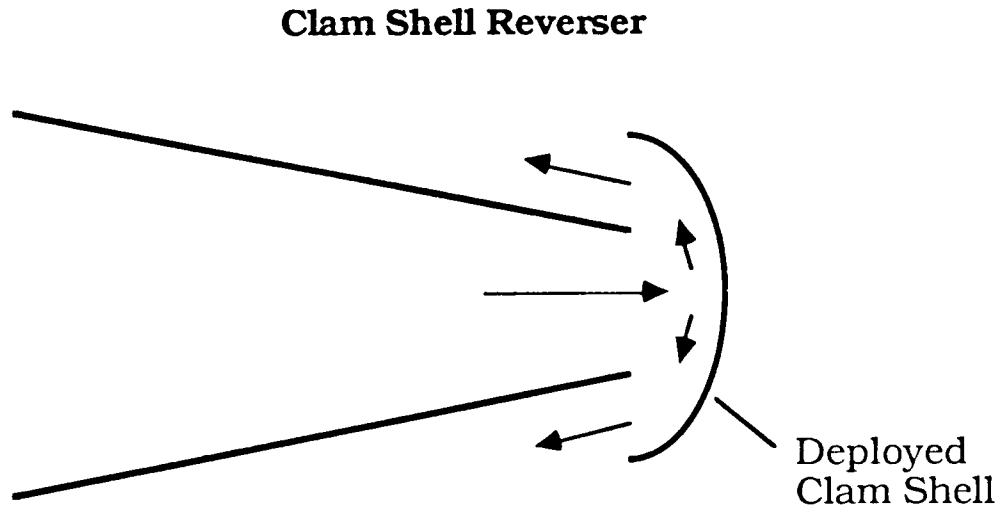
Figure 6.9 -- Thrust Reversing Systems

Fuselage

Afterbody

Nozzle

Engine

Landing Gear
Storage

Inlet
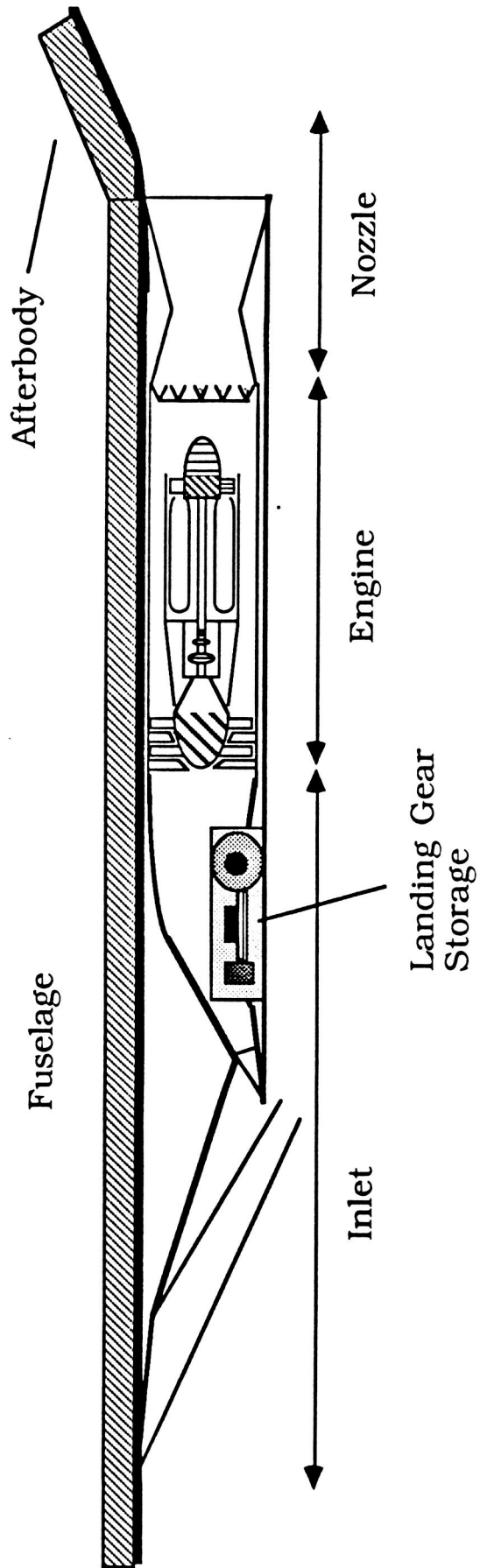
Figure 6.10 -- Propulsion Component Integration

Analysis at altitude (ft)	:	100000.00
Freestream Mach number	:	5.00
First shock angle (deg)	:	18.51
Upper ramp angle (deg)	:	8.00
Second shock angle (deg)	:	30.27
Second ramp angle (deg)	:	16.35
Third shock angle (deg)	:	54.21
Lower ramp angle (deg)	:	19.24
Capture area (sq ft)	:	56.00
Area at normal shock	:	8.34
Mach number exiting normal shock	:	0.58
Compressor face Mach number	:	0.40
Compressor face pressure (psf)	:	4425.17
Compressor face temperature ('R)	:	2345.00
Compressor face density (slug)	:	0.00110
Compressor face total pressure (psf)	:	4972.04
Compressor face total temperature	:	2744.47
Compressor face total density	:	0.00118
Total inlet length (ft)	:	43.00
Inlet height (ft)	:	8.00
Inlet width (ft)	:	7.00
Longitudinal cowl length (ft)	:	23.00
Subsonic diffuser length (ft)	:	15.00
Freestream mass flow (slug/sec)	:	10.68
Burner total pressure (psf)	:	4524.56
Burner total temperature ('R)	:	6000.00
Total gross thrust (lbf)	:	121277.38
Total ram drag (lbf)	:	53638.84
Total net thrust (lbf)	:	67638.54
Specific impulse (sec)	:	2845.79
Specific fuel consumption (1/hour)	:	1.40

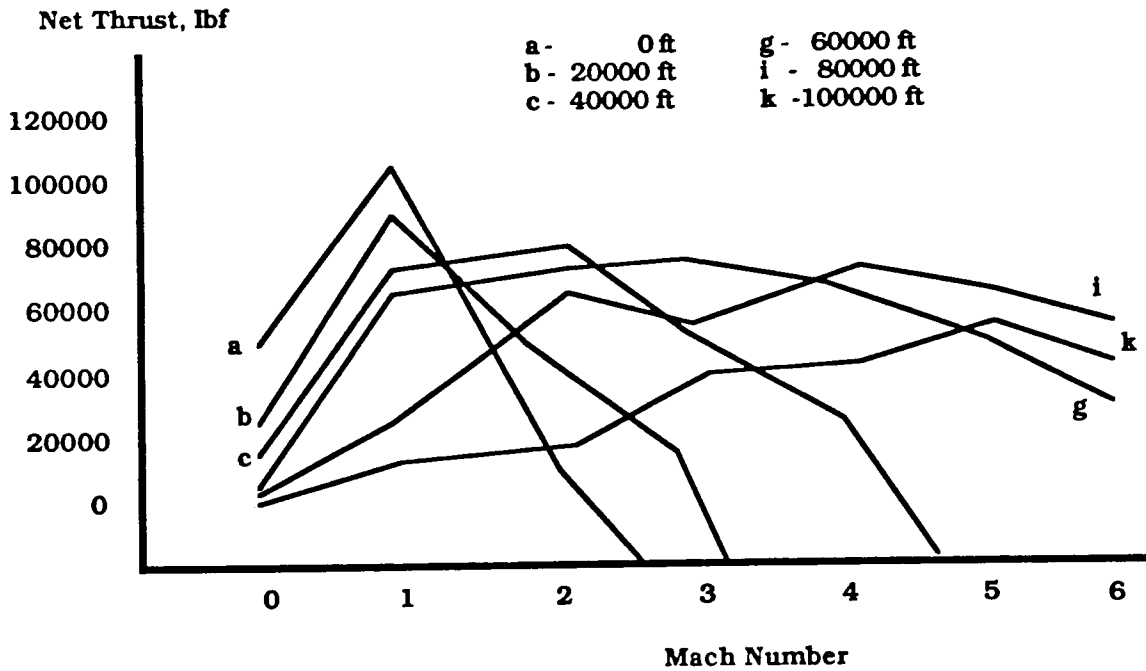# Figure 6.11 -- Output of Propulsion Integration

Net Thrust, lbf

a -   0 ft   g - 60000 ft
b - 20000 ft   i -   80000 ft
c - 40000 ft   k -100000 ft

120000

100000

80000

60000

40000

20000

0

a

b

c

i

k

g

0   1   2   3   4   5   6

Mach Number

Figure 6.12 -- Thrust versus Mach Number at Various Altitudes

Specific Fuel Consumption

lb / hr

a -   0 ft   d - 60000 ft
b - 20000 ft   e -   80000 ft
c - 40000 ft   f - 100000 ft

3.5

3.0

2.5

2.0

1.5

1.0

0.5

a

b

c

d

e

f

0   1   2   3   4   5   6
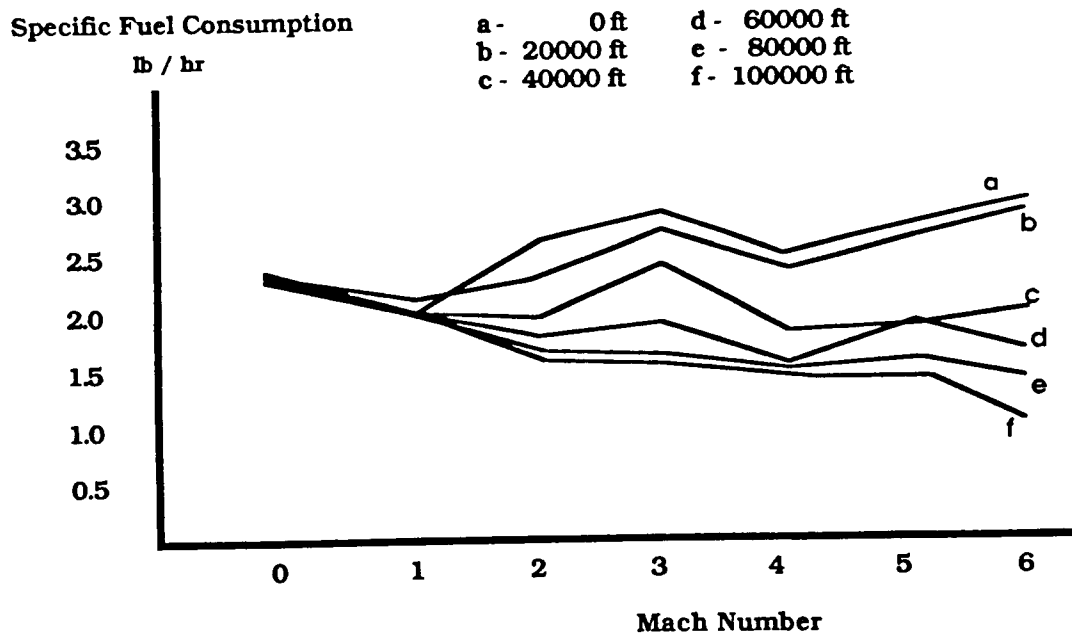
Mach Number

Figure 6.13 -- Specific Fuel Consumption versus Mach Number at Various Altitudes

59

7 WEIGHTS AND BALANCE

The weights analysis for the Waverider was separated into three parts; the preliminary weight estimation, the component weight estimation, and the c.g. location.

7.1 PRELIMINARY WEIGHT ESTIMATION

Initially the aircraft must be sized according to historical data and required performance values. Upon completion of the initial sizing of the aircraft, a detailed breakdown of fuel weights (according to mission phase) and component weights may commence.

In order to begin preliminary sizing of the Waverider, it was necessary to calculate a maximum take-off weight for the aircraft. The first step in this process was to calculate the weight of the fuel required to meet the RFP range requirements of 6,500 nm plus reserves. This was accomplished by using the "Method of Fuel Fractions".

By this method, an initial estimation of the aircraft's maximum gross take-off weight was required. By reviewing weight data of similar aircraft (XB - 70, 747, and Concorde), an initial maximum gross take-off weight of 920,000 lbs was decided upon. Another requirement of the method was the determination of the aircrafts mission profile. The mission profile was readily derived from RFP requirements as discussed in Chapter 2 (see Figure 2.1).

For each flight phase, a ratio of the aircraft's goss weight at the end of the phase to the aircraft gross weight at the beginning of the phase was used as a measure of the fuel consumed during the phase. These "fuel fractions", were obtained from fuel fraction data for similar aircraft, and were utilized on all mission phases except cruise. For the cruise phase, the fuel fraction was determined

using Breguet's range equation.

With the fuel fractions determined, the mission fuel weight was calculated. The fuel fraction calculation takes into account trapped and reserve fuel. The overall fuel fraction, M_f, was calculated to be 0.5277.

To ensure the validity of the estimated gross take-off weight used in the fuel fraction computation, the resulting empty aircraft weight of 355,500 lb was compared to an empty aircraft weight value of 370,00 lb which was obtained from a graph of weight trends for similar aircraft. These values agreed within 5%; therefore, the estimated maximum gross take-off weight was assumed a valid assumption. Figure 7.1 presents the weight breakdown of the Waverider. Additionally, Figure 7.2 presents the fuel weight breakdown of the Waverider.
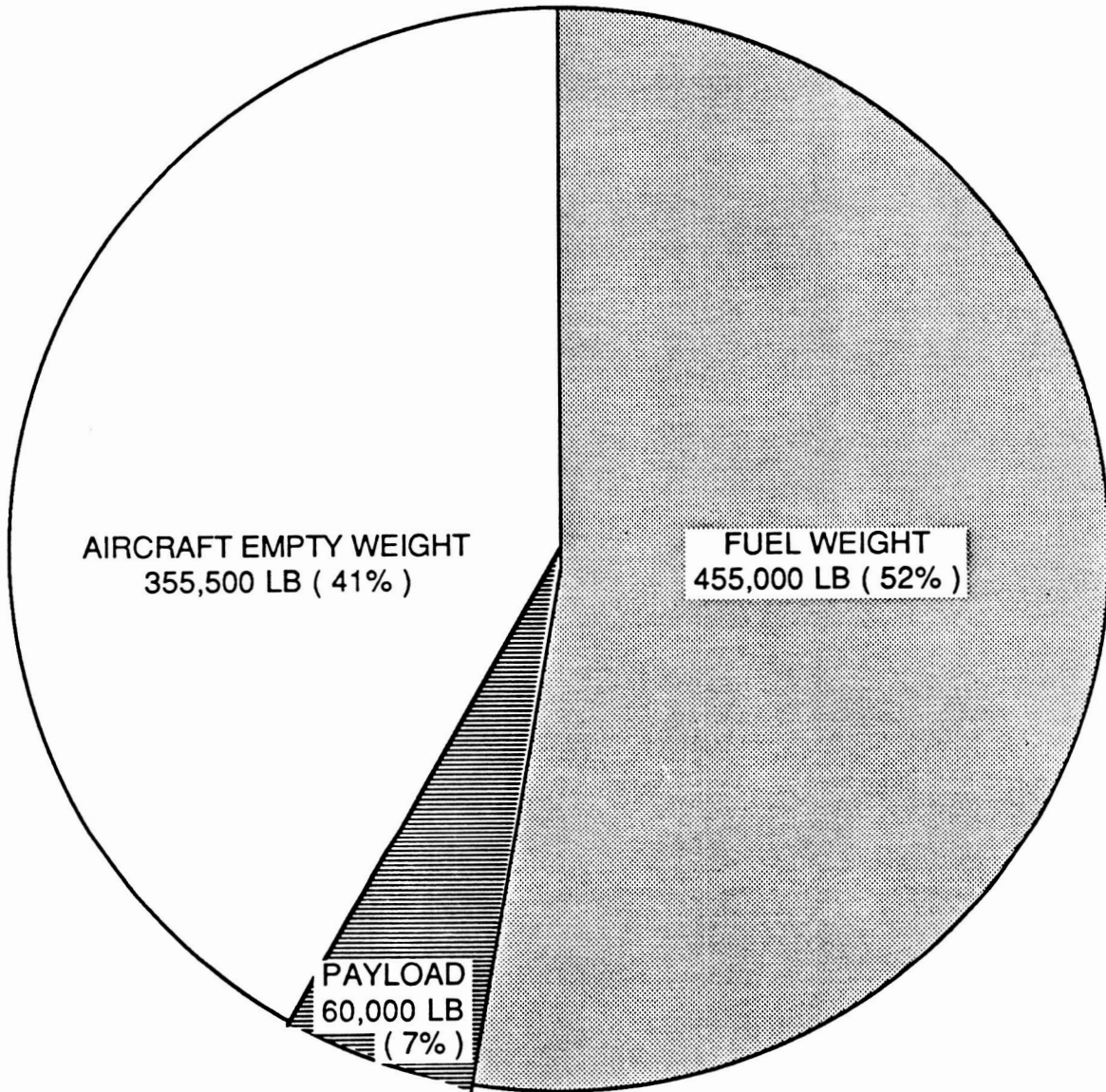
7.2 COMPONENT WEIGHT BREAKDOWN

The second part of the weight analysis involved the determination of component weights. As these computations involved the summation of a large quantity of values, a computer program was written to ease the workload. Upon completing the calculation of component weights, the weights were summed and reported the aircraft empty weight as 355,500 lbs. A breakdown of the component weights is presented in Figure 7.3.

7.3 CENTER OF GRAVITY

The balance analysis involved the determination of the location of the center of gravity (c.g.) of the aircraft. The c.g. calculation was based upon the detailed weight breakdown of the aircraft component weights as reported in section 8.1.2. A plot of c.g. travel is presented in Figure 7.4.
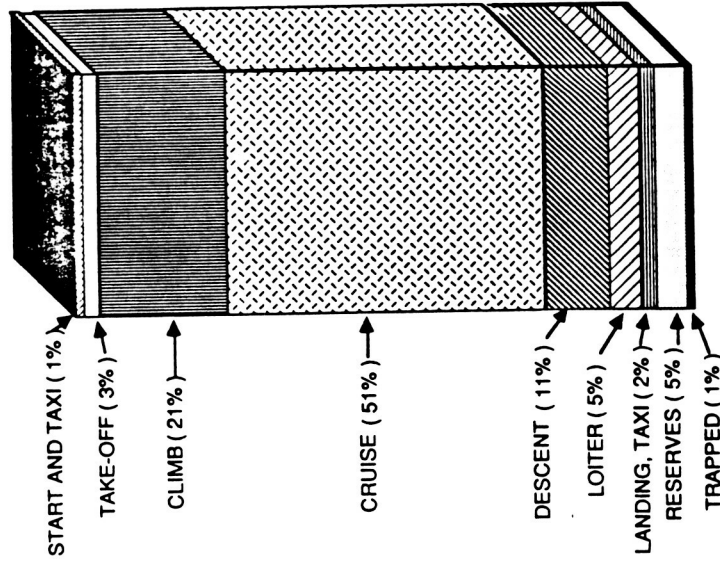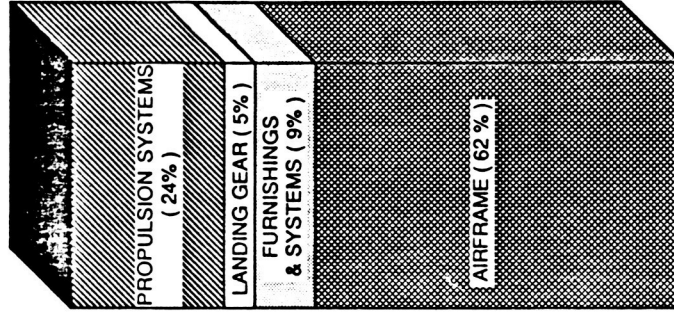
WEIGHT BREAKDOWN

AIRCRAFT EMPTY WEIGHT
355,500 LB (41%)

FUEL WEIGHT
455,000 LB (52%)

PAYLOAD
60,000 LB
(7%)

GROSS TAKE-OFF WEIGHT = 870,500 LB

FIGURE 7.1. WEIGHT BREAKDOWN.

COMPONENT WEIGHTS

PROPULSION SYSTEMS (24%)

LANDING GEAR (5%)

FURNISHINGS & SYSTEMS (9%)

AIRFRAME (62%)

EMPTY WEIGHT = 355,500 LB

FIGURE 7.3. COMPONENT WEIGHT BREAKDOWN.

FUEL WEIGHT

START AND TAXI (1%)
TAKE-OFF (3%)
CLIMB (21%)
CRUISE (51%)
DESCENT (11%)
LOITER (5%)
LANDING, TAXI (2%)
RESERVES (5%)
TRAPPED (1%)

FUEL WEIGHT = 455,000 LB

FIGURE 7.2. FUEL WEIGHT BREAKDOWN.

63

C. G. TRAVEL

WEIGHT (/ 1000 LB)

FUSELAGE STATION (ft)

GROSS

PASS. + WING + AFT FUEL

WING + AFT FUEL

AFT FUEL ONLY

FOREWARD FUEL + PASS.

FORWARD FUEL

EMPTY
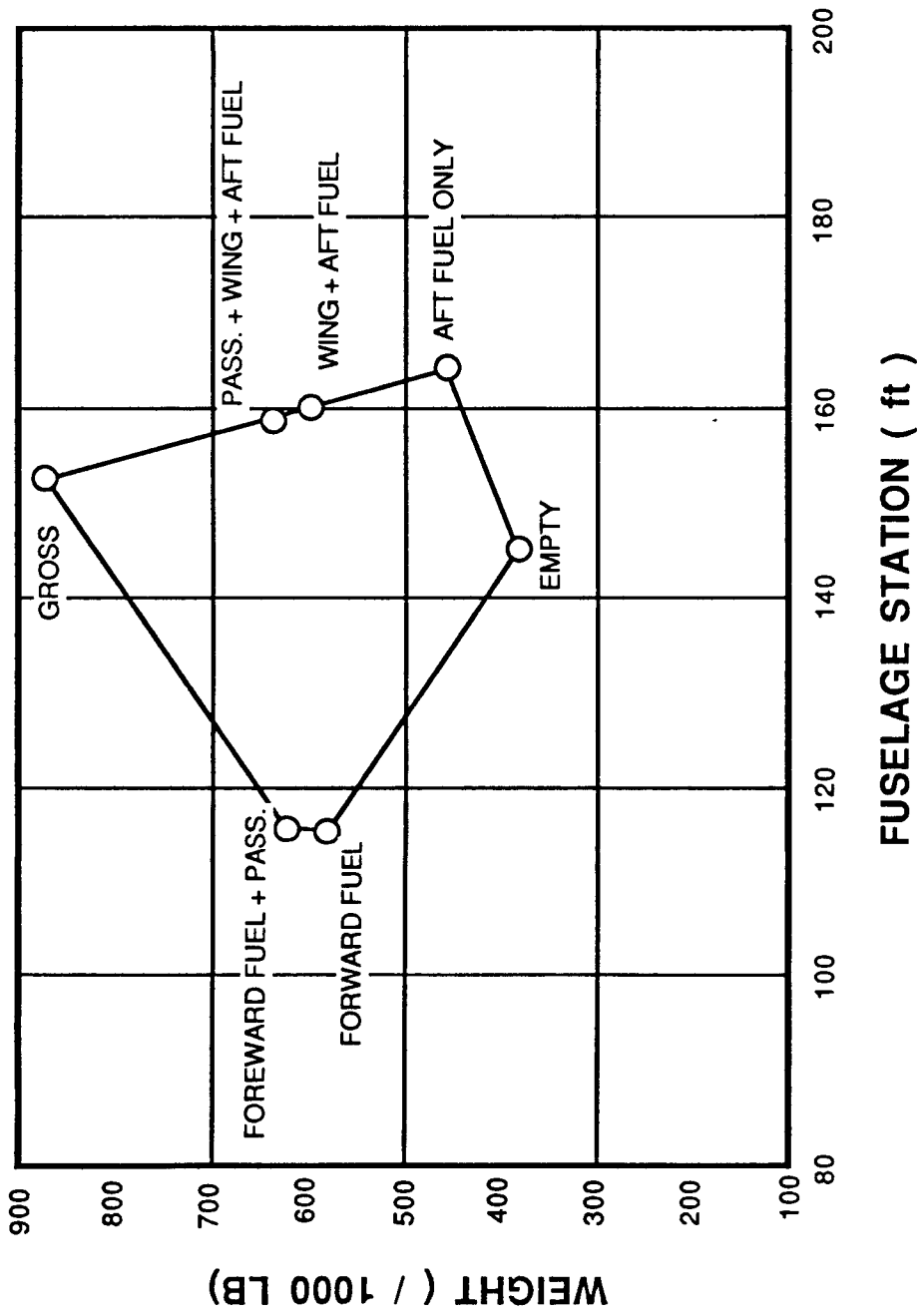
FIGURE 7.4. C.G. TRAVEL.

64

8 PERFORMANCE

The major focus of the Waverider's design was to develop a viable commercial transport. This transport must be compatible with existing airports and associated trafic control areas, as stated in the RFP. The performance analysis of the Waverider includes take-off, landing, and temperature effects on both. Since all the results are obtained from estimation methods; consevative assumptions were made to insure compliance with FAR and RFP requirements.

8.1 TAKE-OFF

A series of approximation methods were used to calculate the take-off ground distance, S_G, rotation distance, S_R, transition distance, S_{TR}, and climb distance, S_{CL}. Refer to Figure 9.1 for take-off flight path geometry. The take-off required no special lift or thust augmentation devices other than the standard ATR afterburner. The take-off performance calculation resulted in a ground roll distance of 4,892 ft, rotation distance of 652 ft, and a transition distance of 1,122 ft and total tke-off ground distance of 6755 ft. At the completion of the transition to climbing flight the Waverider was at an altitude of 65 ft which implies that at the end of transition the aircraft clears a 50 ft high obstacle without further climbing flight. This is due to the aircrafts weight, C_{LMAX}, and takeoff speed. A breakdown of the takeoff distances for standard sea level conditions is also presented in Figure 9.1.

8.2 LANDING

The landing performance is similar to the take-off performance varying only in the approach, flare, and consideration of auxiliary braking devices such as reverse thrusters and speed brakes. For landing performance, approximations methods were used for the airborne distance, S_A, the free-roll distance, S_{FR}, and the braking distance, S_B. Refer to Figure 9.2 for the landing flight path geometry. Results of the landing performance calculation yield an airborne distance of 1,317 ft, free-roll distance of 528 ft. and a braking distance of 7,069 ft. Note that no auxiliary braking devices were employed. This gives a total landing distance (with 30° of plain flap deflection) of 8,914 ft for standard sea level day conditions. Figure 9.2 also presents a breakdown of the landing roll distances. Note that this meets the RFP requirement of operations from 11,500 ft runways.

8.4 SPECIAL CONSIDERATIONS

Although the Waverider's intended route is trans-Pacific and therefore operations will be conducted from the 'cooler' costal airports, the effects of non-standard temperature variations on take-off and landing performance must be considered. Special consideration must be given to the 'hot' days when the take-off and landing roll distances will be increased. See Figure 9.3 and Figure 9.4 for the calculated effects of non-standard temperature variations (up to 100° F) on take-off and landing distances respectively.
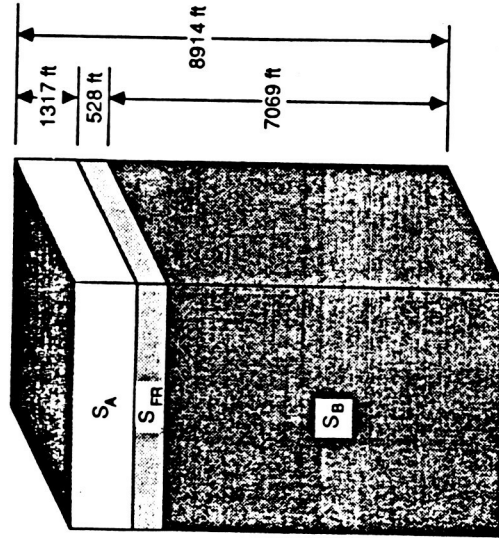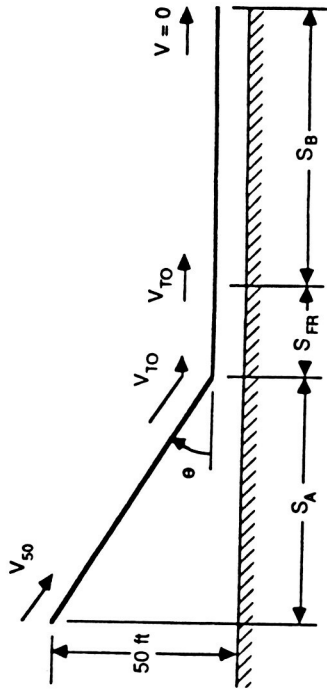
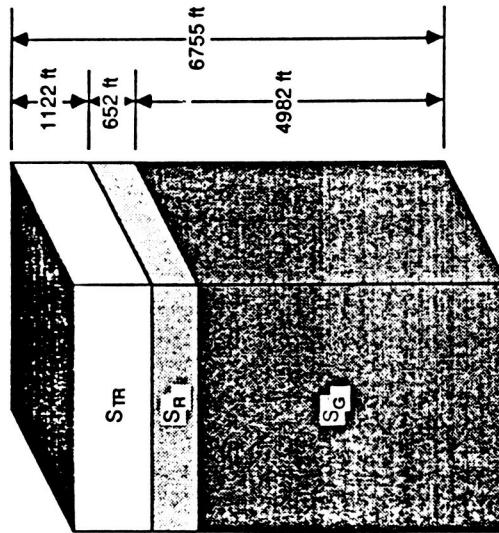## LANDING ANALYSIS

FIGURE 8.2. LANDING.
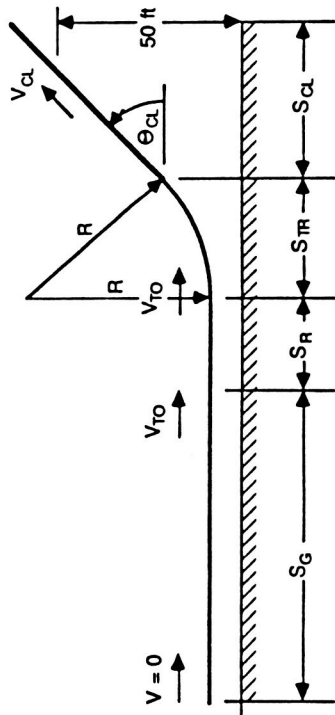
TAKE - OFF ANALYSIS
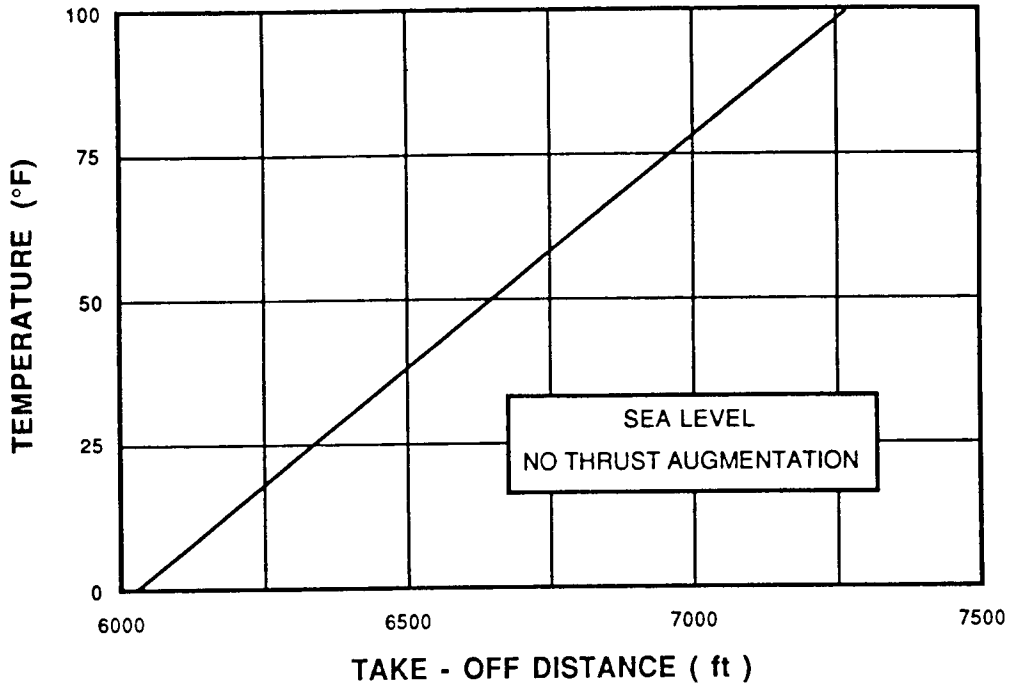

FIGURE 8.1. TAKEOFF.

TAKE - OFF DISTANCES

FIGURE 8.3. TAKEOFF DEVIATIONS.
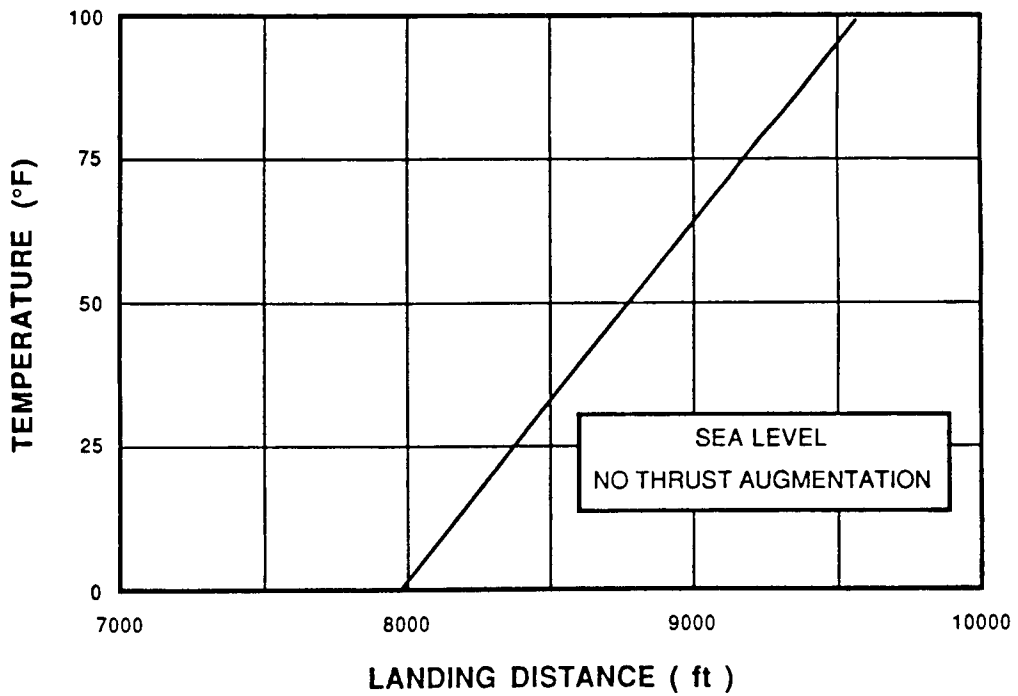
LANDING DISTANCES

FIGURE 8.4. LANDING DEVIATIONS.

9.0 HEAT TRANSFER / STRUCTURES

The advent of high speed, high altitude aircraft has introduced many new problems to the designer. One of the more important problems that arises is caused by the skin temperatures (aerodynamic heating) that are attained at very high velocities. Adiabatic wall temperatures under these conditions can exceed the temperature limitations of structural materials commonly used in the manufacture of such aircraft. It has been the purpose of this analysis to develop a heat transfer model to evaluate the aerodynamic heating conditions to which the Waverider configuration will be exposed.

9.1 THE HEAT TRANSFER MODEL

For purposes of analysis a two-dimensional model has been used (see fig. 10.1) . Geometrically the model is composed of an upper and lower insulated flat plate, and a semicircular nose resembling the geometry of a wing flying a predetermined mission profile fig. 2.1. The general model has been written in Fortran and allows the user to specify geometry such as, nose radius, skin thickness, and number of elements to be analyzed. In order to run the model it is necessary for the user to write into the program functions of time for altitude, mach number, and angle of attack, this allows several users with different flight profiles to conduct the heat transfer analyses. Once the functions of time are entered into the program the user is prompted via screen to enter additional information such as material properties and specific geometry for the model to be analyzed. The model can be easily modified to reflect axisymmetric values by means of Mangler Transformations (ref. 22).

9.1.1 MODELING THE ATMOSPHERE

An international Standard Atmosphere is used as the basic model. It is assumed in this model that the temperature of a "characteristic" atmosphere decreases linearly with height from the surface to a fixed height called the Tropopause, where the fixed height is taken as 36,089 ft. Above this height the temperature remains constant at 390 °R to an altitude of 82,000 ft. Beyond this point the temperature begins to increase linearly, and for purposes of this analysis the upper limit of the atmosphere is taken as 100,000 ft.

The temperature variation below 36,089 ft. is given by

$$T = T_s - Bh \tag{9.1}$$

where B is the lapse rate, given as 0.00356 °R/ft., Ts is the surface temperature, given as 518.7 °R, and h is the altitude. Above 82,000 ft. the temperature variation is given by

$$T = 418.79 + 0.0016(h-100,000) \tag{9.2}$$

The pressure variation in the atmosphere has been modeled using an exponential variation with height up to 36,089 ft given by

$$p = p_s \left[\frac{T_s - Bh}{T_s} \right]^{(g_0/RB)}$$

70

where p_s is the sea level pressure given by 2116 lb/ft^2, g_o is the gravitational constant and **R** the Universal Gas constant 1716 ft^2/(sec^2- °R). Above this region and up to 100,000 ft. the following pressure variation was used

$$p = p_t \, e^{-(g_0/RT)(h-h_t)} \qquad (10.4)$$

where p_t is the pressure at $h_t = 36,089$ ft., and h are heights between h_t and 100,000 ft. Density variations are determined for all heights based on the perfect gas law given by:

$$\rho = p/RT \qquad (9.5)$$

using the values obtained from the above relations.

9.1.2 DEVELOPMENT OF THE MATHEMATICAL MODEL

Since the aircraft will be flying under subsonic and supersonic conditions it is necessary to model the local surface conditions of the aircraft for both regimes.

In the development of this model the one-dimensional isentropic compressible flow relations, and the one-dimensional normal shock relations for a perfect gas with constant specific heat were used (ref. 16). These relations allowed the determination of the total and local properties of the flow over the wing during

71

subsonic and supersonic operating conditions, with the exception of the local pressure distribution, where it is assumed that experimental pressure distributions for hypersonic flow over cylindrical noses follow closely a modified Newtonian relation (ref. 22), this concept is used in the development of the local pressure distribution over the nose of the geometrical model and is given by:

$$p_L = (p_{02} - p)\cos^2\Theta + p \qquad (10.6)$$

where Θ is the angle between the velocity vector and the normal to the suface in question (fig. 9.1), p_{02} is the total pressure behind the shock wave and p is the free stream pressure.

The local viscosity, and the local thermal conductivity are determined using the following relationships:

For the local viscosity

$$\mu_L = \frac{C_1 T_L^{1.5}}{T_L + C_2}$$

where $C_1 = 2.27 \times 10^{-8}$ slug/ft.-sec $^\circ R^{0.5}$, and $C_2 = 198.7$ $^\circ R$, and for the local thermal conductivity

$$k = k_{32} \left[\frac{492 + C}{T_L + C} \right] \left[\frac{T_L}{492} \right]^{1.5}$$

72

where $k_{32}=4.005 \times 10^{-6}$ Btu/ft-sec-°R, and C=225 °R. With this local values it was then possible to compute the local Prandtl number given by

$$Pr = 32.2 \, c_p \, m \, / \, k$$

In order to simplify the analysis it was assumed that the general flow over the wing was turbulent so that the recovery factor would be given by the relation

$$r = Pr^{1/3}$$

Experimental evidence reveals that the above relation is apparently unaffected by compressibility effects and therefore justifies its use in supesonic flow (ref. 24). In order to avoid dealing with variable fluid properties the simple technique recommended by Eckert (ref. 23) is used. That is that the constant property correlations may be used as long as the properties are evaluated at the reference temperature T^*, rather than at the average film temperature. The relation is given by

$$T^* = 0.5(T_s - T) + 0.22(T_r - T)$$

where T_s is the surface temperature of the element, T_r is the recovery temperature, and T is the free stream temperature. The reference temperature was then used to determine the reference thermal conductivity, viscosity, density, velocity, Reynolds number and Nusselt number.

Two forms of the Nusselt number are used for turbulent flow on flat

73

plates, and the relations are taken from the working relations for forced convection in high speed flow in ref. 23. The first one is given for a reference Reynolds number of less than 10^7 as:

$$Nu^* = .0292(Re^*)^{0.8}(Pr)^{1/3}$$

The second relation is given for $10^7 < Pr^* < 10^9$ as:

$$Nu^* = \frac{0.185(Re^*)(Pr^*)^{1/3}}{(\log_{10}Re^*)^{2.584}}$$

The heat transfer coefficient can now be obtained from

$$h = Nu^* \, k^*/L$$

where k^* is the reference thermal conductivity and L is the convection flow length measured from the stagnation point to the point in question.

The stagnation heating rate is computed using an empirical relation for the stagnation point heating rate to a blunt body of revolution in hypersonic flow given in ref. 24 as:

$$q_s = \frac{17600}{\sqrt{R}} \left[\frac{\rho}{\rho_o} \right] \left[\frac{u}{u_c} \right]^{3.15} \left[\frac{T_{SL} - T_{ws}}{T_{SL} - 540} \right]$$

Where R is the nose radius ρ and ρ_o are the free-stream and sea level densities, u is the velocity of the vehicle in question, u_c is the satellite velocity given as 26000 fps., T_{sl} is the stagnation local temperature and T_{ws} is the wall temperature. Since this empirical equation is for an axisymmetric flow it is necessary to convert its results to a two-dimensional form. This is accomplished by means of a transformation given in ref. 26 in which

$$q_{s\,2\text{-}D} = \frac{0.570}{0.763} \, q_{s\,3\text{-}D}$$

The stagnation point radiation relation was also obtained from ref. 24 and was given as:

$$q_{rad} = 10^2 \left[\frac{V}{10^4} \right]^{8.5} \left[\frac{\rho}{\rho_o} \right]^{1.6} R$$

where V is the velocity of the vehicle, R is the nose radius, and ρ and ρ_o are the free stream and sea level densities respectively. Again this relation is for axisymmetric bodies, therefore it is necessary to transform this relation as before.

The heating rates generated at the elements of the model are described by Newton's Law of cooling, and are given by

$$q/A = h(T_{aw} - T_s)$$

were h is the heat transfer coefficient, T_{aw} is the adiabatic wall temperature of the element and T_s is the wall temperature of the elements . The radiation emitted by the elements has been obtained using the Stefan-Boltzmann Law

$$E= \varepsilon\sigma T^4$$

where E is the rate of energy emission per unit area, T is the absolute temperature of the body, $\sigma=4.7611 \times 10^{-13}$Btu/sec-ft.^{2}-°R, and ε is a property of the particular emitting surface known as the emissivity

9.1.3 TEMPERATURE CALCULATION

Now that the mathematical model has been developed it is necessary to satisfy thermal equilibrium.Thermal equilibrium requires that the rate of heat stored in each element be equal to the sum of the rates of heat entering and leaving the element. In this model it is assumed that convection and radiation are the only heating rates entering and leaving the elements, or in mathematical form

$$mc_p dT/d\tau= hA(T_{aw}-T_s) - A\varepsilon\sigma T^4$$

or

$$\rho V c_p dT/d\tau= q_{bl}-q_{rad}=q_{TOT}$$

and by expanding the differential and rearranging

$$T_{wf} = \frac{q_{TOT}}{\rho_m t_c c_p} \Delta t + T_w$$

where T_{wf} is the final temperature of the element q_{TOT} is the net heating rate into or out of the element due to convection and radiation, ρ_m skin material density, t_c is the skin thickness, c_p is the specific heat of the material, Δt is the time increment and T_w is the initial wall temperature.

The stagnation temperature can be obtained in a manner similar to the one presented above.

9.1.5 RESULTS

Several runs were conducted using two models of different material properties . The models were both of 102 ft. in chord with a total of seven divisions for the upper portion and the same number for the lower portion of the model. The first model tested was an Inconel X model of density 15.1863 slug/ft^3, c_p=3.5762 Btu/Slug-°R, and emissivity of 0.81., and the second one was a Chrome-Nickel model of density 16.5221 slug/ft^3, c_p=3.5378 Btu/Slug-°R, and emissivity 0.36.

The models were run by varying the nose radius and skin thickness of the elements in order to determine the variation of temperatures due to this parameters. As expected the leading edge elements for both material models were subjected to higher tempertures.These temperatures reached values of about 2700°R, while the aft elements reached maximum temperatures below 2000°R., see fig. 9.2. Figure 9.3 is a description of the heatings rates and temperatures to which the model is

exposed for a leading endge element, while fig. 9.4 is a comparison of the hetaing rates experienced by a leading and a trailing edge element. In general the increase in thickenss of skin or nose radii has the effect of decreasing the heating rates and therefore the temperatures experienced by the element. A comparison of both materials indicated also that chrome nickel attained in general higher temperatures in the order of 100 to 200°R higher, refer to figure 9.5. It is to be noted that Chrome Nickel has a higher melting temperature than Inconel X, at about 3000°R. This should be a driving consideration in the design of the structure if it is expected to fly the aircraft without any type of cooling system. For lighter structures aluminum may be considered but the structural temperature must remain below 1600°R. Other materials may be cosnisdered nad this include titanium alloys which could also well be used without any cooling system since the melting temperature approximates the 3480°R.

In general this model is to be used as a reference and the temperatures resulting from the runs are to be expected slightly higher than those under full heat transfer conditions since the effects of conduction have been omitted. It is also noted from the results in fig. 9.2. that all elements return to almost sea level temperatures, another result that may indicate low accuracy since the conduction terms have been omitted.

9.2   STRUCTURES

9.2.1   DEVELOPMENT OF THE V-n DIAGRAM

The V-n diagram was developed using Roskam's methods for FAR Cert. airplanes (ref. 25).

With an aircraft $C_{L\max}$ =1.6 the maximum normal load coefficient

resulted in a value of 1.76. With a wing loadingof 66.5941 lb/ft^2 the +1g stall velocity V_{s1} was determined to be 105.66 kts. V_{s1} represents the minimum steady flight speed which can be attained. The design maneuvering speed V_a was determined to be 167.06 kts.,which also results from a positive load factor of 2.5 which is the minimum required by FAR 25. The design speed for maximum gust intensity V_B was determined to be 118 kts., which in turn yields a design cruising speed of 161 kts. From the flight profile the cruise speed is to be M=5.5 at 100,000 ft. this results in an equivalent air speed at sea level of 379.93 KEAS; since this speed is greater than V_c=161 kts., then the design cruising speed is taken as V_c=379.93 KEAS. The design diving speed is given by V_D=1.25V_C, which results in V_D=474.91 KEAS. The negative stall line is determined by assuming $C_{Lmax-neg}$=-1.00, which results in a maximum negative normal load coefficient of -1.1, yielding a negative 1g stall speed of 136.22 KTS. Please refer to fig. 9.6 for details.

Based on the aircraft gto weight of 870,462.33 lb the total load experienced based on the V-n diagram's maximum load factor results in a load of 2,176,155.95 lb, or in a spanwise loading of 17,369.83 lb/ft. which yields a maximum bending moment of about 35,000,000 ft-lb. (refer to fig. 9.7). For design purposes it would be appropiate to design the wing structure with more than one spar to relief some of the excessive loading.
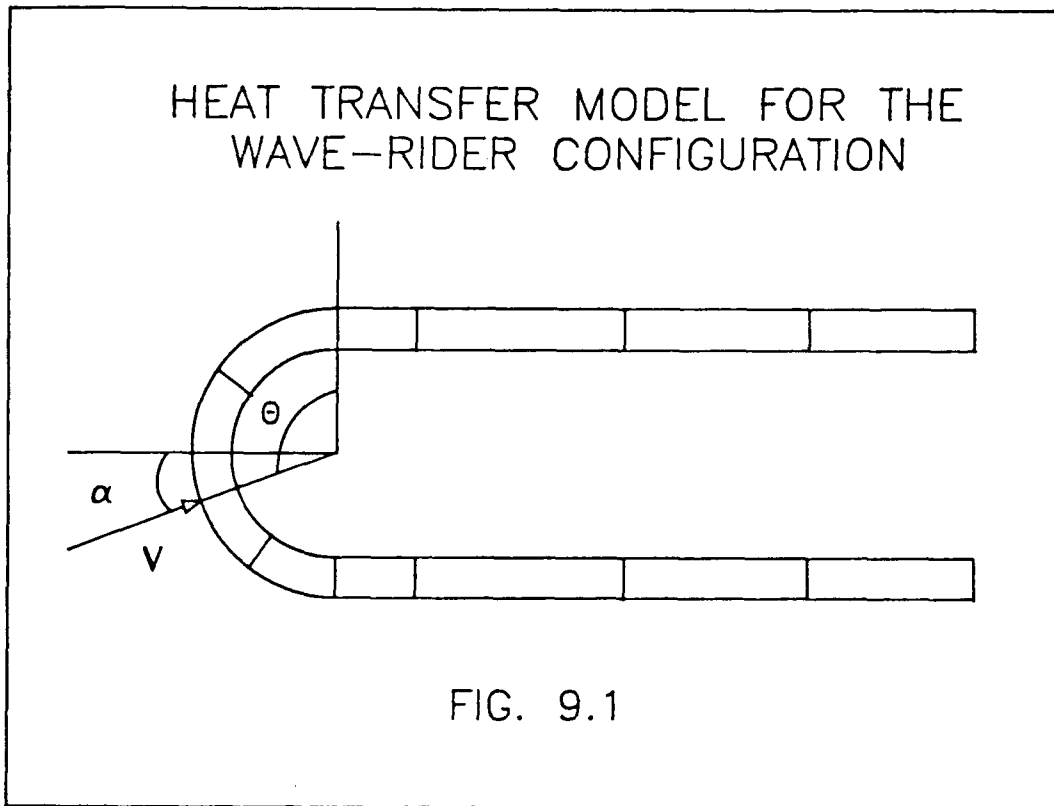
HEAT TRANSFER MODEL FOR THE WAVE-RIDER CONFIGURATION

FIG. 9.1

FIGURE 9.1. HEAT TRANSFER MODEL.

WAVE-RIDER TEMPERATURE HISTORY
Rn=0.0417 ft., Thickness=0.04 ft.

Twall - R

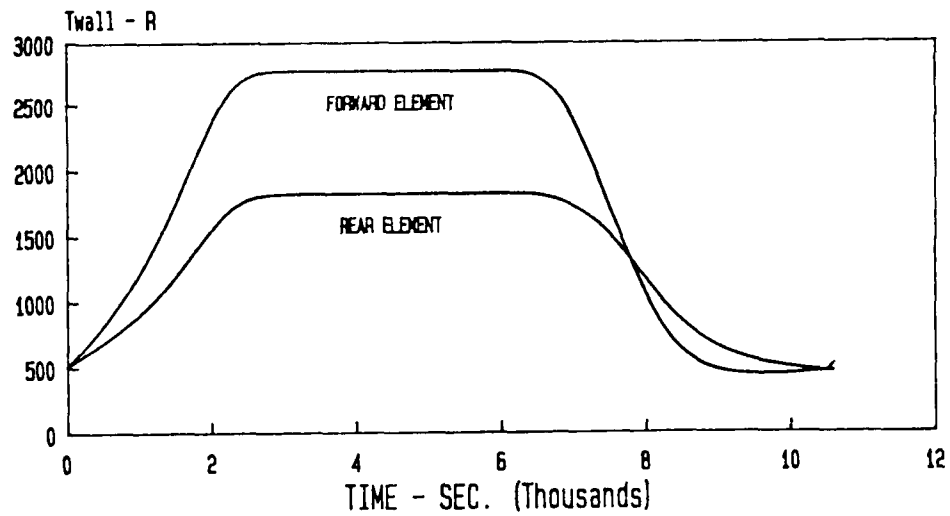FORWARD ELEMENT

REAR ELEMENT

TIME - SEC. (Thousands)

FIGURE 9.2. WAVERIDER TEMPERATURE HISTORY.

Inconel X

80

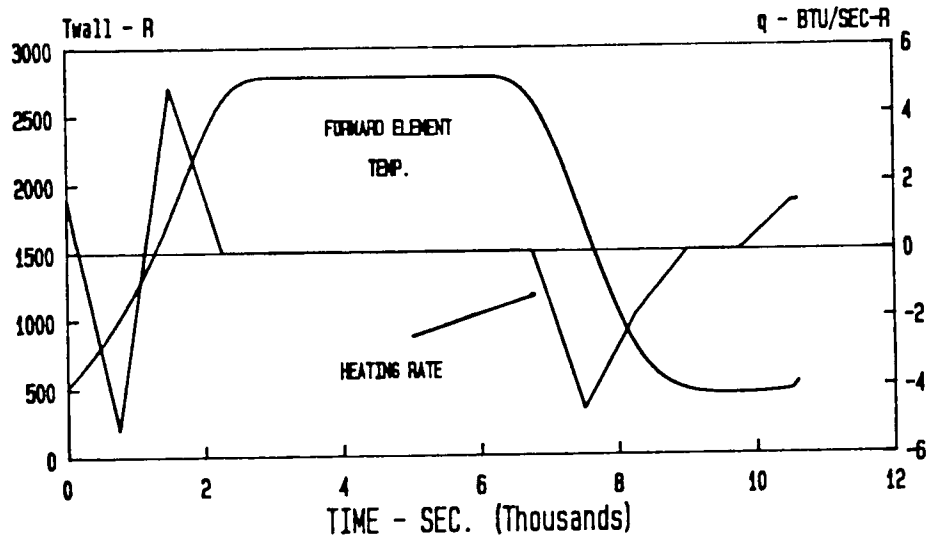WAVE-RIDER TEMP.& HEATING RATE HISTORY
Rn=0.0417 ft., Thickness=0.04 ft.

FIGURE 9.3. WAVERIDER HEATING RATE HISTORY.

Inconel X

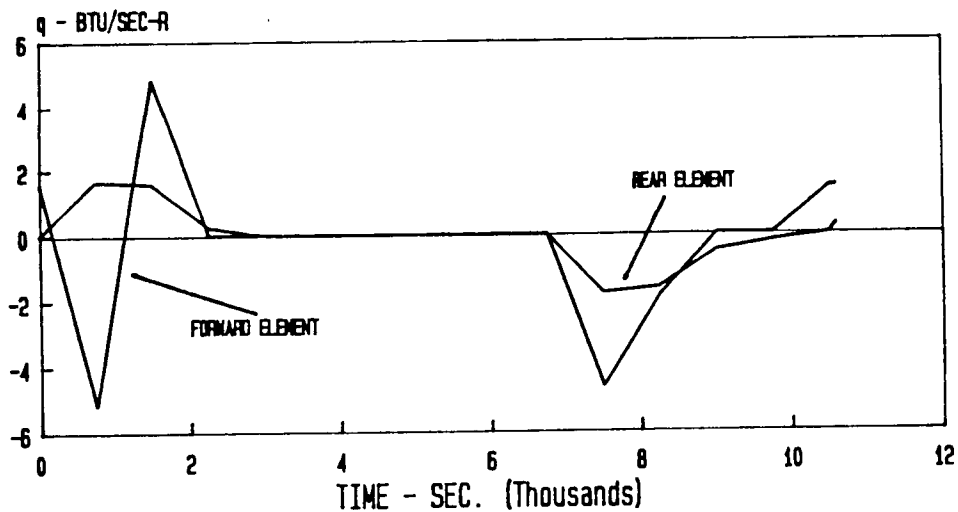WAVE-RIDER HEATING RATE HISTORY
Rn=0.0417 ft., Thickness=0.04 ft.

FIGURE 9.4. TEMPERATURE AND HEATING RATE HISTORY.

Inconel X

81

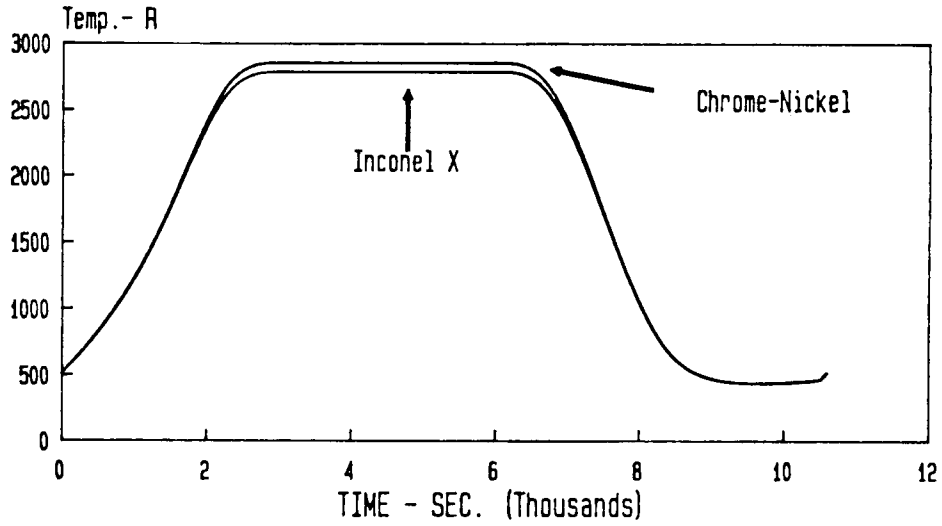## WAVE-RIDER TEMPERATURE HISTORY
MATERIAL COMPARISON

FIGURE 9.5. MATERIAL COMPARISON.
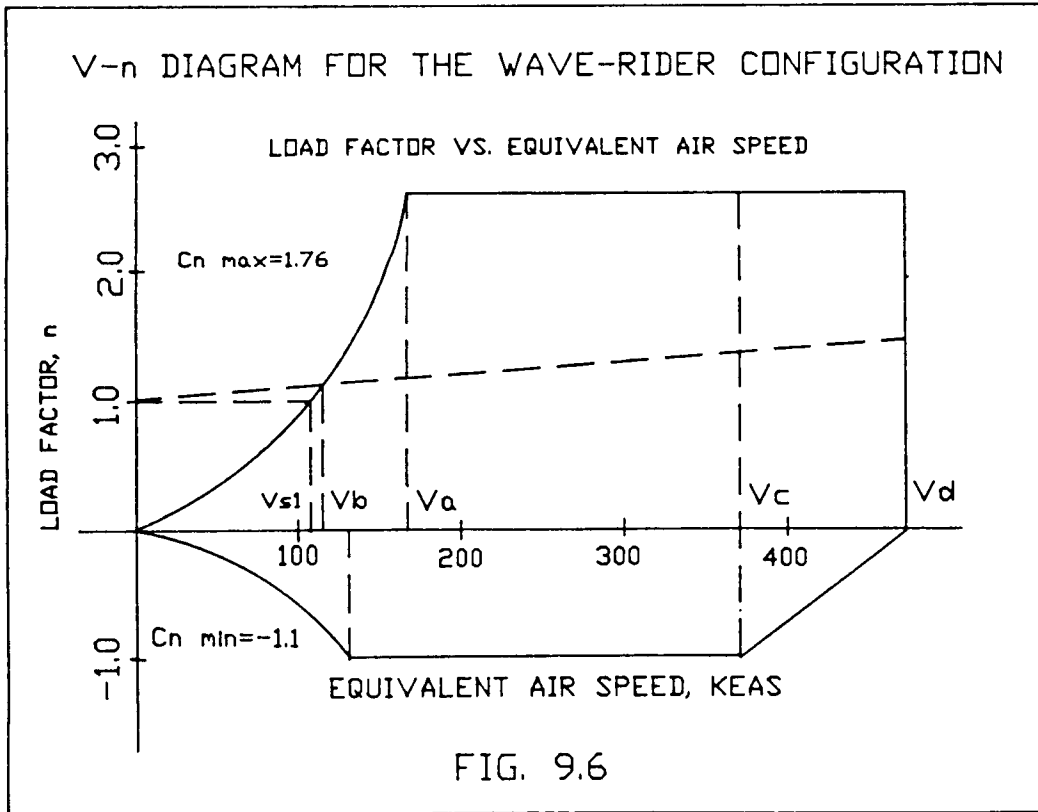
Inconel X & Chrome Nickel

FIGURE 9.6. V-n DIAGRAM.

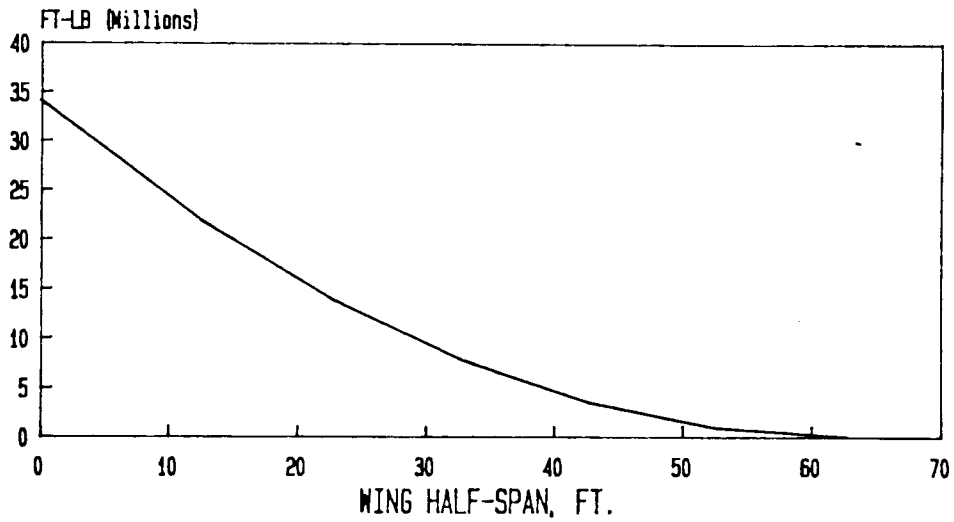## WAVE-RIDER CONFIGURATION
BENDING MOMENT DIAGRAM

FIGURE 9.7. BENDING MOMENT DIAGRAM.

Inconel X

10 NOISE AND POLLUTION

The nature of this aircraft requires daily operations from civilian commercial airports. Because this nature of the operations of this aircraft noise and pollution implications of the aircraft must be considered.

10.1 SONIC BOOM

Inherent to the mission profile of the Waverider is supersonic and hypersonic flight. Any object passing through the air at a velocity greater than the speed of sound will create a sonic boom. This sonic boom is the sudden rise and fall of sound pressure associated with high speed aircraft flight. The change in pressure level comes from the Mach cones eminating from the bow and tail of the airplane. Figure 10.1 shows the bow and tail waves, the typical pressure wave generated near the ground, and a possible ear response to the pressure signal. Most of the sonic boom's energy is concentrated in the infrasonic range (Reference 27). The maximum increase in atmospheric pressure due to the sonic boom is termed the overpressure and is measured in units of pounds force per square foot or in the typical sound unit, the logarithmic decible. Another quantity used to describe the sonic boom is its duration duration measured in seconds or fractions thereof. To gain insight on the decible and frequency sales used in quantifying noise, refer to Figure 10.2. On Figure 10.2 one can compare the dB measurement of an automobile horn to a distant airplane to a soft whisper.

10.1.1 FAR 91.55

FAR 91.55 states that no civil aircraft which is capable of supersonic flight may operate from a United States airport nor may it operate supersonically in U.S. airspace. Landing waivers have been granted to Concorde aircraft to operate from

a few U.S. airports but are prohibited from supersonic flight over land. Current HSCT studies being performed by Mc Donnell Douglas and Boeing aircraft companies assume subsonic flight overland and as little overland travel as possible (Reference 29). The only stipulation to allow supersonic flight in FAR 91.55 is if the pilot is able to determine the sonic boom generated by his aircraft will not reach the ground. It makes no mention of tolerable overpressure levels. The EPA (Reference 29) says there is no public annoyance from one daytime (7 a.m. to 10 p.m.) ground measured boom below 0.75 psf based on a day-night average of 55 dB and therefore recomends, for more than one boom per day, the peak level of each boom should be no less than 0.75 / (N) 1/2 psf or 125 - log (N) dB where N is the number of booms. It is expected the attractions and wide ranging benefits of the HSCT will persuade the public to change these laws and to instead invoke laws which seek compromise between feasible operation of an HSCT fleet and sonic boom tolerances.

10.1.2 PREDICTION METHODS

The prediction methods of Carlson, Sebass, and Morris (References 30,31, and 32 respectively), were used in comparison to estimate the sonic boom signatures produced bythe Waverider. Common to all methods was input information regarding aircraft shape, speed, and altitude.

Morris' (Reference 32) 1960 paper gave the overpressure (dp) as either due to volume effects or lifting effects, whichever is greater. The use of this method requires and relies heavily upon an estimate of the volume shape factor KV and the lift shape factor KL which the author states are generally between 1.5 to 2.0 and 1.4 to 1.63 respectively, for "practical supersonic aircraft shapes." KV would be close to 1.5 for bodies whose maximum thickness occur towards the rear and KL would tend towards 1.63 for shapes similar to delta wings. Morris states that lifting

effects will dominate over most of the altitude range of a large bomber or supersonic transport aircraft. Figure 10.3 shows overpressure as a function of altitude and Mach number for the Waverider aircraft as calculated by Morris' methods.

Reference 31 (Seabass, 1972) gave an equation for the overpressure.This equation utilizes altitude, length, and speed as the primary parameters but also the atmospheric scale height which was not well defined. He states "...the signature shape that is approached asymptotically below the aircraft in an isothermal atmosphere of scale height H is the signature that occurs at a distance $(\pi)H/2$ below the aircraft in a homogenous atmosphere" and "...the ultimate (pressure signal) advance below the aircraft in a stratified atmosphere is the same as that in a homogenous atmosphere when z (the distance below the aircraft) is euqal to $(\pi)H/2$." He states his methods are usable for "exotic configurations" provided the effective lengths and base areas are used. Figure 10.4 shows the Waverider overpressure as a fuction of altitude and Mach using Seabass' procedures.

Reference 30 (Carlson, 1978) published a simplified sonic boom prediction procedure which seems to be the most thorough of the three methods. Carlson employs the combined effects of lift and volume in his effective area equation:

$$Ae(x) = A(x) + B(x)$$

where $B(x)$ is the equivalent are due to lift and $A(x)$ is the cross-sectional area distribution normal to the flight path. Since the aircraft was not assumed to be operating at very large angle of attack, so areas normal to the aircraft longitudinal axis was acceptable. One then calculates the shape factor assuming a parabolic effective area distribution. Carlson gave proof of the validity of the assumption to calculate the shape factor and its accuracy to within 5% to 10% of the values for current supersonic aircraft using more rigorous computer methods. Like Morris,

86

Carlson employed a reflectivity factor, KR, which one must estimate in order to use the procedure. Morris and Carlson agreed that reflectivity factors between 1.8 for marshy terrain to 2.0 for hard flat surfaces are acceptable. Carlson's model may be used for aircraft altitudes as great as 250,000 ft (76 km)ground level altitudes as great as 5,200 ft (1600 m), aircraft in level flight or in moderate climb of decent flight profiles in the standard atmosphere. Acceleration or flight-path curvature effects were not covered. Figure 10.5 shows lines of constant overpressure for varying altitude and Mach number using Carlson's equations.

Seabass' method gave the lowest overpressures but also required the least information for input. Seabass' equations were only sensitive to length and weight (keeping altitude and Mach constant) and since the four HSCT planforms were within 4% of each other's length and at most 16% different in weight one could expectsimilar results. The method did not account for aircraft shape or planform which distinguishes the various HSCT configurations to a greater degree than length and weight. Morris' method required more information about the shape of the airplane as given by the boom due to volume factor, boom due to lift factor, wing span and maximum cross-sectional area inputs. As mentioned above, the volume and lift factors were only estimates; therefore, the same bias possessed by the person doing the calculations exists in the results. Carlson's method seemed the most planform sensitive of the three procedures being that cross-sectional area and span distributions as well as length, weight, aircraft planform area, and flight track information were required for input. This last method also gave the boom time duration, something which the other methods did not mention.

10.1.3 RESULTS

The first method implied overpressures due to lift effects dominated altitudes above 75,000 ft for all Mach numbers for the Waverider. Volume effects were prevalent only at higher Mach numbers and lower altitudes. The second

method gave results which were desired but not necessarily probable. Sonic boom overpressures for this method were as low as 0.87 psf for Mach 1.5 at 35,000 ft altitude and only as high as 1.76 psf for Mach 6.5 at 20,000 ft. A goal of 1 psf for high-speed transports has been set in hope that U.S. law-making bodies will accept this ceiling for supersonic flight over land. The second method's results were encouraging that HSCT designs might be able to accomplish their goal. The third method's results were in better agreement with the first's results. Overpressures for the Waverider were as great as 12.67 psf for Mach 6 at 20,000 ft which seems reasonable from such a large heavy aircraft. Sonic boom decreased as expected at higher altitudes to 1.71 psf at 80,000 ft--the cruise design point of the Waverider aircraft. Boom time durations increased with altitude for constant Mach and increased with increasing Mach for constant altitude. Although one would expect that as he flies higher at the same Mach number the time duration should decrease due to atmospheric attenuation the tren was just the opposit, however, as one flies faster at constant altitude the sonic boom grew stronger and lasted longer as predicted.

10.2 NOISE

The design of any airplane requires a look at the production o noise from its engines. Noise, in any context, is characterized by its sound level, frequency spectrum, and its variation over time. Sound level refers to the listener's subjective conception of loudness and is a function of the magnitude ot pressure fluctuations about the ambient barometric pressure. As the HSCT configuration of this report was employing the air-turbo ramjet, an unconventional engine and noise generators and suppressor techniques were considered. Acoustic liners to act as the inner skin of the engine fairing in parts throughout the entire engine are, in general, effective sound absorbers. In some cases they have reduced the noise by 10 dB but encountered operational problems like freeze-thaw transition and fuel/oil retention.

For those and other reasons, alternative reduction methods for unique stages of the engine must be considered.

10.2.1 SOURCES OF NOISE

Coming from the inlet system of an aircraft engine is noise from the compressor, which is prominent during the approach phase. This noise is characterized by two types--broad band and discrete tone noise. Broad-band noise is turned by the turbulence and flow velocity as it enters and is generated by the compressor blades. The acoustic energy from the turbulent flow is porportional to its velocity to the 5th power. The incidence angles of the compressor blades also play a key role in tnoise production. A one-degree divergence of blade incidence angle from the optimum angle can increase noise by 3 dB. Disrete tones are associated with the fans of low- or high-bypass ratio turbofans but can occur from compressor stages. When the supersonic tips of blades have shock waves that are not identical the familiar buzzsaw noise is produced but also the cyclic pressure field and wake interactions which exist between the rotating and stationary stages are a cause of discrete tones. The correct spacing of the compressor stages and blade sweep-back to defeat the shock problem have been noted as possible solutions. Also proposed is the introduction of a hemispherical honey-comb skin inflow control device to mount in front of the inlet during the landing and approach phases. This device was tested on conventional turbofan engines. A couple of the key factors in helping reduce the internal noise of a two-stage turbofan by 20 dB in addition to the ideas presented above was the elimination of inlet guide vanes, divided or non-circular intakes and introduction of acoustical insulation (Reference 33).

Noise emanating from the combustor region has been difficult to isolate and little is known about it (Reference 34). One item which is known is that combustors generate low frequency noise and is less annoying than the high frequency buzzsaw whine of the compressor and/or fan.

Broad-band and discrete tones are also present in the turbine stage of the engine (Reference 33). To a lesser ratio of stationary to rotating blades than in the fan should be used due to the lower Mach number of the hot flow. High blade loading should be avoided. Large stage spacing is recomended.

Jet noise is probably the most prominent of all engine noise sources especially during the take-off phase. Key factors here are exhaust flow velocity and temperature profiles. Early civilian turbojet engines such as the ones used on early DC-8's were loud due to the flow of high temperature, high velocity gases. The popularity of the high-bypass ratio turbofan grew not only from its lower fuel consumption but also from its quieter exhaust. The idea was (and still is) to surround the hot jet core with cool bypass air. The problem, though, of the hot jet core still exists. One way to combat this problem is to use an inverted-velocity-profile (IVP) coannular jet which has the hot flow at high speed but over a greater area surrounding the low temperature, low speed flow. The hot core which was once a concentrated flow is now disbursed to the atmosphere at a higher rate thus quieting the exhaust. Other suppression techniques include ejectors, thermo-acoustical shields, mechanical chute suppressors, and advanced opperational procedures, the later to be discussed later. The concept behind mechanical suppresors is they slow the jet flow as close to the nozzle as possible such that the shear between exhaust flow and atmospheric air is minimized. The thermo-acoustical shields act as heat and sound energy absorbers and reflectors. The exhaust temperatures are decreased and sound energy is reflected away from the ground rather than towards it. Ejectors create another path of exit for exhaust and thus have mixing characteristics like the IVP coannular jet. In the past, the weight, cost, and drag penalties of ejectors have eliminated tham from widespread usage but the take-off thrust required and the asociated airport noise will probably take priority.

10.2.2 FAR 36

FAR 36, Appendix C, Section 36.5 gives the maximum noise levels for various types of aircraft for take-off, approach, sideline, and landing conditions. The measurement stations are given in Figure 10.6.

The "Stage" level is a function of the take-off weight as seen in Figure 10.7. The maximum take-off weight of the Waverider conicides with the 108 EPNdB FAR requirement. EPNdB is an acronym for Equivalent Percieved Noise level which takes into account the sensitivity of the humanear to frequency and tone annoyance, together with the duration of exposure to the noise (Reference 35). In California, home of major international airports likely to serve the HSCT, the CNEL shall not exceed 65 dBA at the airports' property boundaries. CNEL is the acronym for Community Noise Equivalent Level which is a noise rating method using an average level which exceeds a threshold value and is integrated over 24 hours (Reference 36). FAR 36 gives exception to Concorde making its guidelines Stage 2 rather than the quiter Stage 3 and states: "...the noise levels of the airplane are (or should be) reduced to the lowest levels that are economically reasonable, technologically practicable, and appropriate for the Concorde type design." This statement translates into a proposition that if supersonic transport or HSCT manufacturers/designers reduce noise levels as much as possible, then exemptions and/or exceptions to the law might apply.

10.3 POLLUTION

Methane is what is termed an alkaline or paraffin. It constitutes 50 to 90% of natural gas. Incomplete combustions of methane yields carbon black which is used in rubber compounding and printing ink. Oxygen deficient burning of methane produces carbon monoxide and when heated above 9000 $^\circ$C, it converts or dissociates to its carbon and hydrogen components. The reaction of methane with

oxygen produces carbon dioxide and water in the balanced equation :

$$CH_4 + \frac{3}{2} O_2 >>> CO_2 + 2 H_2O .$$
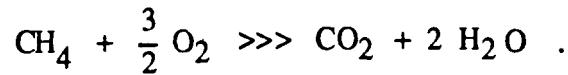
Combustion in air, however, yields the usual carbon monoxide, hydrocarbons, nitric oxides, sulfur oxides (depending on the sulfur content of the fuel) and particulates.

It has been suggested that a fleet of supersonic transports operating at high altitudes would effect the ozone layer. One article(Reference 37) recommended that such a fleet should operate above 95,000 ft as the 80,000 to 95,000 ft layer contains ample free oxygen to provide stability to the 65,000 to 80,000 ft layer which varies in quantity of free oxygen atoms -- one of the key factors to the reformation of ozone. Minimal ozone, however, resides in the 80,000 to 85,000 ft. If the exhaust emissions of the Caret HSCT deplete ozone then it would be advantageous to fly in a region where there exists the least amount of ozone. Figure 10.8 shows an approximate distribution of ozone in our atmosphere. Some attention might be paid to whether patterns and seasons since Johnson of Reference 38 states that ozone concentrations are 10% lower than normal before a storm and 20% higher than normal after a storm. He also states that concentrations are greatest at the high latitudes in Spring.

Emission standards for SST as of 1979 for new manufactured modesl were 3.9, 30.1 abd 9.0 pounds hycrocarbon, carbon monoxide and nitric oxides per 1000 pound thrust per cycle, respectively (Reference 36). Beheim (Reference 39) and Petrash (Reference 40) said that hydrocarbons and carbon monoxide were the dominant emissions at idle conditions where oxides of nitrogen and smoke were dominant at takeoff. Petrash (Reference 40) said that hydrocarbons and carbon monoxide were the dominant emissions at idle conditions where oxides of nitrogen and smoke were dominant at takeoffl. Petrash (Reference 40) suggests to increase the burning zone, increase the residence time by reducing the flooow velocity or by delayed mixing, add more fuel to the fire to raise local temperature and improve

fuel atomiztion to burn lean will reduce idle emission of HX and CO . Running fuel lean, enhancing mixing, increasing flow velocity and again better fuel atomization will reduce the NOx and smoke emission dominating the cruise or high power regimes. The combustor characteristic were realized in the Vorbix combustor of a JT9-D engine. CO was reduced by about 50%, HC was reduced by a factor of 10% and oxides of Nitrogen by 35 %. Catalyzed combustion was also suggested as it aided in nearly pollutant-free combustion.

There was an article (Reference 41) found which opposed the belief of many texts which had proof nitric oxides did not affect ozone. A study done in the early 60's of nuclear tests revealed that the large quantity of nitric oxide created from a total of some 340 megatons of nuclear explosions over a four year period showed no evidence of any decreas of any decrease in ozone. Such a large quantity of NOx would be " perhaps three times that of upper estimates predicted from 500 SSTs flying 7 hr. a day for a year". The scientists of this study had 22 stations in the Arctic and 2 stations in the Antarctic recording 12,000 ft altitude nuclear detonation activity during ther years of 1961 and 1962. Nuclear explosions were also made in the Pacific at equatorial latitudes where introduction of large concentrations of NOx with sunlight are suppose to be even more contributory to catalytic ozone reduction.
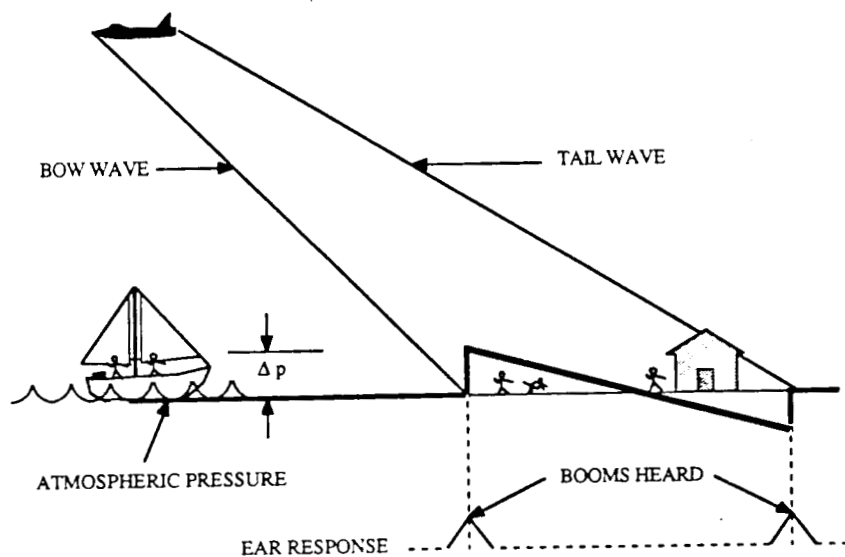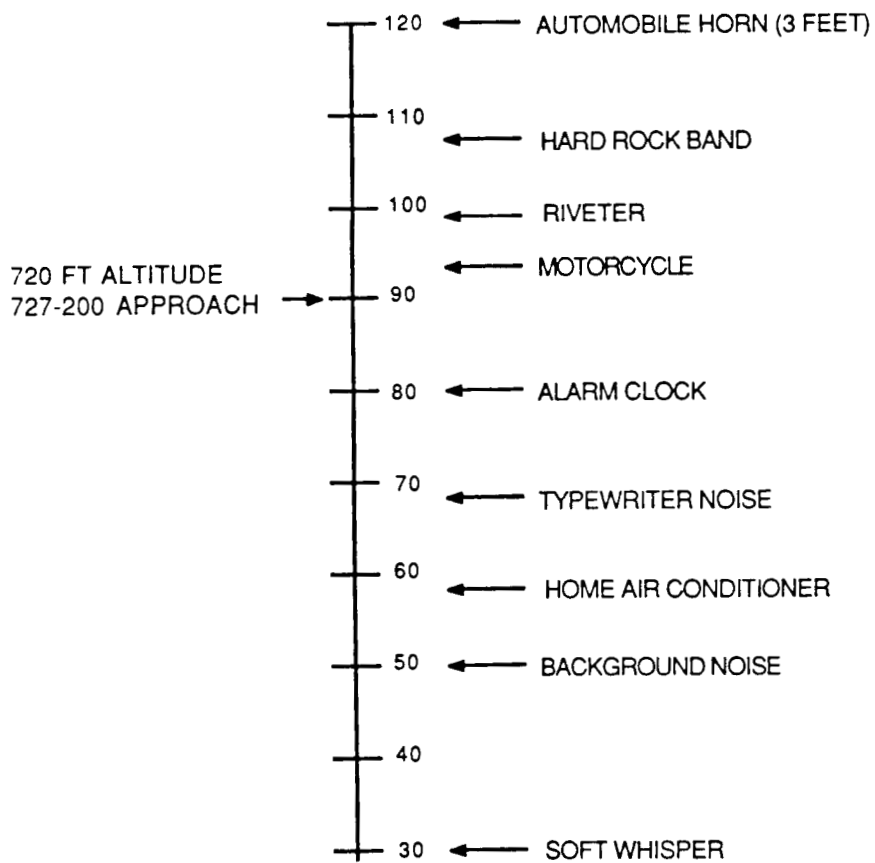
NATURE OF THE PROBLEM

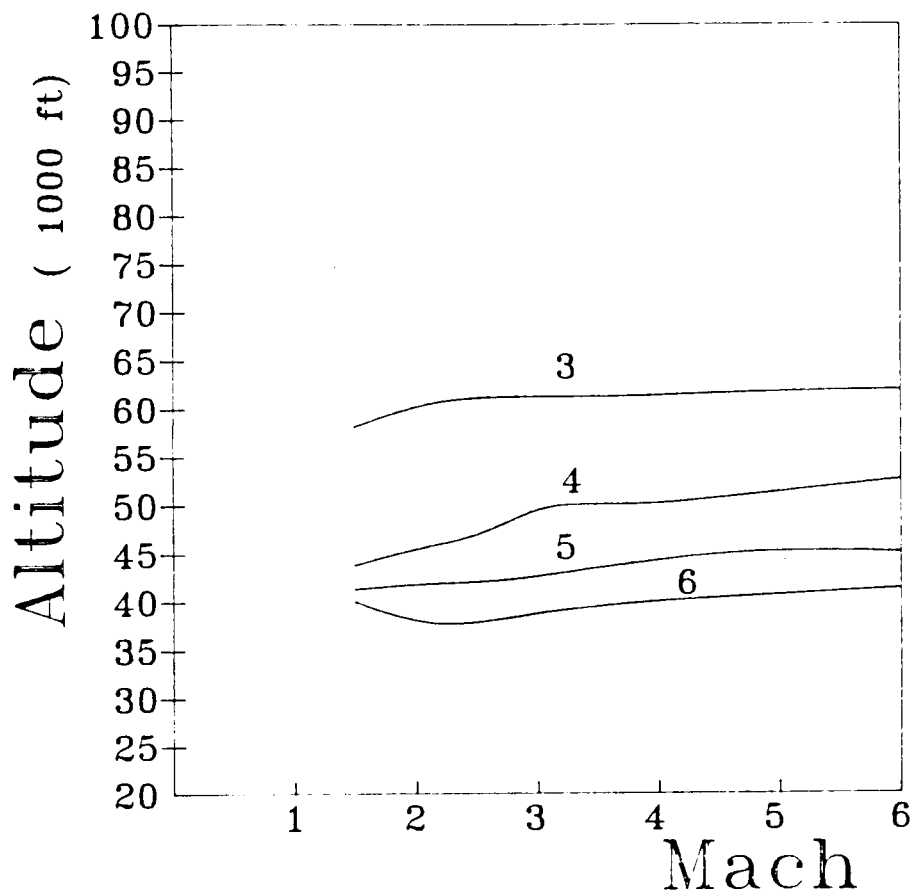FIGURE 10.1. SONIC BOOM.

TYPICAL NOISE LEVEL

120	AUTOMOBILE HORN (3 FEET)
110	HARD ROCK BAND
100	RIVETER
	MOTORCYCLE
720 FT ALTITUDE 727-200 APPROACH → 90	
80	ALARM CLOCK
70	TYPEWRITER NOISE
60	HOME AIR CONDITIONER
50	BACKGROUND NOISE
40	
30	SOFT WHISPER

FIGURE 10.3. OVERPRESSURE PREDICTION USING MORRIS.
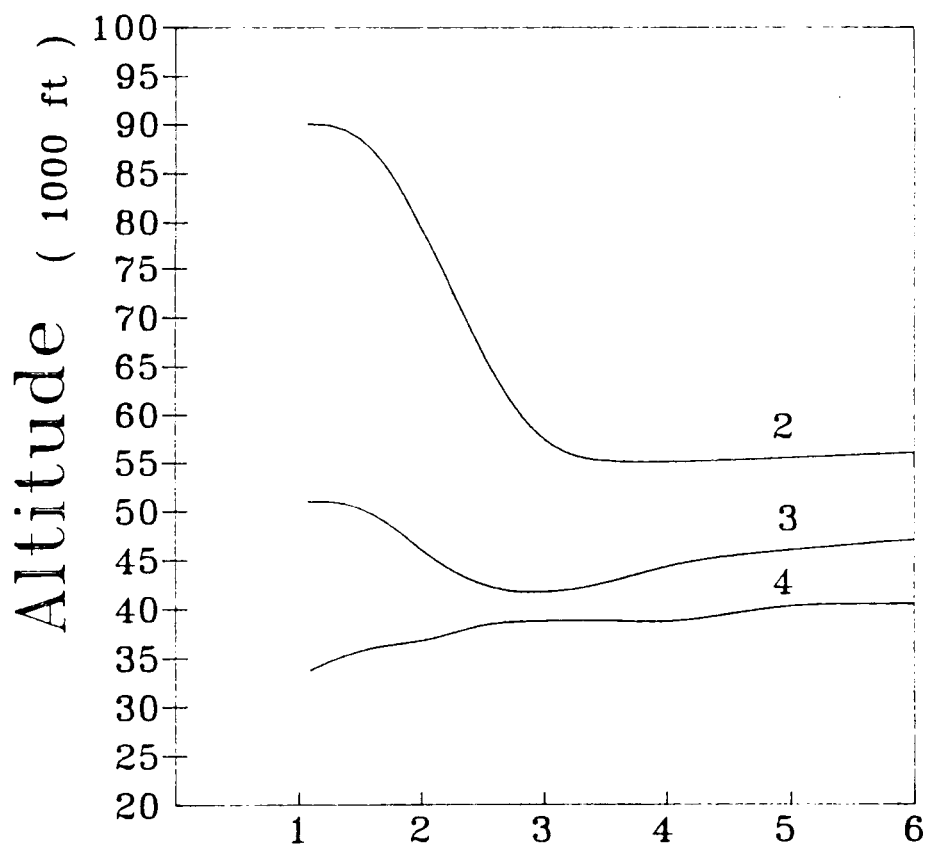
FIGURE 10.4. OVERPRESSURE PREDICTION USING SEABASS.
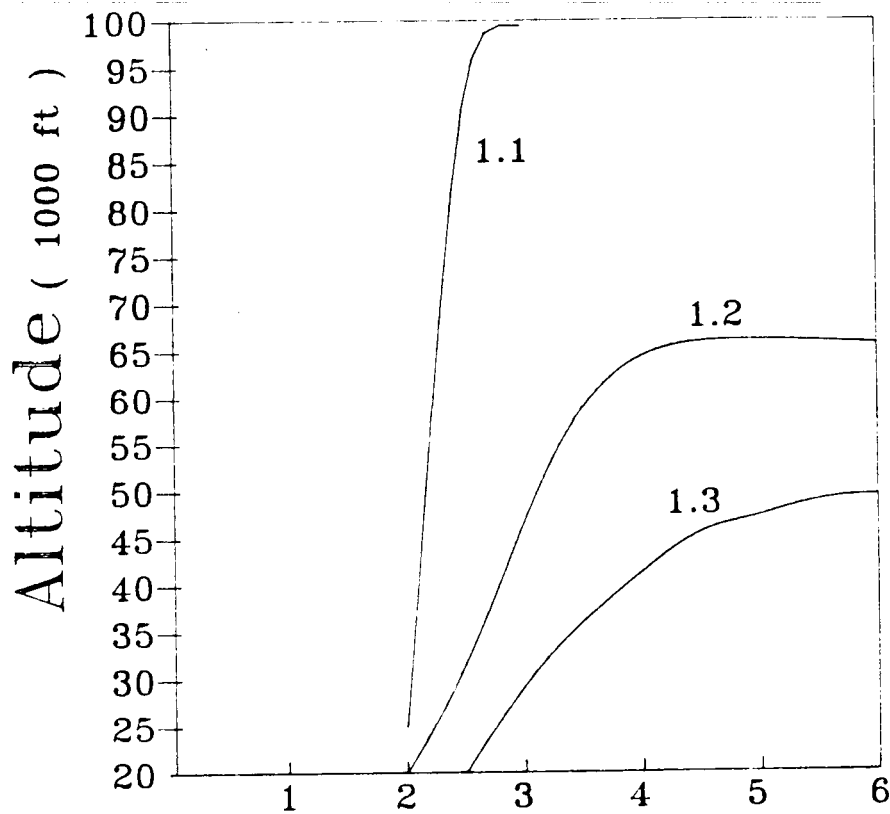
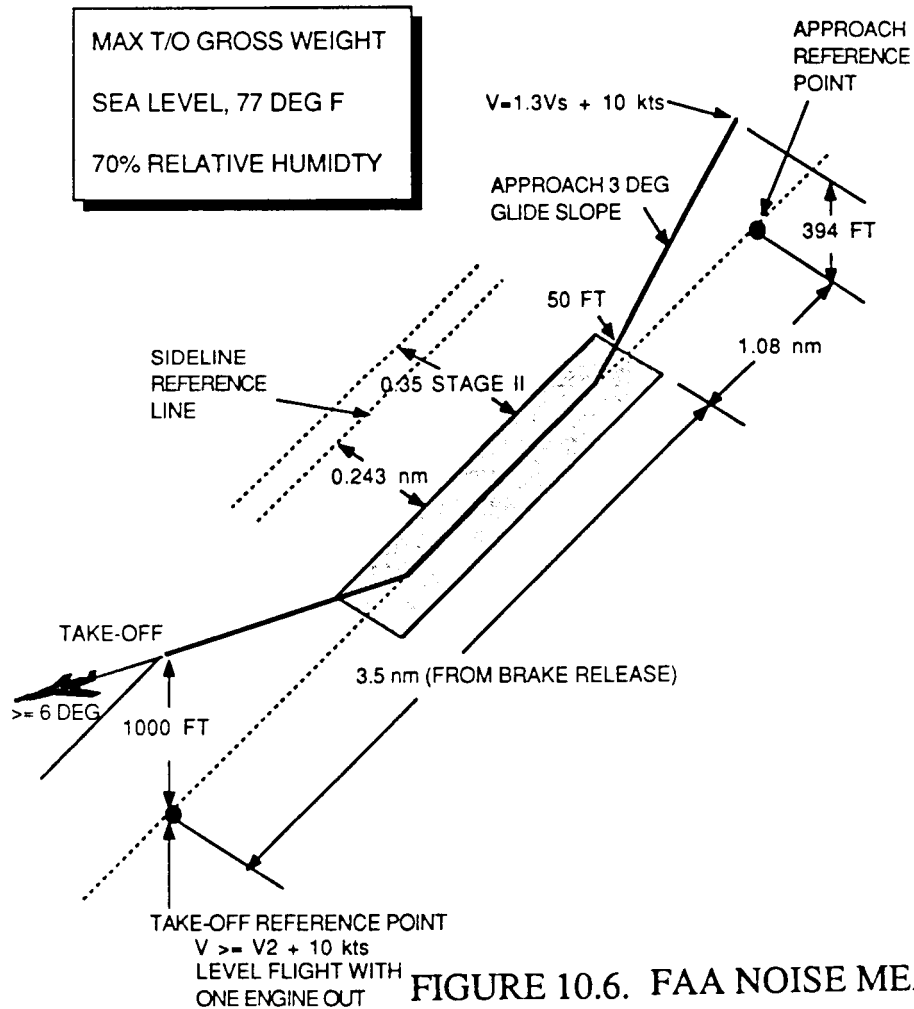FIGURE 10.5. OVERPRESSURE PREDICTION USING CARLSON.

FAA NOISE - MEASURING POINTS

MAX T/O GROSS WEIGHT

SEA LEVEL, 77 DEG F

70% RELATIVE HUMIDTY

V=1.3Vs + 10 kts

APPROACH
REFERENCE
POINT

APPROACH 3 DEG
GLIDE SLOPE

394 FT

50 FT

1.08 nm

SIDELINE
REFERENCE
LINE

0.35 STAGE II

0.243 nm

TAKE-OFF

>= 6 DEG

1000 FT

3.5 nm (FROM BRAKE RELEASE)

TAKE-OFF REFERENCE POINT
V >= V2 + 10 kts
LEVEL FLIGHT WITH
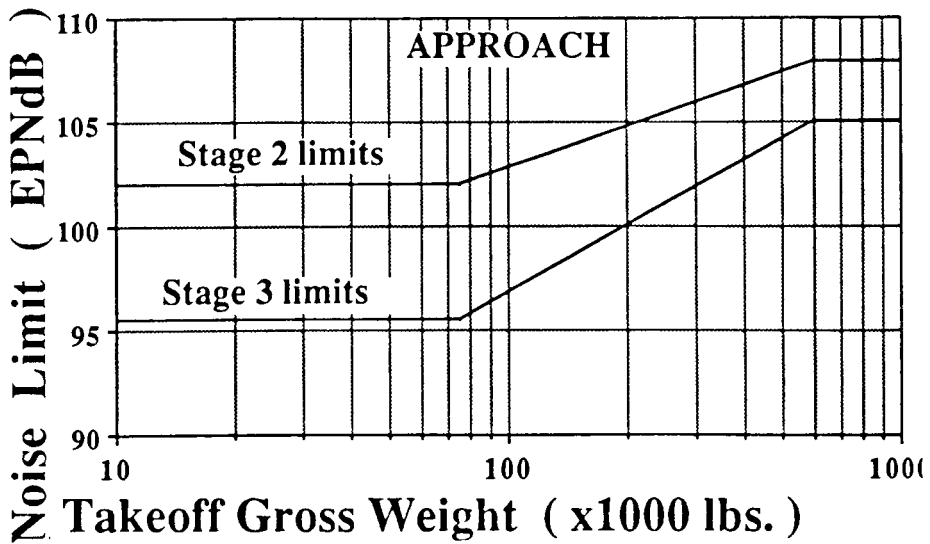ONE ENGINE OUT

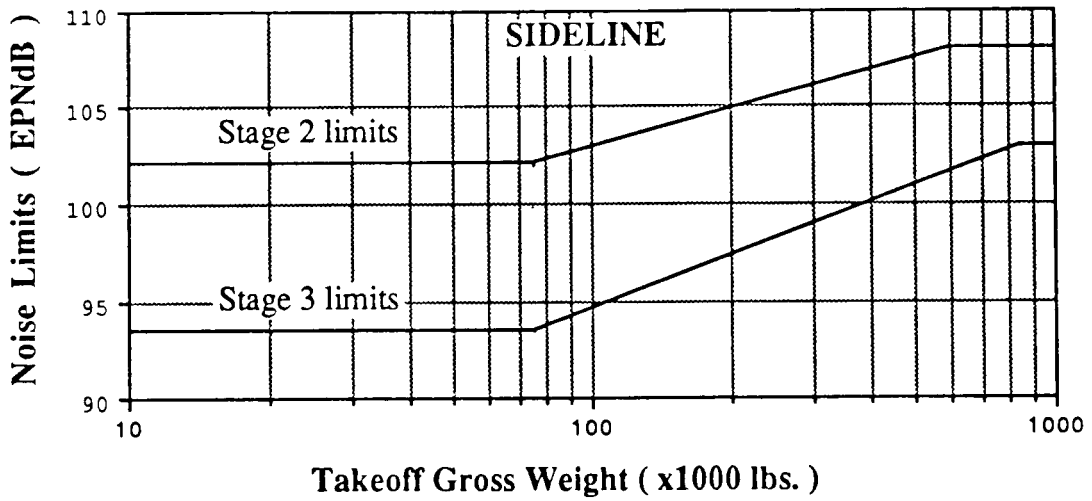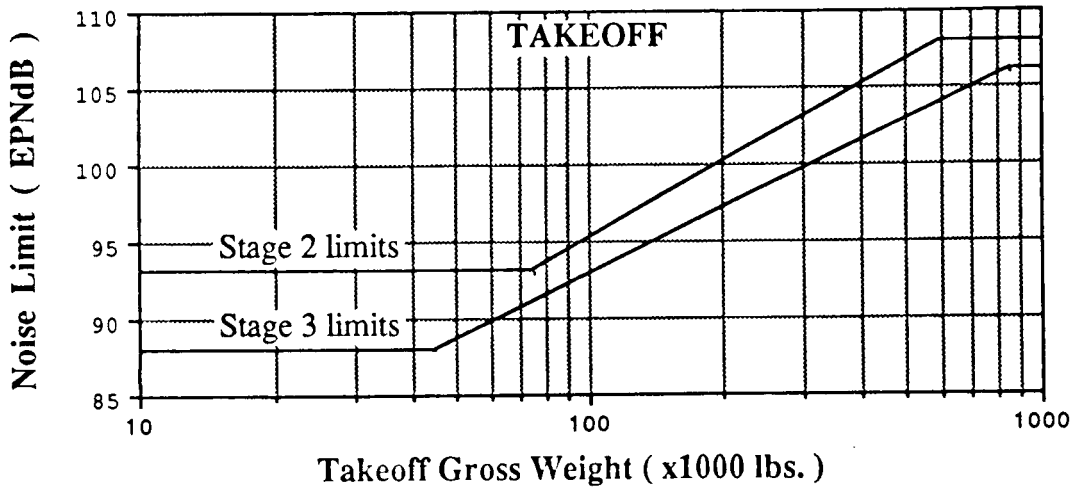FIGURE 10.6. FAA NOISE MEASURING POINTS.

96

FIGURE 10.7. STAGE LIMITATIONS.

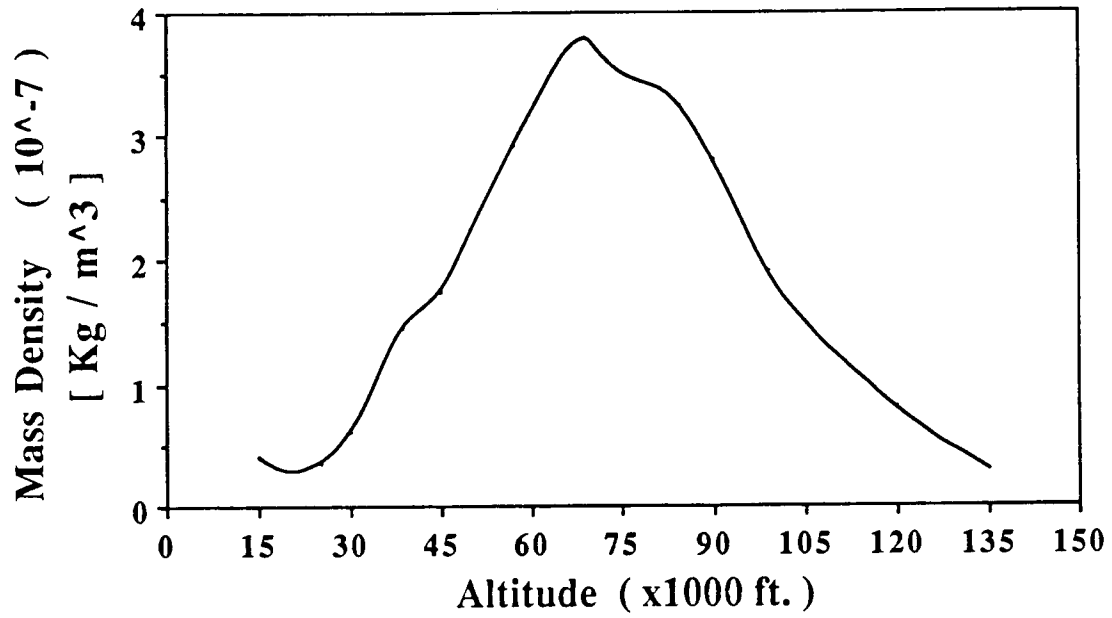97

Ozone Model Atmosphere

FIGURE 10.8. OZONE CONCENTRATIONS.

11 COST ANALYSIS

As subsonic travel is loosing its ability to keep up with the pace and needs of today's traveler, the modern and future business person will turn towards ever faster and efficient means of transportation. Concorde sought to fill this need but with current trans-atlantic fares of $5,500, its inability to fly into many U.S. airports because of noise and intolerable sonic boom overland, Concorde has not found its niche. Responding to the demand will be the Waverider High Speed Civilian Transport (HSCT), however, if the monetary risks of building such an airplane are too high, as was the case with the early 1970's U.S. SST, the program will die. It is the objective of this section to examine the costs and feasibility of the Waverider configuration.

11.1 METHOD

The cost estimation was done with a paper published by the Rand Corporation. The report was the result of the reduction of cost data on post World War II cargo, tanker, fighter, bomber and trainer aircraft as well as aircraft in the 1970 era -- A-7, F111-A, C141 and OV-10. These aircraft were composed mostly of aluminum alloy, 5000 to 113,000 lbf in AMPR weight (to be described later) and had maximum speeds of Mach 0.5 to Mach 2.2 . The method outputs development and production costs of aircraft airframes and subsystems such as engines and avionics, in a long-range planning context.

The Development phase was defined as the nonrecurring manufacturing effort undertaken in support of engineering. It includes manufacturing labor, material for mock-ups, test parts and static test items. Development costs of, say, M aircraft include development support, flight test operations and cumulative cost of M flight test aircraft plus N operational aircraft. Test facilities or manufacturing

99

facilities were included. Flight test operations cost includes costs incurred by the contractor to carry out flight tests, engineering, planning, data reduction, manufacturing support, instrumentation, spares, fuel, oil, pilots, facilities and insurance. Tooling costs encompass tool design, planning, fabrication, production of test equipment, maintenance of tooling, production planning and various changes which might take place during the production phase. Material costs include that for raw material, hardware and purchased parts for the major structure. The method decreases material cost per lbf of aircraft with quantity produced due to a built-in learning curve. Prototype costs cover limited tooling, few test articles, off-the-shelf engines and avionics but do not furnish production planning. Avionics costs, like materials, have a learning curve associated with it. One of the paper's disclaimers stated, " it is emphasized that far greater uncertainty exists when the (cost) equations are applied to aircraft whose technological or performance characteristics are outside the range of the sample." . Clearly, the Waverider HSCT planform, like the other planforms of the overall study, lie outside the range of the sample. Therefore, great uncertainty will plague calculations done for the HSCT.

The four major parameters required by the method were the desired production quantity, maximum speed of the aircraft, AMPR weight and the production rate. AMPR weight was defined as " the empty weight of the airplane less 1) wheels, brakes, tires and tubes, 2) engines, 3) starter, 4) cooling fluid, 5) the rubber on nylon fuel cells, 6) instruments, 7) batteries and electrical power supply and conversion equipment, 8) electronic equipment, 9) turret mechanism and power operated gun mounts, 10) remote fire mechanism and sighting and scanning equipment, 11) air-conditioning units and fluid, 12) auxilliary power plant unit, and 13) trapped fuel and oil." .

Also required as input information was engineering, tooling and manufacturing hourly rates, profit for the project, type of engine(s) used and maximum thrust or shaft horsepower of each engine. The hourly rates should

100

incorporate direct labor, overhead, burden, general and administrative costs and other miscellaneous direct charges.

11.2 RESULTS

To parallel the ongoing Douglas HSCT report (Reference XX), a production quantity of 275 airframes was used. The production rate was chosen to be 5 per month in order to have the project last 4 years. AMPR weight of the Waverider wing was 336,500 lbf while the maximum design speed was Mach 5.5 at 100,000 ft altitude (standard day) . Figure 11.1 shows a breakdown in cost for a prototype running with estimated avionics throughput of $200 millions and first production package of $15 million while doubling engineering hours and engine production costs. The first run yielded a unit cost for 275 airframes of $89 millions while the second (inflated) run yielded a unit cost of $107 millions in 1988 dollars. Figure 11.2 shows the breakdown cost of development for airframe, engine and avionics of the flight test aircraft.
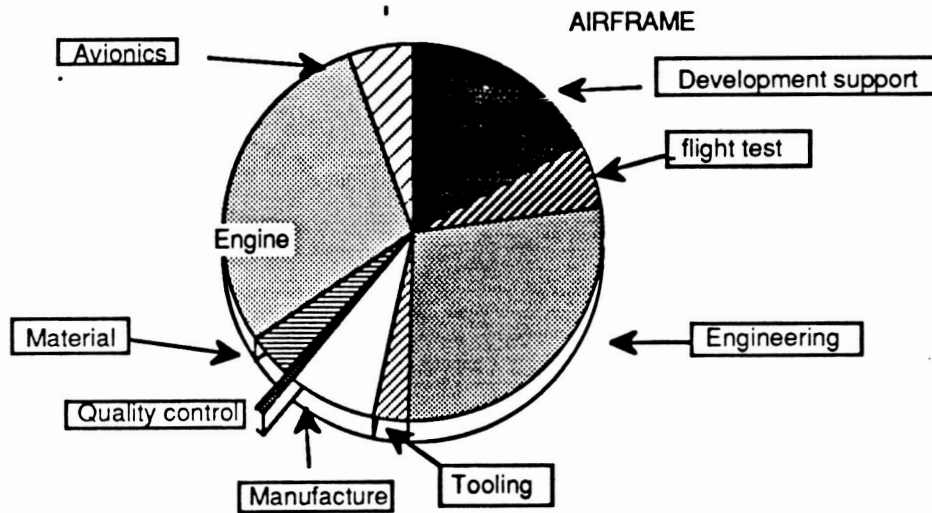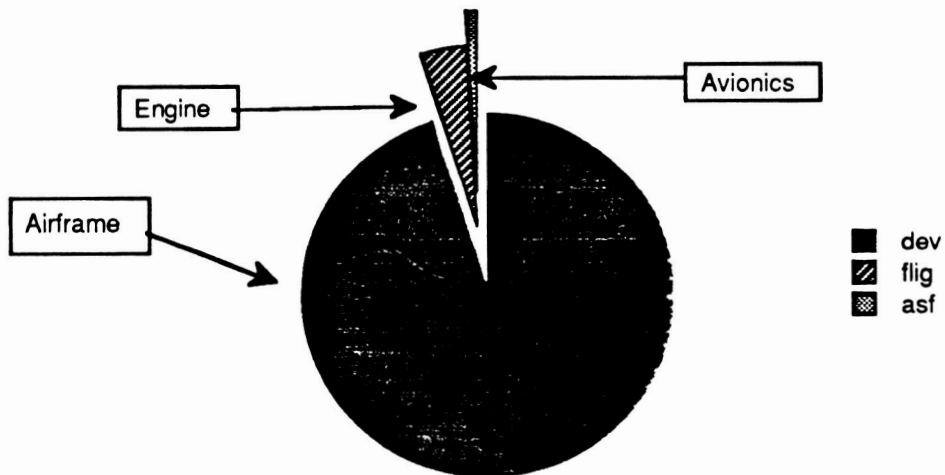
FIGURE 11.1. COST BREAKDOWN OF PROTOTYPE.

FIGURE 11.2. DEVELOPMENT COST FOR FLIGHT TEST.

REFERENCES

1. Ames Research Staff,"Equations, Tables, and Charts for Compressible Flow," NACA Report 1135, 1954.

2. Bertin and Smith, *Aerodynamics for Engineers*, Prentice Hall, New Jersey, 1979.

3. Grimminger, G. ,Williams, E.P., and Young,G.B.W.,"Lift on Inclined Bodies of Revolution in Hypersonic Flow," *Journal of Aeronautical Sciences*, November, 1950.

4. Kuchemann, D., *The Aerodynamic Design of Aircraft*, Pergamon Press, Oxford, 1978.

5. McCormick,B., *Aerodynamics, Aeronautics, and Flight Mechanics*, New York, 1979.

6. Nicolai,L., *Fundamentals of Aircraft Design*, METS, Inc., San Jose, Ca., 1984.

7. Pace, S., *North American Valkyrie XB-70A*, Aero Series Vol. 30, Aero Publishers, Inc., Fallbrook,Ca.,1984.

8. Roe,P.L.,"Aerodynamics at Moderate Hypersonic Mach Numbers," *Aerodynamic Problems of Hypersonic Vehicles*, Pankurst,R.C.(Editor), AGARD-LS-42, Vol. 1, July 1972, pp. 1.1-1.8.

9. Roe,P.L.,"Optimum Shapes," *Aerodynamic Problems of Hypersonic Vehicles*, Pankurst, R.C.(Editor), AGARD-LS-42, Vol. 1, July 1972, pp. 2.1-2.21.

11. Roe,P.L.,"Theory of Waveriders," *Aerodynamic Problems of Hypersonic Vehicles*, Pankurst, R.C.(Editor), AGARD-LS-42, Vol. 1, July 1972, pp. 3.1-3.17

11. Roskam, Jan *Airplane Flight Dynamics and Automatic Flight Controls* Roskam Aviation and Engineering Corp. Ottawa, Kansas; 1979.

13. Finck, R.D. Primary investigator for *USAF Stability and Control DATCOM* with McDonnell-Douglas Corporation, U.S. Department of Commerce. Springfield, Virginia; Revised 1975.

14. Dusa, D.J. *High Mach Propulsion System Installation and Exhaust System Design Consideration*, AIAA-87-2941; Sept 1987

15. Mattingly, Jack D., *Aircraft Engine Design* American Institute of Aeronautics and Astronautics. New York; 1987.

16. Anderson, John D., *Modern Compressible Flow* McGraw-Hill Inc., San Francisco, 1982.

17. Young, Lou Interview. Professor, California State Polytechnic University, Pomona.

18. DeMeis, Richard "Multimodes to Mach 5" *Aerospace America* American Institute of Aeronautics and Astronautics. New York; September 1987.

19. Constantine, Marc "Statement by (author) before the Subcommittee on Transportation, House of Representatives (on the Air-Turbo Ramjet)" Aerojet Corporation. Sacremento; July 1985.

20. Straight, David M "Performance of a 2D-CD Non-axisymetric Exhaust Nozzle on a Turbojet Engine at Altitude". NASA TM-82881; June 1982.

21. Hartsel, James E. "General Electric Study Engines For High Speed Transport" General Electric Corporation. Cincinnatti, February; 1988.

22. Truitt, Robert Wesky, *Fundamentals of Aerodynamic Heating,* N.Y. The Ronald Press Co. 1960

23. Chapman, Alan Jesse, *Heat Transfer*, 3rd ed. N.Y. Macmillan 1974

24. Detra, Kemp, and Riddell, "Addendum to Heat Transfer to Satellite Vehicles Re-entering the Atmosphere," *Journal of Jet Propulsion*, Dec 1957.

25. Roskam, Jan *Airplane Design, Part V: Component Weight Estimation,* Roskam Aviation and Engineering Corp.

26. White, Frank M. *Viscous Fluid Flow,* N.Y. McGraw Hill 1974.

27. Cuniff, Patrick F., *Environmental Noise Pollution*, John Wiley & Sons, Inc., NewYork, 1977

28. Ott, James, "HSCT Research Defines Weight, Fuel Issues," *Aviation Week and Space Technology*, March 28, 1988, pp. 88-90.

29. Anon. "Information on Levels of Environmental Noise Requisite to Protect Public Health and Welfare with Adequate Margin of Safety," United States Environmental Protection Agency, March 1974.

30. Carlson, Harry W., "Simplified Sonic Boom Prediction," NASA TP 1122, Scientific and Technical Information Office, 1978

31. Seabass, R. and George, A.R., "Sonic Boom Minimization," *The Journal of the Acoustical Society of America*, Volume 51, Number 2, Part 3, 1972, pp. 686-694.

32. Morris, John, "An Investigation of Lifting Effects on the Intensity of Sonic Booms," *The Journal of the Royal Aeronautical Society*, Volume 64, Number 598, October 1960, pp. 610-616.

33. Nelson, P.M., *Transportation Noise Reference Book*, Chapter 21, pp. 8-9, 1987.

34. Feiler, Charles E., "Noise Reduction," Aeropropulsion 1979, NASA CP-2092.

35. Clark, F.G. and Gibson, A., *Concorde: The Story of the World's Most Advanced Passenger Aircraft*, Paradise Press, Inc.

36. Anon., "Summary 707-727-737-747 Noise and Emission Reduction Activities," Boeing Commercial Airplane Company, Seattle, Washington, 98124, January 1978.

37. Bunin, Bruice L., "The Required Technology Combinations for High Speed Commercial Aircraft," Douglas Aircraft Company, McDonnell Douglas Corporation, February 17, 1987, Aerospace Engineering Conference and Show.

38. Johnson, F.S., "SST's, Ozone and Skin Cancer," *Astronautics and Aeronautics*, Volume 2, Number 7, p. 16, July 1973.

39. Beheim, M.A., Antl, R.J. and Poodney, J.H., "Advanced Propulsion, Cleaner and Quieter," *Astronautics and Aeronautics*, Volume 10, Number 8, p. 37, August 1972.

40. Petrash, Donald A., Diehl, Larry A., Jones, Robert E., and Mularz, Edward J.,

"Emission Reduction," Aeropropulsion 1979, NASA CP-2092.